Università degli Studi della Tuscia di Viterbo

Dipartimento per la Innovazione nei sistemi Biologici, Agroalimentari e Forestali

Corso di Dottorato di Ricerca in

Scienze, Tecnologie e Biotecnologie per la sostenibilità - XXXII ciclo

USE OF LOW-COST SENSORS FOR MEASURING GAS EXCHANGES IN ECOSYSTEMS

Settore scientifico-disciplinare

AGR/05

Tesi di dottorato di:
Dott.ssa Adriana Mariotti
Firma (Signature)
Adriana Mariotti

Coordinatore del corso
Prof. Andrea Vannini
Firma (Signature)

Tutore
Prof. Dario Papale
Firma (Signature)

Co-tutore
Prof. Ines Delfino
Firma (Signature)

A.A. 2019/20 (A.Y. 2019/20)

Università degli Studi della Tuscia di Viterbo

Dipartimento per la Innovazione nei sistemi Biologici, Agroalimentari e Forestali

Corso di Dottorato di Ricerca in

Scienze, Tecnologie e Biotecnologie per la sostenibilità - XXXII ciclo

USE OF LOW-COST SENSORS FOR MEASURING GAS EXCHANGES IN ECOSYSTEMS

Settore scientifico-disciplinare

AGR/05

Tesi di dottorato di:
Dott. Adriana Mariotti
Firma (Signature)....

Coordinatore del corso
Prof. Andrea Vannini
Firma (Signature)....

Tutore
Prof. /Dott. Dario Papale
Firma (Signature)....

Co-tutore
Prof./Dott. Ines Delfino
Firma (Signature)....

A.A. 2019/20 (A.Y. 2019/20)

Sommario

Abstract

The global climate warming observed over the last 50 years is receiving serious attention from scientists, policymakers and citizens. Quantifying greenhouse gases (GHGs) emissions and uptakes is crucial to assess global policy to reduce climate warming. Among the GHGs, carbon dioxide (CO_2) is a key contributor to the issue. Sequestration or release of atmospheric CO_2 by terrestrial ecosystems can significantly influence the stabilization of atmospheric CO_2. To understand the carbon dynamics of a given ecosystem, it is important to estimate the size of the several carbon fluxes depending on it, i.e. the net carbon balance. The eddy covariance technique and the flux-chamber technique are two widespread methods for understanding the biological components of the net C balance, and in particular of the so-called net ecosystem exchange (NEE) of CO_2. The calculation of the ecosystem storage term is key to a correct estimation of the NEE in several circumstances, while flux-chambers method is used to characterize the soil respiration and its variability. Hence, increasing the accuracy of both the storage and the flux-chamber systems translates into an enhanced accuracy in the estimates of NEE and ecosystem respiration. Improving the quality of these measurements encounters some limitations though, especially in terms of costs of CO_2 concentration sensors and auxiliary data (temperature, air humidity) probes. However, low-cost sensors are currently available on the market that would make it possible to build storage and chamber systems at a reduced cost, thus allowing to increase the spatial representativeness by a higher number of systems deployed.

Hence, the key question of this PhD research is: can a higher number of storage and flux-chamber systems made of low-cost sensors compensate for their expected lower accuracy?

For that aim two low-cost prototypes for measuring CO_2 fluxes were developed and tested for exploring their potential use in flux chambers and storage flux measurements.

The first part of the PhD activities, described in Chapter 2, concerned the laboratory tests of a set of CO_2, temperature and relative humidity low-cost sensors. The laboratory experiments followed a defined protocol designed to evaluate the sensor's performances in terms of intra model variability, linearity, accuracy, precision, short-term drift, long-term drift and sensitivity to temperature and relative humidity. Test results were analyzed to evaluate sensor potential use with flux-chambers and storage measurements.

The second part of the PhD activities concerned the set up of the prototypes. Both were realized by selecting a subset of the tested sensors, according to the laboratory results, and tested in the field.

The first prototype, a low cost system to measure storage fluxes, was tested at SMEAR II forestry station, located in Hyytiälä, Southern Finland. The aim of field tests was both to evaluate the low-cost prototype performances to measure the storage flux in comparison with the standard systems and to evaluate if this new approach could be a useful instrument to improve the storage horizontal spatial representativeness. Description of prototype, field measurements and results are presented in Chapter 3.

The second prototype, a low cost system to measure CO_2 soil fluxes, was only tested in one single application to explore the low-cost sensors suitability for soil fluxes measurement. Prototype and field tests are described in Chapter 4.

List of abbreviations

AT	air temperature
EC	eddy covariance
FCh	flux-chamber
Fc	turbulent flux
GA	gas analyzer
GHG	greenhouse gas
LCS	low-cost sensors
MP	multipoint approach
NEE	net ecosystem exchange
PT	low-cost prototype
RH	relative humidity
S	storage flux
SP	single point approach

1 General Introduction

Climate change is not a new phenomenon in the Earth's history, our climate, indeed, is subjected to continual changes with a turnover of ice ages and warmer interglacial periods, (Snyder, 2016). However, over the past century, the rate at which the climate is changing is unprecedented, (Karl and Trenberth, 2003; IPCC, 2001). Each of the last three decades has been successively warmer at the Earth's surface than any preceding decade since 1850, (IPCC, 2001; Wallington et al, 2004). The period from 1983 to 2012 was likely the warmest 30-year period of the last 1400 years in the Northern hemisphere, due to the global Earth's surface temperature warming, around 0.9 °C (IPCC, 2015). The temperature record is not the only indication of a changing climate (IPCC, 2001; IPCC, 2015). There are many other indicators such as the substantial retreat of mountain glaciers, decrease of snow cover in the Northern hemisphere, decrease of tropical precipitation, rising of sea level, decrease and thinning of Arctic ice (IPCC, 2001). The combined data prove beyond a reasonable doubt that global climate is changing, (Wallington et al, 2004; IPCC 2015).

Most of the warming observed is associated with the releasing of gases such as carbon dioxide in the atmosphere, especially due to human activities, (IPCC, 2015; Bryan et al, 1982). The link between CO_2 and climate warming has caught the attention of scientists and politicians, because of the well-known "greenhouse effect" (Matthews et al, 2004; Wallington et al, 2004). The greenhouse effect is a natural process that warms the Earth's surface. When the Sun's energy reaches the Earth's atmosphere, the portion that passes through the atmosphere as short wave radiation is absorbed by the biosphere, and re-emitted as longwave radiation. CO_2 and other gases naturally present in the atmosphere (e.g. water vapor and methane) are able to "capture" this longwave radiation causing heat to remain "trapped", (Houghton, 1997). This "natural greenhouse effect" maintains the average surface temperature of the Earth around 15°C, without which it would be approximately -19°C (Wallington et al, 2004). "Global warming" refers to the enhanced greenhouse effect due to an increase in atmospheric concentration of CO_2 and other greenhouse gases (GHG) resulting from emissions associated with anthropogenic activities (Matthews et al, 2004; Wallingtonet al, 2004; IPCC, 2001). Scientific research has well established the relationship between CO_2 and global warming, due mainly to its radiative forcing and long atmospheric lifetime, (Houghton, 1997; Bryan et al, 1982). Radiative forcing (RF) is a measure of the effect of different greenhouse gases on radiative balance at the tropopause, and is used to assess and compare the climate impact of greenhouse gases as it can be linearly related to the global mean surface temperature change

(Ramaswamy, 2000). RF is computed based on GHG concentration rate of change relative to 1750's values and its efficiency in absorbing available infrared radiation. The amount of carbon dioxide in the atmosphere has increased, since pre-industrial times, from 278 to 420 ppm (parts per million) resulting in a radiative forcing change of approximately 1.46 Wm^{-2}, larger than other greenhouse gases (e.g. methane: 0.47 Wm^{-2}) (Wallington et al, 2004). In addition the CO_2 atmospheric lifetime is around 100 years, higher than other greenhouse gases (e.g. methane: 12 years), producing a greater impact on long-term period, (Wallington et al, 2004).

The importance of CO_2 to the climate has moved the research focus on the global carbon cycle (Houghton, 2007; Prentice et al., 2001; Pinty et al,2019). The global carbon cycle refers to the exchanges of carbon within and between four major reservoirs: the atmosphere, the oceans, land, and fossil fuels, (Prentice et al., 2001). It has been widely recognized that terrestrial ecosystems, by sequestration or release of atmospheric CO_2, can significantly influence the stabilization of atmospheric CO_2, and, thus, the dynamics of the global climate system (Fowler et al, 2009; Shevliakova et al, 2013; IPCC, 2015). To understand the ecosystem carbon dynamics it is important to estimate the size of all carbon fluxes, i.e. the net carbon balance of the ecosystem of interest.

The net carbon balance of an ecosystem represents the overall ecosystem balance from all carbon sources and sinks: physical, biological, and anthropogenic (Chapin et al, 2006). A portion of the net carbon balance is the so-called NEE (net ecosystem exchange), the net CO_2 flux from the ecosystem to the atmosphere, which corresponds to the difference between photosynthesis and ecosystem respiration (Baldocchi, 2003; Chapin et al, 2006). A positive NEE indicates a CO_2 source, while a negative NEE reveals a CO_2 sink (Baldocchi, 2003; Chapin et al, 2006; Oertel et al, 2016). During the last decades the development of integrated infrastructure to measure, provide and analyze data on CO_2 and other greenhouse gases fluxes occurred, such as Euroflux, AmeriFlux and ICOS (Aubinet et al, 2000; Baldocchi et al, 2001; Franz et al, 2018). These networks determine spatial distributions and temporal evolutions of CO_2 terrestrial fluxes using long-term series of harmonized high-precision data (Raupach et al., 2005). Two main methods used by these networks to measure the CO_2 fluxes are the eddy covariance technique and the flux-chamber technique (Aubinet, 2005).

1.1 NEE measurements methods: eddy covariance and flux-chamber techniques

The eddy covariance (EC) technique is based on micrometeorological theories. It allows for continuous and non-disturbing measurements and provides spatially averaged fluxes on a scale of a few hectares to several square kilometers (Baldocchi, 2003). Flux-chamber technique (FC) is used to measure the NEE especially for small-scale field plots, generally ranging from 0.1 to 1 m^2, (Holland et al, 1999) and non-uniform surfaces where the assumptions of eddy covariance are not met (Lee et al., 2004, Wang et al, 2013).

1.1.1 Eddy covariance: theory and equations

The atmospheric turbulence is the dominant transport mechanism in the boundary layer, i.e. the part of the atmosphere that is directly influenced by the Earth's surface and responds to surface characteristics changes in a timescale of one hour (Stull, 1988). Within this layer fluxes are constant with the height and representative of the underlying surface, and they can be measured by the eddy covariance approach (Stull, 1988; Aubinet et al, 2012).

The eddy covariance method leads to the estimate of the exchanges of heat, mass (e.g. CO_2) and momentum between a surface and the atmosphere. Under ideal conditions, such as strong turbulent mixing, horizontal homogeneity of surface (topography, surface roughness, canopy density, etc), and flat terrain with an extended upwind distance, the net exchange become mono-dimensional and the vertical flux density can be calculated as the covariance between the turbulent fluctuation of vertical wind speed and the quantity of interest, (Montgomery, 1948).

The turbulent motion of any variable X, e.g. wind components or the gas concentrations, applying the Reynold decompositions, can be expressed as the sum of the mean component ($\underline{X}$) and the turbulent component (X'):

$$X = \overline{X} + X' \qquad (1.1)$$

After applying the Reynolds decomposition, simplifications of the mass conservation equation, and a spatial integration over a control volume of height z, neglecting the horizontal turbulent flux divergence and the horizontal variation of the vertical flux, lead to the computation of the net ecosystem exchange related to the scalar of interest (s) (Aubinet et al., 2012; Foken et al, 2006; Rebmann et al., 2018), given by :

$$NEE = \frac{1}{V_m}\overline{w'\chi'_s} + \int_0^z \frac{1}{V_m}\frac{\delta\overline{\chi_s}(z)}{\delta t}\,dz + \int_0^z \frac{1}{V_m}\overline{w}(z)\frac{\delta\overline{\chi_s}(z)}{\delta z}\,dz + \int_0^z \frac{1}{V_m}\left(\overline{u}(z)\frac{\delta\overline{\chi_s}(z)}{\delta x} + \overline{v}(z)\frac{\delta\overline{\chi_s}(z)}{\delta y}\right)dz$$

(1.2)

Where V_m is the molar volume of dry air ($m^3\ mol^{-1}$), t the time (s), u,v and w represent the wind velocity components in the horizontal (x,y) and vertical (z) directions and χ_s is the scalar concentration (expressed as mixing ratio, mol mol^{-1}). It should be noted that the amount of a scalar in the atmosphere can be expressed in many units: density (kg m^{-3}), molar fraction, (ratio between scalar's moles and total moles of the wet air mixture, mol mol^{-1}) and mixing ratio (ratio between scalar's moles or mass and total moles or mass of dry air (mol mol^{-1} or kg kg^{-1}). Between these, only the mixing ratio has conservative properties, and does not change with changes in temperature, pressure and humidity (Aubinet et al. 2012). If it is not possible to directly measure the mixing ratio, corrections taking into account such effects need to be performed on densities and molar fractions, the quantities that are normally measured in the field, that are not conservatives (Webb et al., 1980).

The first term of the Equation (1.2) is the turbulent vertical flux (Fc) measured by the EC system at the reference height *z.* The second term is the rate of change in storage of CO_2, i.e. storage flux (S) usually estimated from vertical profile measurements. S is an accumulation of CO_2 in the air volume below the EC measurement level, generally due to a weakness of turbulence and an increasing stability of the atmosphere, and it is conventionally assumed negative in case of accumulation and positive in case of depletion, (Aubinet et al, 2012; Montagnani et al, 2018; Nicolini et al, 2018). The third and fourth term are the non-turbulent vertical and horizontal advection fluxes. NEE is generally expressed in μmol m^{-2}s^{-1}, and conventionally positive when directed from the ecosystem to the atmosphere (source), and negative otherwise (sink) (Aubinet et al, 2012; Baldocchi et al, 2003; Chapin et al, 2006).

The vertical and horizontal advection are currently neglected, especially due to technical problems related to the direct measurement (Aubinet and Feigenwinter, 2010), while the storage is often estimated, thus the Equation 1.2 can be simplified as:

$$NEE = Fc + S \qquad (1.3)$$

Since the early tests performed with eddy covariance systems, many researchers (Ohtaki, 1984; Anderson et al., 1984; Goulden et al., 1996) highlighted that the eddy covariance method underestimates the CO_2 flux in stable conditions, i.e. when the atmosphere is stratified. This underestimation, known as the *night flux problem*, mainly occurs during the night when turbulence is suppressed and there is a net emission of CO_2 by the ecosystem, accumulating below the measurement level (Aubinet et al., 2012; Aubinet and Feigenwinter, 2010).

The most widely used methods to overcome the night-flux problem is discarding data obtained during calm, nocturnal periods and replacing data using a parameterisation of the night flux (gap-filling methods) (Goulden et al, 1996; Falge et al, 2001; Papale & Valentini, 2003; Reichstein et al, 2005). This criterion is based on the friction velocity (u*), a generalized velocity dependent on surface nature (topography, roughness and heterogeneity) and wind intensity representing the strength of wind stress. It is defined as (Foken 2008):

$$u^* = (-\overline{u'w'})^{1/2} \qquad (1.4)$$

where u and w are expressed in m s^{-1}

Hence, data measured when u* is below a given threshold, u^{*crit}, generally used as a threshold to identify windy (u*> u^{*crit}) from calm events (u*<= u^{*crit}), are discarded and replaced (Aubinet et al., 2012). Since the friction velocity depends on the surface nature, u^{*crit} is site-specific and needs to be evaluated case by case (Aubinet et al, 2012; Gu et al, 2005).

However u* correction method should be applied with care (Aubinet et al, 2012; Papale et al, 2006). When the CO_2 is accumulated under the canopy, as soon as the turbulence restarts, the flux is restored, and it's captured by the eddy covariance system, (Aubinet et al, 2012; Papale et al, 2006). In these conditions the u* correction leads to counting this flux twice (Aubinet et al, 2012; Papale et al, 2006). The addition of the storage component to Fc avoids this problem. Reliable measurement of storage fluxes are then necessary (Papale et al., 2006).

The storage flux can be computed by Eq. 1.5, a discrete form of the second term of Eq.1.2. It is given by the difference in the instantaneous vertical profiles of the gas concentration, c(z, t) at the beginning and end of the averaging period divided by the averaging interval Δt. Normally the instantaneous difference are replaced by the difference between time-averaged vertical profiles centered on the beginning and the end of the flux-averaging period (Finnigan, 2006),

$$S = \overline{\rho_d}(z) \sum_{i=1}^{i=n} \frac{\Delta \overline{c}(z_i)}{\Delta t} \Delta z_i \qquad (1.5)$$

where n is the total number of profile sampling levels, ρ_d is air molar density, Δc is the CO_2 dry molar fraction difference at height z_i over the time period Δt, Δz_i is the vertical extent of the corresponding i-th air layer. Storage flux is expressed as a flux density (generally μmol $m^{-2}s^{-1}$).

S can be significant over short-term intervals (e.g. 30 min), especially during the morning and evening hours (Finnigan, 2006). During the night, when the atmosphere stratification is stable and the turbulence suppressed, S can be equivalent to or exceed Fc, notably in forests (Nicolini et al, 2018).

The EC system uses a single point of measurement, placed over the canopy, to measure Fc and typically also S (Papale et al, 2006, Rebmann et al, 2018). The single point approach (SP) assumes that, due to the turbulence, the profile concentration of CO_2 below the measurement system is linear

(Nicolini et al, 2018). However during low turbulence, when air stratifications occur, the linear profile could not be representative of the CO_2 concentration distribution, and using a single level of measurement can lead to errors in S quantification, (Van Gorsel et al, 2009; Nicolini et al, 2018). Moreover the CO_2 concentration horizontal variability could have large difference under specific meteorological conditions even in homogeneous forests (Montagnani et al., 2018), especially at night, during calm wind and stable atmosphere, when the storage, represented by a portion of the respiratory CO_2 from soil and plants, is trapped in the lowest profiles levels (Yang et al., 2007). It is well established that increasing the number of concentration measurement levels in the vertical profile and along horizontal directions, to consider the spatial distribution, would increase the accuracy of S measurements (Nicolini et al., 2018; Yang et al., 2007; Montagnani et al, 2018). The multipoint sampling approach (MP) requires a number and position of the sampling points or levels which depend on the type of the ecosystem and the EC measurement height (Al-Saidi et al., 2009). As example if the EC system is placed at 35 mt, the vertical profile needs 10 sampling points and a minimum of 4 and 2 sampling points should be installed on horizontal planes across the two lower profile levels near the ground, in a radius of minimum 5 meters from the vertical profile (Nicolini and Papale, 2017; Montagnani et al, 2018).

1.1.1.2 Equipment and instruments

EC approach requires the setting-up of fixed stations (towers) high enough to place the sensors at the top layer above the surrounding plant canopy, with a single sampling point (Aubinet et al, 2012; Rebmann et al, 2018). This technique allows for continuous measurements and does not disturb the local environment. Turbulent flux measurements involve a sonic anemometer and a fast-response analyzer for measuring turbulent fluctuations in CO_2 concentrations at high frequency (Aubinet et al, 2012; Rebmann et al, 2018). Currently, most sites use a non dispersive infrared absorption analyzer (commonly referred to as infrared gas analyzer – IRGA), in either an open- or closed-path configuration (Aubinet et al., 2012). The multipoint sampling approach (MP) for measuring S fluxes requires a vertical profile with multiple sampling levels. Each level is equipped with an air temperature and relative humidity sensor, while the gas concentration at each level can be sampled in different ways, depending on the configuration chosen. Typically, three different multipoint configurations are currently used to assess the S profile: the ‘separate sampling’ configuration, which provides for a dedicated gas analyzer at each sampling level, the ‘sequential scheme’ configuration, which is made up by a single gas analyzer used to sequentially sample all the levels, and the ‘simultaneous’ configuration, where a single gas analyzer is used for the all the sampling levels, (Nicolini and Papale, 2017).

Instruments generally used are high-precision sensors. As example, the minimum sensor requirements stated by ICOS network are: for the CO_2 gas analyser, a range of measurement that include the range of expected CO_2 ambient values (350-650 ppm), accuracy equal to 0.5 µmol mol^{-1} and a frequency of measurement between 5-10 Hz (Nicolini and Papale, 2017; Rebmann et al, 2018). Concerning the air temperature sensor, the range of measurement should be between -55 and 55 °C, with accuracy equal to 0.1 K and a frequency of measurement of 0.033 Hz (Nicolini and Papale, 2017; Rebmann et al, 2018). Relative humidity sensors should measure in a range between 5-100 %RH, with accuracy equal to 3% and a sampling frequency equal to 0.033 Hz, (Nicolini and Papale, 2017; Rebmann et al, 2018).

1.1.2 Flux-chamber: theory and equations

Flux-chamber technique allows the direct measurements of CO_2 fluxes, due to processes such as photosynthesis and respiration, of the different ecosystem compartments (soil, trunks, leaves etc.), and can be used for replicated measurements in multiple small plots, (Wang et al, 2013).

They basically consist of accumulation chambers, enclosing the portion of the ecosystem investigated, that allow gases to accumulate in the chamber headspace over time, (Livingston and Hutchinson 1995; Rochette and Hutchinson, 2005). Depending on the recirculation system of the air, chambers can be differentiated in steady-state (open system), when an external air flow passes through the chamber and non-steady-state (closed system) when the air passes through the chamber in a closed loop (Livingstone and Hutchinson, 1995; Rochette and Hutchinson, 2005; Guidolotti et al, 2017). Concerning the open system, the flux is calculated as follows (Rochette and Hutchinson, 2005):

$$F_{ch} = (f/A)\,(C_0 - C_i)/M_v \qquad (1.6)$$

where A is the chamber area (m^2), Mv is the molar volume of air at chamber air temperature and pressure (m^3 mol^{-1}), f is the constant rate of air passing through the chamber (m^{3}s^{-1}) and C_0 and C_i the gas concentrations entering and leaving the chamber.

Concerning the closed system, the flux is calculated as follows, (Rochette and Hutchinson, 2005):

$$F_{ch} = (\delta C/\delta t)\,(V/A)/M_v \qquad (1.7)$$

where $\partial C/\partial t$ is the rate of gas accumulation (μmol mol^{-1} s^{-1}), V/A is the chamber volume/area ratio (m) and Mv is the molar volume of air at chamber air temperature and pressure (m^3mol^{-1}).

Flux estimation depends on chamber headspace CO_2 concentration measurements that are influenced by several factors, including air temperature and air moisture, soil temperature and soil moisture and pressure fluctuations (Holland et al., 1999; Pihlatie et al., 2013; Rochette & Hutchinson, 2005). It follows that the chamber deployment and the air samples should be taken in a short time as possible to keep the influencing factors under control to avoid over- or underestimation of F_{ch},

1.1.2.1 Equipment and instruments

FC are usually fabricated with non-permeable and inert materials, e.g. Polyvinyl Chloride (PVC), Polypropylene (PP), Polyethylene (PE), stainless steel or aluminium (Holland et al, 1999). The chamber design depends on the purpose of the measurements. When only the fluxes deriving from the respiration are to be measured, opaque chambers are generally used, while to account for the photosynthesis activity, transparent chambers are the choice (Guidolotti et al, 2017; Butterbach-Bahl et al, 2016; Rochette and Hutchinson, 2005). Chamber shape (generally cylindrical) and dimensions depending on the portion of the ecosystem, e.g. soil, root or vegetation, that should be enclosed in the system. The chamber closure time should be around 5 minutes, to allow the CO_2 to accumulate in the headspace and avoid perturbations from the influencing factors (temperature, moisture, etc) (Parkin and Venterea, 2010; Holland et al, 1999).

Depending on the sampling method, chambers are divided into automated or manual, (Holland et al, 1999; Rochette and Hutchinson, 2005). Automated chamber are a combinations of chamber with a fast response gas analyzer, such as tunable diode lasers (TDL), quantum cascade lasers (QCL), Fourier transform infrared spectroscopy (FTIR) or cavity ring-down spectroscopy (CRDS). Instruments using these spectroscopic techniques require a continuous air flow through the instrument, need to be at the study site and physically connected to chambers, and need a continuous power supply (Butterbach-Bahl et al, 2016). As example, the minimum requirements stated by ICOS for the CO_2 gas analyser are: continuous measurements for each chamber at least every two hours, range of measurement equal to 100-2000 ppm, sampling frequency equal to 0.1 Hz and accuracy at least equal to 2% of the readings (Rebmann et al, 2018).

Manual chambers are cheap to make, usually do not require electricity and are easily transported and deployed. Gas manual samples, at least 4 for each chamber enclosure time, are collected using vials and shipped to a laboratory to be analyzed. The frequency and timing of sampling have to take into account the gas fluxes temporal variability. To account for diurnal variability, gas samples should be collected at the daytime that corresponds to the daily average temperature, i.e. mid morning and early evening, while to account for seasonal variability, samples should be collected at least weekly (Parkin and Venterea, 2010). Gas chromatography is the most commonly used analytical technique to assess CO_2 concentrations in gas samples from manual chambers.

It is recommended, to assess the CO_2 spatial variability, to use as many chambers as possible and employ a sampling design that takes into account similar landscape elements (e.g. soil type or vegetation) or hotspots (Parkin and Venterea, 2010; Rochette and Hutchinson, 2005). Using automatic chambers, a high temporal resolution of the measurements can be obtained, however, spatial coverage is likely to be even smaller than for manual chambers, due to their much higher costs, (Butterbach-Bahl et al., 2016).

1.2 Thesis objectives

In order to estimate the storage flux as accurately as possible, considering the vertical and horizontal distributions of CO_2 concentrations is crucial. Vertical concentrations should be measured using vertical profiles with a multipoint sampling system, while the horizontal concentrations should be measured increasing the profile sampling points at the lowest levels to take into account the spatial variability. A multipoint sampling configuration (MP) can be difficult to manage and really cost demanding (Nicolini et al, 2018; Nicolini and Papale, 2017; Montagnani et al, 2018). For this reason storage measurements are not always available at all eddy sites or are based only on the concentration at the tower top, reducing the accuracy of measurement (Papale et al, 2006).

Concerning the FC methods, due to cost-related (automatic chambers) and logistical problems (manual chambers), it is often difficult to employ this method for long-term measurements, or having enough measurement units to account for spatial variability and to obtain statistically reliable results (Rochette and Hutchinson, 2005).

New low-cost sensors available on the market, to measure CO_2 concentrations and auxiliary data such as air temperature (AT) and relative humidity (RH), would make it possible to build storage and chamber measurement systems at a reduced cost, thus allowing to increase the spatial representativeness by a higher number of systems deployed.

The main objective of this thesis was to develop a low-cost approach to measure the storage fluxes using a vertical profile with a multipoint sampling configuration and evaluate its potential use to account for the storage horizontal spatial variability.
The secondary objective of this thesis was to explore the suitability of a low-cost approach to measure the CO_2 soil fluxes in conjunction with the flux-chamber method.
To achieve these results, the working plan was structured in several phases. As the low-cost technology is rather new and there is a lack of structured information regarding the sensors performances, a set of CO_2, AT and RH low-cost sensors was chosen and tested in the laboratory. The protocol test was designed to evaluate specific sensor features needed for the applications here considered, i.e. CO_2 storage and soil fluxes measurements. Description of the sensors, laboratory test and results are presented in Chapter 2. According to the laboratory tests results, a subset of the tested sensors has been selected and used to set up two prototypes that were tested in the field. The first prototype, a low-cost approach to measure the storage fluxes, was compared with the multipoint and single point approach to evaluate its performance to estimate the fluxes and to evaluate if this tool could be suitable to enhance the storage spatial variability. Description of the prototype, field tests and results are presented in Chapter 3. Description of the second prototype, a low-cost approach to measure CO_2 soil fluxes in conjunction with FC, field test and results concerning the potential use are presented in Chapter 4.
The following chapters are structured to be submitted as scientific papers, for this reason some main concepts may be redundant, especially in the introductory sections.

2 Laboratory tests for the use of low-cost sensors in environmental applications

2.1 Introduction

Eddy covariance (EC) method is based on micrometeorological theories, and under the assumption of horizontal homogeneity of surface, leads to the CO_2 net ecosystem exchange (NEE) estimation, given by the sum of the turbulent flux and the storage flux (Aubinet et al, 2012). The establishment and setup of an eddy-covariance tower requires the use of high-frequency gas analyzers and ultrasonic anemometers and instruments to measure the auxiliary data, such as air temperature (AT) and relative humidity (RH) (Rebmann et al, 2018). The used configuration for turbulent flux measurement is made up of a single sampling point (single point approach, SP), placed over the canopy, which is generally used to measure also the storage flux (Papale et al, 2006; Aubinet et al, 2012; Rebmann et al, 2018). However, to assess the storage flux more accurately a multipoint approach (MP) is deemed necessary, especially for tall canopies, but not exclusively (Papale et al, 2006; (Nicolini et al, 2018; Montagnani et al, 2018). MP approach consists of setting up along the tower a vertical profile of sampling points (Nicolini et al, 2018; Montagnani et al, 2018). Each sampling point should be equipped to measure CO_2 concentrations, air temperature and relative humidity (Rebmann et al, 2018). The storage flux is given by the difference between half-hourly instantaneous vertical profiles of the gas concentration, (Aubinet et al, 2012; Finnigan, 2006). Normally the instantaneous difference are replaced by the difference between time-averaged (generally 5 minutes) vertical profiles centered on the beginning and the end of the flux-averaging period (Finnigan, 2006)

Flux chambers technique basically consists of accumulation chambers and is widely used to measure the CO_2 soil flux, a part of NEE (Rochette and Hutchinson, 2005; Butterbach-Bahl et al., 2016). Chambers are sealed to collars, placed on soil surface, that allow CO_2 to accumulate in the chamber headspace over time and estimate the rate of change of gas concentration (i.e. the flux), (Rochette and Hutchinson, 2005; Davidson et al., 2002). CO_2 concentration measurements in the chamber headspace are influenced by several factors, including air temperature and air moisture (Holland et al., 1999; Pihlatie et al., 2013; Rochette & Hutchinson, 2005). It follows that the chamber deployment and the air samples should be taken in as short a time as possible to keep the influencing factors under control to avoid flux over- or underestimations (Rochette & Hutchinson, 2005; Holland et al., 1999; Butterbach-Bahl et al., 2016). The recommended closure time should be

around 5 minutes, to allow the CO_2 to accumulate in the headspace and avoid perturbations from the influencing factors (Parkin and Venterea, 2010; Holland et al, 1999).
Gas samples are manually collected from each chamber and subsequently analyzed using gas chromatography (manual chamber) or measured directly in the field using a chamber equipped with a gas analyzer (automatic chamber) (Rochette and Hutchinson, 2005; Butterbach-Bahl et al., 2016).
Both the storage and flux chambers methods have advantages and limitations. The major drawbacks are related to the high cost of instruments used and to the spatial resolution of measurements. Many eddy covariance sites are not equipped with a multipoint system to measure the storage because of its costs (Papale et al, 2006), up to 500K Euros for a tall forest site, (ICOS Handbook, 2019). To capture the dynamics of ecosystems CO_2 soil fluxes, both manual and automatic chambers should be replicated in time and space, i.e. more units are needed to be deployed in the field for long-term measurements (Davidson et al, 2002; Savage and Davidson, 2003; Savage et al, 2014). To increase the soil chamber spatial and temporal coverage the major limitations are related to the labor-intensive measurement (manual chamber) and the cost of gas analyzers (automatic chambers).
New low-cost sensors (LCS) to measure CO_2 concentrations are currently available on the marketplace. These sensors obviously do not have the same high performance (in terms of accuracy, precision, frequency of measurement) as instruments for measurements in environmental science (Castell et al. 2016). However, despite this limitation, over the last few years, researchers have addressed their attention to LCS, not only for measuring CO_2 concentrations, but also AT and RH. For example, Yasuda et al (2012) developed a low-cost portable CO_2 measurements device, with the aim to improve an urban monitoring system. The study compared CO_2 measurements from the device against high-precision CO_2 analyzers (LI-6262, Licor Co, Ltd). Results showed a good agreement of the outputs between the CO_2 analyzer and the developed device (Yasuda et al, 2012).
Young et al (2014) developed an urban temperature monitoring system using a wireless network of low-cost sensors, and the tested sensors have proven to be more than fit for the application: accuracy resulted < 0.22°C between -25 and 30°C, (Young et al, 2014).
Researchers are focusing on these sensors mainly because LCS could potentially fill the gap between the costly research instruments and the enhancing of spatial measurement resolution; the lower cost, indeed, can allow for simultaneous deployment of a large number of units, (Harmon et al., 2015; Hensen et al, 2013; Jiao et al., 2016; Primicerio et al., 2013).
Common limitations of LCS are: 1. designed for indoor measurements, 2. relatively low accuracy, 3. performance not coherent even among units of the same model, (Castell 2016; Shrestha, 2009).

All of the above result in a potentially high uncertainty. Also, it is not straightforward for the users to know a priori if sensor performances are sufficient to obtain a good data quality for the intended application.

The aim of this study was to explore LCS potential use with storage measurement for EC technique and soil chambers. Concerning the storage flux measurement, LCS could be configured as an array of sensors to set up a vertical profile of sampling points and replicate the heavier, more expensive EC sensing systems. However, to fit with the application, sensors should be able to measure half-hourly CO_2 concentration differences in the range between 350-650 ppm and to be suitable for long-term measurements in the field. Concerning the soil chambers technique, LCS can be an opportunity to overcome the main drawback related to capturing the spatial heterogeneity of CO_2 soil fluxes, because their lower cost allows the deployment of a simultaneous number of measurement units. However, to fit with the application, sensors should be able to measure the CO_2 increasing concentration in the chamber headspace over a time of 5 minutes, and not be sensitive to temperature or relative humidity.

A set of LCS was selected to measure CO_2 concentrations, AT and RH and specific features were tested under laboratory conditions, following a defined protocol, to evaluate if the sensor performance was suitable for the intended applications.

2.2 Materials and methods

2.2.1 Low-cost Sensors

The sensor models to test were chosen on the basis of their sensing technology and technical specification. Concerning the CO_2 sensors, the Non-Dispersive Infrared sensing (NDIR) was chosen among the available technologies. NDIR is a technology based on infrared spectroscopy. An infrared spectrum is obtained by passing infrared radiation through a sample and determining what fraction of the incident radiation is absorbed at a particular energy. By measuring the amount of absorbed light, it's possible to measure the number of molecules of a given species, (Dinh et al, 2016). The relation between absorbance A and gas concentration c is described by the Beer-Lambert's law:

$$A = log\,(Io/Id) = s * c * d \qquad (2.1)$$

where A is the absorbance, *Io* is the light source of known intensity, *I*d the light intensity after traversing the gas to the detector, *d* the optical path length and *s* the molar absorption coefficient. In practice, knowing *s, d* and *Io*, it is possible to apply the Beer-Lambert's law to measure *c*.
The basic architecture of the NDIR sensor includes an infrared light source, an optical tube containing the target gas, and an infrared sensor, with a specific wavelength filter and a detector. The NDIR sensor key feature is that fixed narrow-band filters are used with individual IR detectors to identify a few gas absorption lines over a limited wavelength range, cutting the cross-sensitivity with other gases. These sensors, indeed, have been proven to be sufficiently stable and robust against interference from other gases, and to reach a good accuracy if compared with a fast response gas analyzer (Martin et al., 2017). A microprocessor computes the final concentration and the data could be read using a serial connection.
Concerning the AT/RH sensors, the CMOS technology was chosen for AT readings and the capacitive sensing technology for RH readings. The integrated CMOS (complementary metal-oxide semiconductor) smart temperature sensors are widely used in many different commercial applications, based on the proportional-to-absolute temperature (PTAT) principle of operation, (Cahoon and Baker, 2008). The PTAT principle is based on the voltage difference between two bipolar transistors, which have different areas and conduct the same current. The voltage difference, proportional to absolute temperature, increases linearly with temperature, and it could be translated into temperature values, (Makinwa, 2010). Capacitive sensing is based on the variation of capacitance. Capacitive sensors consist of a sandwiched structure with two electrodes separated by a dielectric polymer film. Water vapour is adsorbed or desorbed by the film, creating a variation of the polymer dielectric constant and hence changes in capacitance. Humidity changes are detected by measuring the changes of capacitance, (Farahani et al, 2014).
The first approach to select the sensors, among the different alternatives, was to analyze the minimum requirements for gas analyzers and thermo-hygrometers stated by the ICOS network and here used as reference, (see Chapter 1). A first selection was made considering the alternatives that meet or approach the scientific instruments measurement ranges: 100 ─ 2000 ppm, -55 ─ 55 °C and 5 ─ 100% RH.
A second selection was then made by analyzing the highest possible measurement frequency and accuracy.
The minimum required sampling frequency for scientific thermo-hygrometers is equal to 0.033 Hz, and the minimum accuracy equal to ±0.1°C and ±3%RH. The low-cost thermo-hygrometers

available, after the first selection, met the sampling frequency and the RH accuracy and approached the temperature accuracy, with values ranging between ±0.3 and ±0.5 °C, that were considered affordable for the intended application.

The minimum requirements for CO_2 gas analyzer, in terms of sampling frequency and accuracy, are 0.1 Hz and <2% of readings for flux-chamber method, 1 Hz and 0.5 ppm for storage measurement, (Nicolini and Papale, 2017; Rebmann et al, 2018).

CO_2 low-cost sensors that have measurement frequencies higher than 1 Hz are rather uncommon, so a consideration about the sampling strategy should be made. Flux-chamber deployment time should be equal to 5 minutes with a minimum of 4 gas samples, while storage flux should be calculated using half-hourly CO_2 profiles, computed on 5 minutes averaged data (see Chapter 1). As a result, measurement frequencies up to 1/30 Hz were considered to be appropriate to obtain a reliable data set with at least 10 observations. A further consideration was made on the accuracy of CO_2 low-cost sensors, which obviously do not reach the accuracy of gas analyzers. It should be taken into account that to estimate the CO_2 fluxes, both methods are based on concentration gradient, i.e. the rate of concentration change over time (see Chapter 1), so we are interested in the accurate evaluation of the differences of the quantities more than their absolute values. Taking all these considerations, 4 models of low-cost NDIR CO_2 sensors and 4 models of low-cost CMOS/capacitive thermo-hygrometers were selected. Detailed sensors' specifications are described in Table 2.1 (CO_2 sensor models) and Table 2.2 (AT/RH sensor models), alongside with a code used thereafter, to identify the models. Among the chosen AT/RH sensors, it should be underlined that the Sensirion SHT11 model is integrated on board on the SenseAir CO_2 Engine K33-LP T/RH.

Two units for each model were purchased and used in the experiments.

According to the sensor technical specifications (power input, current consumption) and communication protocol, a circuit was designed and built to power and connect the sensors to a microcontroller (Seeduino Stalker V.3, www.seeedstudio.com), over Universal Asynchronous Receiver/Transmitter (UART) or Inter-Integrated Circuit (I2C) serial connections, depending on the specific case. The microcontroller was programmed to read the serial data using the open source Arduino Software IDE 1.8.13 (www.arduino.cc). Data was collected using the open source software RealTerm (www.realterm.sourceforge.net) which allowed a 1-Hz sampling rate.

Manufacturer		Gas Sensing Solution www.gassensing.co.uk	Gas Sensing Solution www.gassensing.co.uk	Alphasense www.alphasense.com	SenseAir www.senseair.com
Model		CozIR Ambient	Sprint IR	ARC-A1 with transmitter board	CO_2 Engine K33-LP T/RH
Code		**CO2_M1**	**CO2_M2**	**CO2_M3**	**CO2_M4**
Range of measurement (ppm)		0-2000	0-50000	0-5000	0-5000
Power supply (V)		3.25 -5.5	3.3 -5	10-30	5-12
Average current consumption (mA)		< 1.5	< 15	20	< 1.5
Peak current consumption (mA)		33	100	100	300
Resolution (ppm)		10	10	15	5
Accuracy (ppm)		± 50 ± 3% of reading	±70 ± 5% readings	±50	±30 ± 3% readings
Frequency of measurement (Hz)		1	20	1	1/30
Operating range	**T (°C)**	0 to +50	0 to +50	-30 to +50	0 to +50
	RH (% RH)	0-95 non condensing	0-95 non condensing	0-95 non condensing	0-95 non condensing
Dimensions (mm -LxWxH)		50x50x7.5	40x25x22.7	72 x39x16.5	51x57x12.5
Price	**€**	~120 €	~140 €	~122 €	~100 €

Table 2.1. Catalog specifications of NDIR CO_2 models chosen for the laboratory tests

			Aosong Guangzhou Electronics Co.,Ltd	Sensirion	Adafruit	Sensirion
Manufacturer			Aosong Guangzhou Electronics Co.,Ltd	Sensirion	Adafruit	Sensirion
Model			DHT22	SHT11	SHT31-D	SHT75
Code	**T**		**AT_M1**	**AT_M2**	**AT_M3**	**AT_M4**
	RH		**RH_M1**	**RH_M2**	**RH_M3**	**RH_M4**
Range of measurement	**T (°C)**		-40 to 80	-40 to 123.8	-40 to 125	-40 to 123.8
	RH (%RH)		0 to 99.9	0-100	0-100	0-100
Power supply (V)			3.3-5.5	2.4-5.5	2.4-5.5	2.4-5.5
Average current consumption (mA)			0.8	0.028	0.002	0.03
Peak current consumption (mA)			2.1	1	1.5	1
Resolution	**T (°C)**		0.1	0.01	0.015	0.01
	RH (%RH)		0.1	0.05	0.01	0.05
Accuracy	**T(°C)**	**Typ**	±0.5	±0.4	±0.3	±0.3
		Max	±1	±1.5	±1.5	±1.5
	RH (%RH)	**Typ**	±2	±2	±2	±1.8
		Max	±4.5	±5	±2.5	±4
Frequency of measurement (Hz)			1/2	1/30	1	1
Dimensions (mm -LxWxH)			25x15x7	8x5x 2.5	2.5x2.5x1	19.5x5x3
Price			~10 €	~15 €	~15 €	~20 €

Table 2.2. Catalog specifications of AT/RH models chosen for the laboratory tests

2.2.2 Experimental apparatus

A chamber (diameter of 26 cm, height of 54 cm, polypropylene) was designed and fabricated for this study to carry out the sensor tests. A thermostatic water bath was connected to the chamber, the water was piped up to a radiator inside the chamber, equipped with a fan, to maintain the desired temperature and avoid any stratification.

Relative humidity inside the chamber was controlled using saturated solutions of three different salts (LiCl , $Mg(NO_3)$, $BaCl_2$) that are able to provide a known relative humidity (11%, 50%, 90%, respectively) over a temperature range between 5° to 50°C, (Greenspan, 1977). The CO_2 concentration inside the chamber was regulated using two standards at 5000 ppm and 2000 ppm plus a cylinder of compressed air to create the desired mixing.

A LI-7000 (LICOR, Lincoln, NE) non-dispersive infrared (IR) CO_2/H_2O gas analyzer was used as the reference instrument for CO_2 concentration. LI-7000 CO_2 measurements are based on the difference in absorption of IR radiations through two sampling cells: a reference cell and a sample cell. A compressed tank of nitrogen was the input to the reference cell to have 0 ppm of CO_2. LI-7000 sample cell inlet and outlet were connected with two tubes to the top of the chamber, to create a closed air cycle between the chamber and the gas analyzer. The LI-7000 auxiliary pump was used to provide the chamber sample gas to the sample cell. Data from LI-7000 was collected using the software provided by the producer with a sampling frequency of 1 Hz. A MP102A-T4-W4W (Rotronic, www.rotronic.com) thermo-hygrometer was used as the reference instrument to measure AT and RH inside the chamber. The thermo-hygrometer has been positioned inside the chamber. Data from the thermo-hygrometer was recorded by a Campbell Scientific CR1000 data logger with a sampling frequency of 1 Hz (Campbell Scientific, www.campbellsci.com). Reference instruments specifications are presented in Table 2.3. All the sensors have been positioned inside the chamber, paying attention that CO_2 sensors were as close as possible to the gas analyzer inlet, to avoid any potential difference in the sampled air.

Manufacturer	LI-COR www.licor.com	Rotronic www.rotronic.com
Model	LI 7000 CO2/H2O Gas Analyzer	MP102A-T4-W4W
Range of measurement	0-3000 ppm	-40 to 60 ° C 0-100 %RH
Resolution	0.01 ppm	0.1 °C < 0.5 %RH
Accuracy	1% of readings	± 0.3 °C ± 1.5 %RH
Frequency of measurement (Hz)	0-50	< 1/12

Table 2.3. Catalog specifications of reference instruments used for the laboratory tests

2.2.3 Test methodology

A custom laboratory protocol was defined on the basis of those published by Polidori (2016) and Spinelle (2013), to test the following features: intra-model variability, linearity, accuracy, precision, short/long term drift and sensitivity to temperature and humidity.

Both methods here considered, soil chamber and storage measurements, are related to the plant and soil respiration process (Rochette and Hutchinson, 2005; Aubinet et al, 2012; Montagnani et al, 2018). Respiration is mainly correlated with the increase of soil temperature and with the growing season (spring and summer) (Lavigne et al, 2004; Wohlfahrt et al, 2005; Zha et al, 2003). For all these reasons, sensors were tested over the following range of temperature and relative humidity: ~10-40 °C and ~10-100 %RH.

Range of CO_2 concentrations for storage measurement are expected between 300-650 ppm (Aubinet et al, 2012), while concentrations in the chamber headspace could reach higher values. To assess a reliable range over which to test the sensors, typical CO_2 soil fluxes have been analyzed from the study of Oertel et al (2016). Each flux value was processed to simulate the rate of gas accumulation, hence the expected concentrations, in a closed chamber with a deployment time of five minutes. Chamber dimensions used in the simulation (diameter of 16 cm, height of 15 cm) were chosen on the basis of those recommended by USDA-ARS GRACEnet Protocol (Parkin and Venterea, 2010). From the simulation it was observed that the expected increase of gas concentration could reach

1200 ppm for CO_2 soil fluxes equal to 25 µmol $m^{-2}s^{-1}$. It follows that CO_2 sensors should be tested at least over the range 0-2000 ppm, which includes the narrower concentration range for storage measurements (350-650 ppm). However the range was enlarged up to 3000 ppm to reach the typical gas analyzer measurement range (Aubinet et al, 2012) and to approach the whole measurement range of most selected sensors.

All features are defined as follows while details on the test conditions are described in Table 2.4.

			Test conditions						
Feature	**note**	**Trials**	**CO_2 sensors**			**AT sensors**		**RH sensors**	
			CO_2	T	RH	T	RH	RH	T
			ppm	°C	%RH	°C	%RH	%RH	°C
Intra model Variability	Several trials at steady state conditions	1	420.00 ±1.00	25.00 ±1.00	53.00 ±1.00	9.00±0.20	55.00 ±5.00	14.00 ±2.00	25.00 ±1.00
		2	554.00±1.00			26.00±0.20		53.00 ±2.00	
		3	1386.00±5.00			40.00±0.20		94.00 ±2.00	
		4	2551.00±5.00						
Linearity	Ramping experiment		0-3000	25.00 ±1.00	~10-40	~10-100	51.00 ±20.00	~10-100	25.00 ±1.00
Accuracy and Precision	Several trials at steady state conditions	1	2.50±0.50	25.00 ±1.00	55.00 ±5.00	8.30±0.01	55.00 ±5.00	13.50 ±0.50	25.00 ±1.00
		2	282.50±0.50			25.50±0.01		52.00 ±0.20	
		3	430.00±0.50			39.65±0.01		91.00 ±0.10	
		4	491.50±0.50						

		5	1396.50±0.50						
		6	2562.50±1.00						
Short-term drift			425.00±5.00	25.00 ±0.20	51.00 ±2.00	25.00±0.20	51.00 ±2.00	51.00 ±2.00	25.00 ±0.20
Long-term drift			425.00±5.00	25.00 ±0.20	51.00 ±2.00	25.00±0.20	51.00 ±2.00	51.00 ±2.00	25.00 ±0.20
Sensitivity to T			425.00±5.00	-10-40	51.00 ±2.00			10-40	51.00 ±2.00
Sensitivity to RH			425.00±5.00	25.00 ±1.00	10-100	25.00±1.00	10-100		

Table 2.4. Test conditions related to each feature evaluated in the laboratory. Different test conditions depending on the target of the tested model (CO_2, AT, RH)

2.2.3.1 Intra-model variability

Intra-model variability (IMV) is related to how close the measurements from the units of the same sensor model are to each other. The IMV was calculated for each model using the following formula and compared to a defined threshold of 20% (Polidori, Papapostolou and Zhang, 2016), to determine if the measurements of the sensor units from the same model could be averaged,

$$IMV(\%) = \frac{Mh - Ml}{Ma} * 100 \qquad (2.2)$$

Mh = highest of sensors' average readings
Ml = lowest of sensors' average readings
Ma = average of sensors' average readings
IMV was computed at four different concentrations for CO_2 models, at three different temperatures and relative humidity for AT/RH models.

2.2.3.2 Linearity

The datasets acquired from the CO_2 concentration, temperature and relative humidity ramping experiment, trying to keep the other parameters constant, were used to calculate the linearity of response, evaluated by the ordinary least square regression between the sensor measurements against the corresponding reference instrument values. The squared correlation coefficient (R^2, dimensionless) and root mean square error (RMSE, expressed in ppm, °C or %RH, depending on the variable measured) were used to evaluate the goodness of fit. An R^2 near 1 reflects very good agreement between the sensors and reference readings, and small values indicate a complete lack of correlation. High value of RMSE indicates a poor fitting quality.

It should be noted that, due to the limitation of experimental apparatus, the only parameter that was not possible to keep constant was the relative humidity during the experiment regarding the AT sensors.

2.2.3.3 Accuracy and precision

The test procedure for the evaluation of accuracy required measurements at varying CO_2, temperature and relative humidity levels. The sensors reading deviations from reference instrument at every steady-state level, represent the accuracy (A) test result:

$$A = \underline{X} - \underline{R} \qquad (2.3)$$

Where $\underline{X}$ are the averaged readings by the models units and $\underline{R}$ are the reference averaged readings at each steady-state condition. The lower the results, the more accurate the sensor.

The precision (P) was estimated using the standard deviation (SD) of sensor readings.

$$P = \sqrt{\frac{\sum_{i=1}^{n} (x_i - \bar{x})^2}{n-1}} \qquad (2.4)$$

$\underline{x}$: mean of readings by the model, n: number of measurements, x: value readings

CO_2 and AT/RH models were tested over different conditions to evaluate the accuracy and precision: CO_2 sensors over 6 concentrations spanning between 0-3000 ppm, AT models over 3 temperature levels spanning between ~10-40°C and RH models over 3 relative humidity levels spanning between ~10-100 %RH.

2.2.3.4 Short- and long-term drift

Short-term drift (STD) was evaluated using the difference between reference and sensor measurements over three consecutive daily measures of half an hour each. Long-term drift (LTD) was instead evaluated considering measurements collected over two months, using fortnightly measures, lasted half an hour each. Differences within the manufacturer's tolerance range were not taken into account in this analysis.

2.2.3.5 Sensitivity to temperature and relative humidity

Sensitivity to temperature was tested setting the relative humidity at constant levels, and measuring temperature in ramping experiments. Vice-versa for sensitivity to relative humidity, RH measurements were performed at constant temperature values. The slope of a linear fit of the sensor's readings against the temperature and the relative humidity gives the sensitivity coefficient for the influencing variable (Spinelle, Aleixandre, & Gerboles, 2013). Concerning the CO_2 sensors, tests were performed at steady-state gas concentrations. Biases within the manufacturer's tolerance range were not taken into account in this analysis.

2.2.4 Raw data treatment

The first analysis of raw data, i.e. the data as reported by the sensor before any correction or processing, highlighted the presence of outliers in CO2_M1 and CO2_M2 dataset. Data from CO2_M3 and CO2_M4 and from all the AT/RH sensors didn't show the same issue. It should be considered that the CO2_M2 has a high measurement frequency (20 Hz), more susceptible to outliers. Furthermore, the CO2_M2 data collected are instantaneous measurements, and logged with a frequency of 1 Hz. The probability of having an outlier among the CO2_M2 dataset is certainly higher than the other sensors with lower measurement frequencies. For this reason, before any data analysis, an outlier detection method, based on Chebyshev's inequality, was used to clean the CO_2 time series collected with CO2_M1 and CO2_M2 models. This method was designed to determine a lower bound of the percentage of data that exists within k number of standard deviations from the mean, (Amidan, Ferryman and Cooley, 2005):

$$P(|X - \mu| \leq k\,\sigma) \geq \left(1 - \frac{1}{k^2}\right), \qquad (2.5)$$

with X= sensor measurements, μ = mean, σ = standard deviation.
Choosing k=2, about 95% of the data will fall within two standard deviations from the mean. After the outlier detection, the dataset was averaged over 30 seconds.

2.3 Results

2.3.1 Intra-model variability (IMV)

AT/RH models IMV results were under the 2.00%, showing a really good agreement between the readings of the same model units. CO_2 models IMV results were all under 10%. According to the test protocol, since the differences between measurements from units of the same model were under the defined threshold of 20% , they were considered not varying significantly from each other and averaged to calculate the other features of the subsequent tests. However it should be noted that IMV results for CO_2 sensors (Table 2.5) showed different behaviours depending on the model. CO2_M4 results spanned between 0.92 and 1.04%, showing a low variability between the readings from the units of the same model, followed by the CO2_M3 with results spanning between 0.7 and 3.50%. CO2_M1 and CO2_M2 showed the greatest variations of IMV results over all the trials, probably due to the noisier dataset despite averaging over 30 seconds and the detection of the outliers.

	Trial	CO2_M1	CO2_M2	CO2_M3	CO2_M4
IMV (%)	1	9.99	3.57	2.95	0.24
	2	7.95	8.64	0.7	0.09
	3	3.23	5.52	3.50	1.04
	4	3.97	3.90	1.62	0.92

Table 2.5. CO_2 model IMV results related to all the experimental trials

2.3.2 Linearity

Figure 2.1 presents regression lines and Table 2.6 gives the regression results of the CO_2, AT/RH models using the ordinary least square regression. All the sensors showed a really good squared correlation coefficient, with values lower than 1.00 only for CO2_M2 (0.96). However, RMSE results showed that linear fits had an error, ranged between 11.67 (CO2_M3) and 164.95 ppm (CO2_M2) for CO_2 models, between 0.63 (RH_M2) and 1.64 %RH (RH_M1) for RH models while was rather constant (0.32 or 0.40 °C) for AT models. It should be noted that CO2_M2 regression results are due mainly to the noisy dataset (Figure 2.1, top row) despite the averaging and outlier detection.

	CO2_M1	**CO2_M2**	**CO2_M3**	**CO2_M4**
R^2	1.00	0.96	1.00	1.00
RMSE (ppm)	24.72	164.95	11.67	38.92
	AT_M1	**AT_M2**	**AT_M3**	**AT_M4**
R^2	1.00	1.00	1.00	1.00
RMSE (°C)	0.32	0.32	0.28	0.40
	RH_M1	**RH_M2**	**RH_M3**	**RH_M4**
R^2	0.99	1.00	1.00	1.00
RMSE (%RH)	1.64	0.63	0.81	0.79

Table 2.6. CO_2, AT and RH model linearity test results

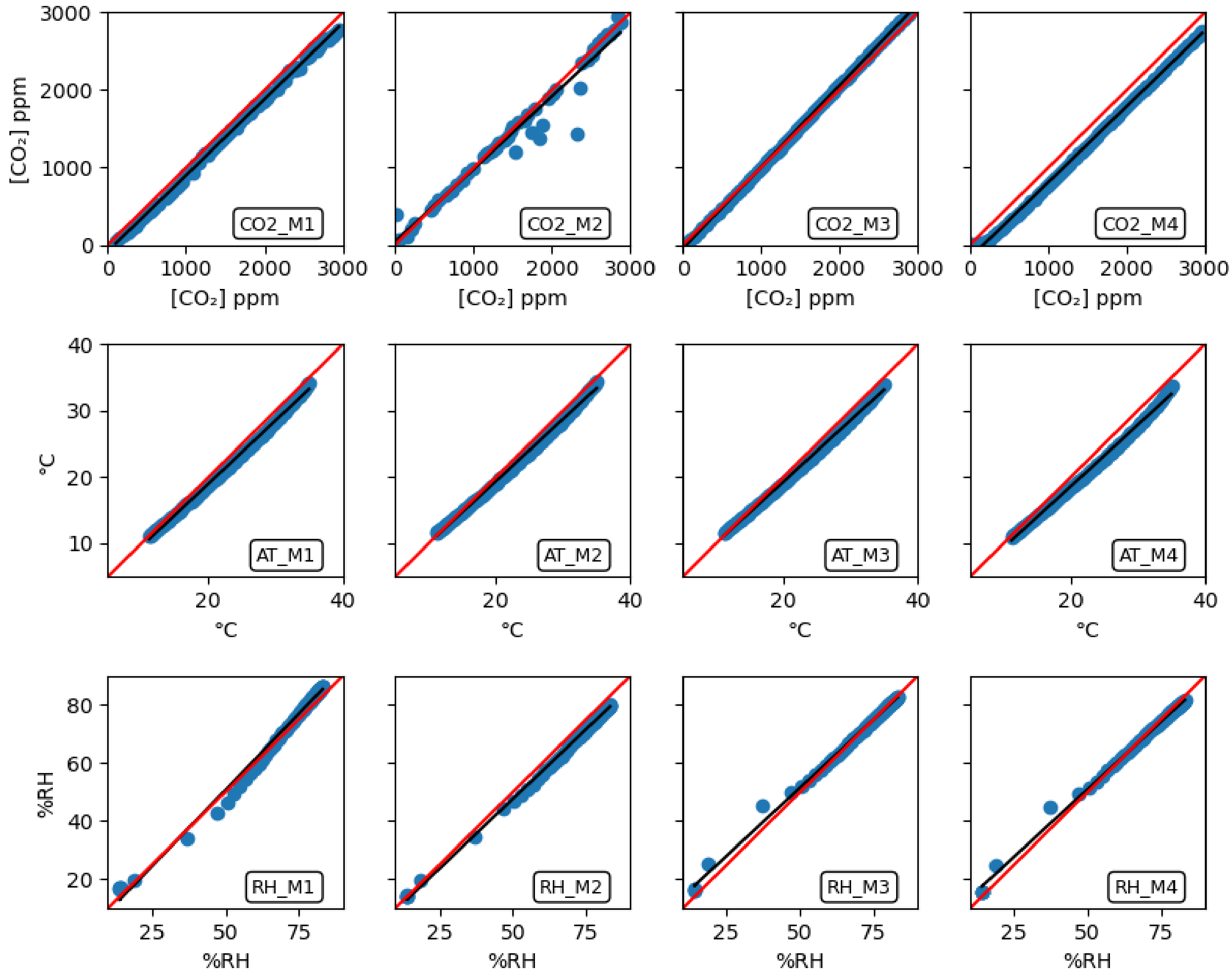

Figure 2.1. Linear regression analysis between CO_2 models readings (top row), AT models readings (central row) and RH models readings (bottom row) against respective reference instruments. Black lines are the fitted models and red lines represent the 1:1 relation. The error of each data point is equal to the tolerance stated by the manufacturer, collected in Table 2.1 (CO_2 models) and Table 2.2 (AT/RH models)

2.3.3 Accuracy and Precision

Accuracy test results are presented graphically in Figure 2.2 (CO_2 models: top row, AT models: central row, RH models: bottom row). Each plot represents the sensor model deviation from the reference at each accuracy test trial and also illustrates the manufacturer-specified typical (grey shadow area) and maximum (light grey shadow area) tolerance, listed in Table 2.1 and Table 2.2. Numerical results related to each experimental trial are provided in Table 2.7.

Concerning the CO_2 sensors, the accuracy decreased as the gas concentration increased, as expected considering the stated tolerance of all the models except for the CO2_M3. CO2_M1, CO2_M2 and CO2_M4 deviations were within the manufacturer-tolerance range in all the accuracy test trials, while CO2_M3 deviations didn't match the declared tolerance at fifth and sixth trial showing a maximum discrepancy equal to 113.59 ppm at 2562.50±1.00 ppm. It should be noted that CO2_M1 was tested at 2562.50±1.00 ppm (sixth trial) outside its range of measurement, equal to 0-2000 ppm, not showing any discrepancy with the spec tolerance.

AT models showed similar accuracy values over all the trials. AT_M2, AT_M3 and AT_M4 deviations at trial 1, spanning between 1.12 and 1.18 °C, were not within the maximum tolerance (±1.00, ±0.40, ± 0.40 °C respectively), and AT_M4 deviation at trial 2, equal to 0.44 °C, was not within the maximum tolerance (±0.30 °C).

RH models deviations fell within the maximum tolerance range at all RH levels tested, except for the RH_M1 at trial 2 that showed a deviation equal to 3.13 %RH, outside the declared maximum tolerance (±2.80%RH).

Precision test results are collected in Table 2.7. AT/RH models, with constant and close to 0.00 values of SD, over all the trials, showed a really good precision. CO2_M4 showed the best precision performance with values spanning between 0.00 and 0.25 ppm over all the tested levels, followed by the CO2_M3 with precision values ranging between 0.53 and 2.41 ppm. CO2_M1 showed precision values decreasing with the increase of concentration, ranging from 2.05 to 18.30 ppm. CO2_M2 showed precision values rather variable over all the trials, ranging between 8.45 to 17.13 ppm.

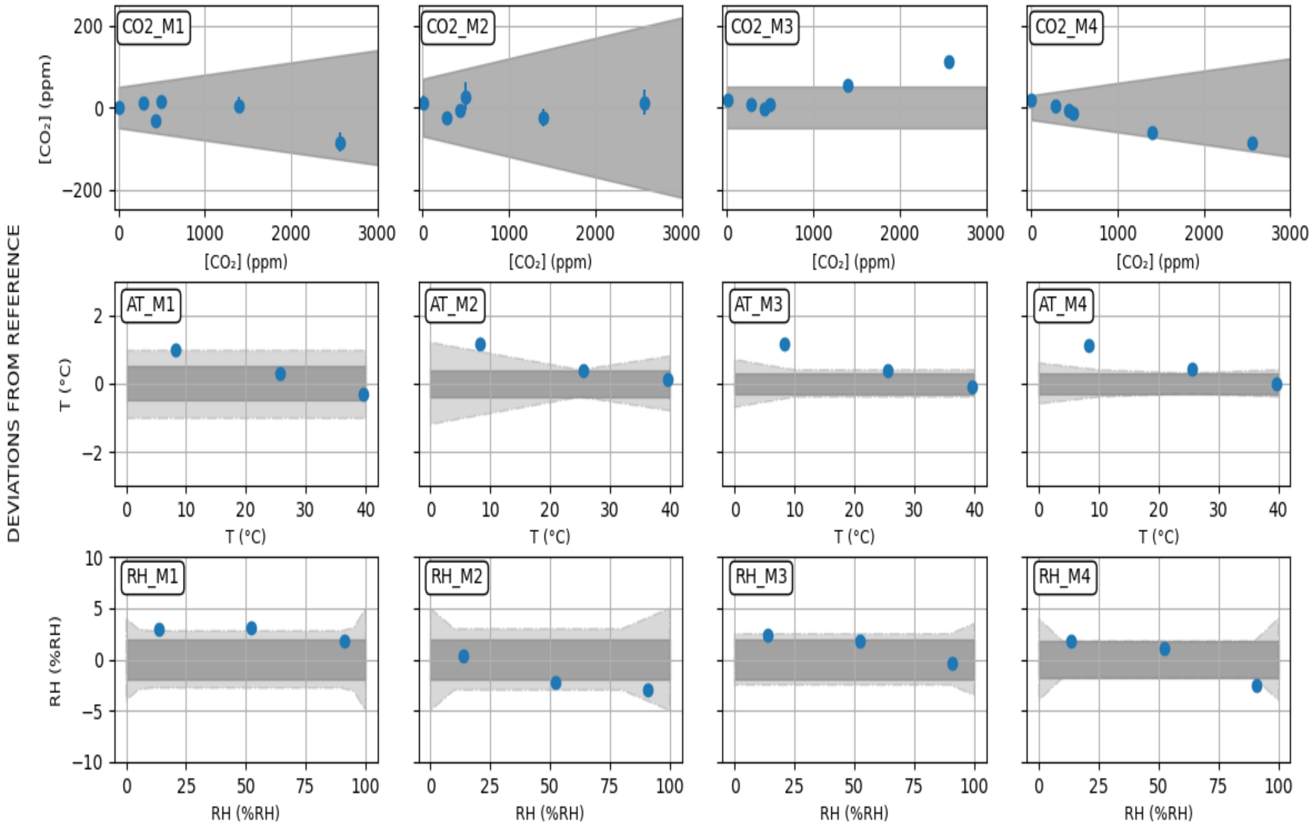

Figure 2.2. Accuracy test results. Plots show the deviations from the reference value for the CO_2 models (top row), AT models (central row) and RH models (bottom row). The gray and the light grey shadow areas represent the manufacturer-stated typical and maximum tolerance and the errorbar the standard deviation.

	CO2_M1		**CO2_M2**		**CO2_M3**		**CO2_M4**	
Trial	**P (ppm)**	**A (ppm)**	**P (ppm)**	**A (ppm)**	**P (ppm)**	**A (ppm)**	**P(ppm)**	**A (ppm)**
1	2.05	1.19	8.00	11.77	0.63	17.35	0.25	18.86
2	4.25	10.45	11.97	-26.38	1.04	6.85	0.18	4.66
3	8.45	-33.90	11.67	-6.87	0.53	-2.64	0.20	-6.59
4	5.95	15.92	12.01	26.16	0.94	6.96	0.00	-12.92
5	10.69	5.11	9.85	-26.05	1.49	52.75	0.13	-60.69
6	18.30	-84.49	17.13	11.77	2.41	113.59	0.25	-85.38

	AT_M1		AT_M2		AT_M3		AT_M4	
Trial	**P (°C)**	**A (°C)**	**P (°C)**	**A (°C)**	**P (°C)**	**A (°C)**	**P (°C)**	**A (°C)**
1	0.00	0.99	0.01	1.18	0.01	1.15	0.01	1.12
2	0.00	0.30	0.00	0.38	0.00	0.38	0.00	0.44
3	0.00	-0.30	0.01	0.13	0.00	0.11	0.01	-0.03
	RH_M1		**RH_M2**		**RH_M3**		**RH_M4**	
Trial	**P(%RH)**	**A(%RH)**	**P(%RH)**	**A(%RH)**	**P(%RH)**	**A(%RH)**	**P(%RH)**	**A(%RH)**
1	0.00	2.94	0.00	0.34	0.02	2.36	0.02	1.76
2	0.01	3.13	0.00	-2.19	0.01	1.85	0.00	1.12
3	0.00	1.78	0.00	-2.91	0.03	-0.39	0.03	-2.45

Table 2.7. CO_2, AT and RH models precision (P) and accuracy (A) test results related to each experimental trial at steady state conditions.

2.3.4 Short- and long-term drift

Short-term drift (STD) and long-term drift (LTD) results are presented as the deviations from the reference measurement every 24 hours over three days and every two week over two months of continuous measurements, respectively.

Concerning the STD, none of the CO_2, AT and RH models showed a clear drift in measurements.

Regarding the LTD, two out four CO_2 models, CO2_M1 and CO2_M3, showed a long-term drift around the 36th day of the test, (Figure 2.3, top row). CO2_M1 bias was equal to 10.53 ppm on day one, after 14 days was equal to -35.93 ppm, and then started to increase up to 194.21 ppm, outside the spec tolerance range. CO2_M3 bias was equal to -6.43 and -10.13 ppm, over the first two weeks, but after the 14th days, it decreased to -57.76 ppm (day 36), to -64.64 ppm (day 52), falling outside the tolerance range.

Two out four RH models, RH_M1 and RH_M3, showed a long-term drift too, (Figure 2.3, bottom row). RH_M1 bias was equal to -0.84%RH during the first days of the experiment. RH_M1 started to increase its drift, equal to 2.33 %RH, around the 14th day of experiment, up to 3.07 %RH at 36th day of test, falling outside their manufacturer accuracy. RH_M3 bias was equal to 1.36 %RH during the first day of the experiment, then started to increase up to 2.67 %RH, falling outside the spec accuracy during the 52th day of the test.

None of the AT models showed a LTD.

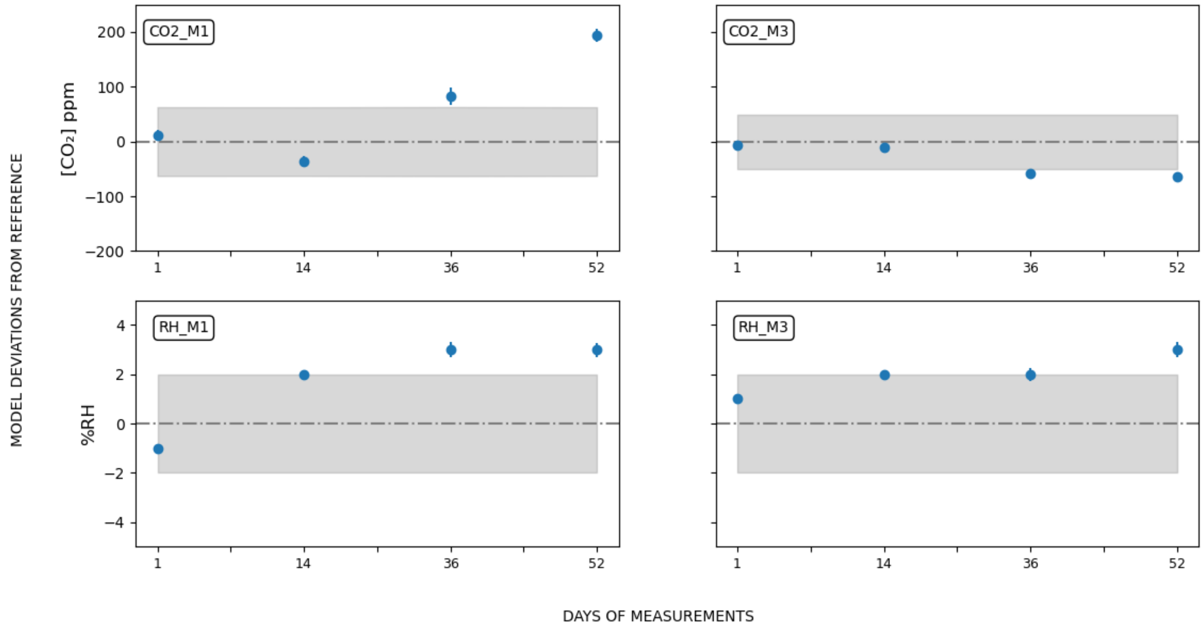

Figure 2.3. LTD test results. Figure represents only the four sensor models (CO2_M1, CO2_M3, RH_M1 and RH_M3) that showed a LTD. Plots show the deviations from the reference value for the CO_2 models (top row), and RH models (bottom row) over 52 days of measurements. The grey shadow areas represent the manufacturer-stated typical tolerance, and the errorbar the standard deviation.

2.3.5 Sensitivity to temperature and relative humidity

AT and RH model sensitivity coefficients, all equal to zero, suggested that relative humidity or temperature variations do not affect AT and RH measurements.

CO2_M1, CO2_M3 and CO2_M4 showed low sensitivity to relative humidity, with sensitivity coefficient values equal to 0.57, 0.59 and 0.44 ppm/%RH, respectively. CO2_M2 showed a higher sensitivity to relative humidity with coefficient value equal to 6.462 ppm/%RH.

CO2_M1, CO2_M2 and CO2_M3 showed a clear sensitivity to temperature with increasing coefficient values from 1.43, 2.59 up to 8.88 ppm/°C, while CO2_M4 was the only model that showed the lowest sensitivity to temperature, with coefficient value equal to 0.13 ppm/°C

CO_2 models sensitivity coefficients are collected in Table 2.8.

	CO2_M1	CO2_M2	CO2_M3	CO2_M4
RH sensitivity (ppm/%RH)	0.57	6.46	0.59	0.44
T sensitivity (ppm/°C)	1.43	2.59	8.88	0.13

Table 2.8. Sensitivity coefficient of CO_2 models to temperature and relative humidity

In order to understand the magnitude of the error that could affect the values detected by CO_2 models, another analysis was performed. Sensors were tested under three combinations of temperature and relative humidity ranges: low (7-15°C/10-40%RH), medium (15-27°C/40-60%RH) and high (27-40°C/60-100%), and the error was evaluated for each individual unit of the considered models, (see Figure 2.4). It was decided to perform this analysis not using the averaged data of the two sensors to understand if the results concerning the sensitivity coefficients were consistent with each other.

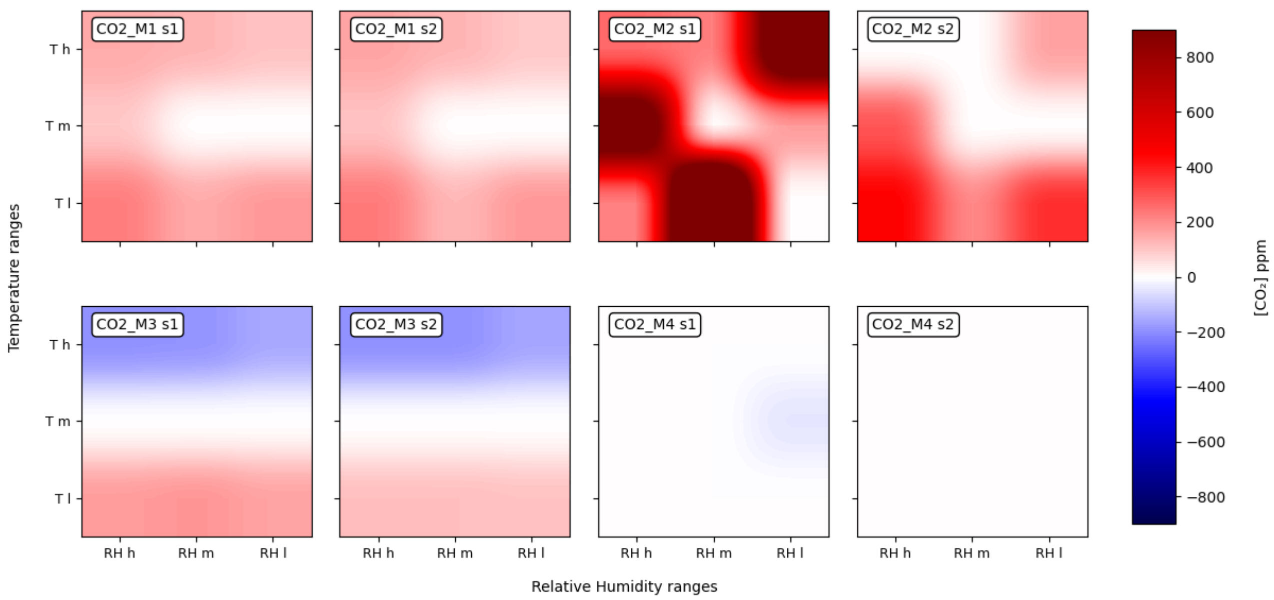

Figure 2.4. Plots show the bias respect to the reference value for each of the two units (indicated as s1 or s2) considered for the CO_2 models, under nine combinations of temperature (T) and relative humidity (RH) ranges (low, medium and high).

CO2_M4 units didn't show, in this test too, a sensitivity to temperature and relative humidity. CO2_M1, CO2_M2 and CO2_M3 bias was compliant to the sensitivity coefficients estimated, however its magnitude was larger than expected. CO2_M3 showed a clear sensitivity to temperature, underestimating the true values at high temperature and vice-versa at low temperature, while it didn't show any bias over all the ranges of relative humidity (low, medium and high) at medium temperature.

Bias pattern of CO2_M1 and CO2_M3 units was similar while CO2_M2 units showed different magnitudes of bias, probably due to a specific sensitivity of the purchased unit.

2.4 Discussion

Four models of low-cost NDIR CO_2 sensors and four models of low-cost thermo-hygrometers were selected and tested in the laboratory. The protocol for the tests was designed to evaluate specific sensor features needed for the applications here considered, i.e. CO_2 storage and soil fluxes measurements.

Storage flux is measured using a vertical profile with sampling points equipped to continuously measure CO_2 concentrations, AT and RH, for long-term field measurements. In order to fit with this application, LCS sensitivity to AT and RH should be as low as possible or negligible for the considered ranges, and sensor measurements should be stable over time significantly longer than the characteristic time scale of the variation of the measured variables, to be deployed for long-term periods. AT and RH sensors should measure absolute values with a good accuracy, while, considering that the storage flux is given by the difference between half-hourly CO_2 vertical profiles, the CO_2 sensors should be stable over time and precise more than accurate in absolute value readings.

Soil flux is measured using the CO_2 rate of change inside the chamber headspace, with generally a closure time of 5 minutes to avoid perturbation, due to temperature and relative humidity changes. In order to fit with this application, CO_2 sensors should be able to measure increasing concentrations over five minutes and not be sensitive to temperature and relative humidity variations. Furthermore, in order to measure the CO_2 soil spatial variability, a number of the same sensor should be deployed in fied for long-term measurements, it follows that readings should be as stable as possible over time.

To evaluate the sensors, the following features were tested: intra-model variability, linearity, accuracy, precision, short and long term drift and sensitivity to temperature and relative humidity.

Concerning the CO_2 models, laboratory results show a wider variation in sensor performance, despite all the models using the same sensing technology (NDIR). So the discussion will concern each single model.

1.CO2_M1. Long-term drift test results suggest that this model is suitable for a deployment period shorter than two weeks (Figure 2.3). For long-term deployment to avoid bias in measurements, sensors would probably need to be replaced or recalibrated. Anyway, the major limitation to be suitable with long-term measurements, such as storage flux estimation or soil flux chambers method to account for the spatial variability, is due to the sensor sensitivity to temperature. Test results (Table 2.8, Figure 2.4), indeed, suggest that CO2_M1 readings are temperature-sensitive and could be affected by a bias between 100-200 ppm with the sensor exposure to low RH ranges and high and low AT ranges. However, this model could be used for soil flux chambers that involve daily field campaigns in order to be easily replaced or calibrated after the field measurement, within a temperature and relative humidity range equal to 15-27°C and 40-100%RH. It was observed, indeed, that this sensor can measure CO_2 increasing concentrations, over the range 0-3000 ppm, with a good correlation with respect to the reference value (Figure 2.1, Table 2.6), accuracy compliant to the manufacturer tolerance, ± 50 ppm ± 3% of readings (Figure 2.2), and precision ranging between 2.05-18.30 ppm (Table 2.7). However, due to the sensor sensitivity to temperature (Table 2.8), special attention is needed to monitor the temperature inside the chamber headspace to avoid biased measurements.

2. CO2_M2. Concerning this model, it should be noted that readings were affected by outliers and out-of-scale values, probably due to the frequency of data logging. This sensor had a frequency of measurement equal to 20 Hz, while the data was logged at 1 Hz. The probability of having an outlier among the CO2_M2 dataset was higher than sensors with lower measurement frequencies. However, after averaging over 30 seconds and performing the outlier detection, the dataset still showed noisy values. IMV and linearity results point out this aspect, indeed this model shows the highest IMV over all the experimental trials (Table 2.5) and the higher RMSE error, equal to 164.95 ppm, in the linearity test (Figure 2.1). This model doesn't show any short- or long-term drift, anyway, the high sensitivity to relative humidity and temperature (Table 2.8, Figure 2.4) allow us to say that this model could not be suitable for the considered applications that involve field campaigns with climatic variations. Results suggest that these sensors should be used preferably for indoor measurements, at stable ambient temperature and relative humidity (25°C-50%RH). Under these conditions, over the range 0-3000 ppm, sensor accuracy is compliant to the manufacturer

tolerance, ±70 ppm ± 5% readings (Figure 2.2), and precision ranges between 8.00-17.13 ppm (Table 2.7).

3. CO2_M3. As pointed out for CO2_M1, long-term drift and temperature sensitivity test results (Figure 2.3) suggest that this sensor could not be suitable for storage flux estimation or soil flux chamber measurements to account for the spatial variability. These sensors, indeed, show a clear sensitivity to temperature, (Figure 2.4). This behaviour narrows the range of temperature which the sensor should be exposed to 15-27°C. However, in that temperature range, CO2_M3 could be used for daily measurement with soil flux chambers. Linearity test results (Table 2.6, Figure 2.1) suggests, indeed, that these sensors could follow the CO_2 increasing concentrations in the chamber headspace with the lowest RMSE error (11.67 ppm) with respect to the other tested models. It should be noted that the observed readings are compliant to the stated tolerance, ±50 ppm, only within the range 0-1000 ppm (Figure 2.2), with mean precision around ±1.00 ppm (Table 2.7). In addition, due to the sensor sensitivity to temperature (Table 2.8), special attention is needed to monitor the temperature inside the chamber headspace to avoid bias or drift in measurements.

4. CO2_M4. Long-term drift test results show that over 52 days CO2_M4 is not affected by any drift, hence could be used in the field for at least one month avoiding to be calibrated or replaced. Furthermore, sensitivity test results (Table 2.8, Figure 2.4) allow us to say that CO2_M4 could be exposed in the field over both a wider range of temperature and relative humidity (10-40 °C and 10-100%RH) and temperature and relative humidity variations, without bias in measurements. It follows that this model is suitable for long-term deployment applications such as storage flux estimation and soil chamber to measure the spatial variability. Over the tested range of CO_2 concentrations (0-3000 pmm), which included the expected storage measurement range, CO2_M4 showed the best precision (0.00 ppm), within the manufacturer stated tolerance range equal to ±30 ppm ±3% of readings (Table 2.7). Linearity results show that this sensor could follow the CO_2 increasing concentrations in the chamber headspace with a RMSE equal to 38.92 ppm (Table 2.6, Figure 2.1). Taken together these results suggest that this model could be suitable not only for short-term measurement such as daily soil chamber campaign, but also for long-term measurements, such as storage flux or soil chambers to account for the spatial variability.

Concerning the AT and RH models, linearity and precision test results suggest that these sensors could be used over the range 10-40 °C and 10-100%RH with a really good agreement between sensor readings and the reference value, (Figure 2.1, central and bottom row), high precision, and accuracy range equal to ±0.39°C and ±3.13%RH (Table 2.7). None of the tested models show a sensitivity to temperature or relative humidity, suggesting that they can be used in the field within the tested ranges, without any potential bias. However, these models were evaluated with the final aim to be used for storage estimation. Considering that this method involves long-term measurement, only RH_M2 and RH_M4 are suitable for measurement periods longer than two weeks, Figure 2.3. Furthermore the lower readings variation between units of the same model (i.e. IMV results, Table 2.5) provide further support for the hypothesis that AT/RH_M2 and AT/RH_M4 could be used as an array of sensors, to measure AT and RH absolute values at each storage profile sampling point.

2.5 Conclusions

This work evaluated the performance of a set of 4 low-cost NDIR CO_2 sensor models and 4 low-cost thermo-hygrometers models to explore their potential use with soil chambers and eddy covariance method for storage estimations. It should be highlighted that tests were not carried out in a certified laboratory and results are not a quantitative evaluation but a general sensor performance evaluation to define which sensor could be suitable for the considered applications. Three out of four CO_2 models could be used for daily measurement with soil chambers, but special attention is needed to monitor the temperature range of exposure and the data quality. One out of four CO_2 models could be suitable for long-term measurement with soil-chamber methods to account for the soil flux spatial variability and with eddy covariance techniques for storage estimations. All four low-cost thermo-hygrometer models could be used for short-term measurements but only two out of four models could be suitable for the long-term deployment needed for storage measurement. Laboratory results show that significant variations in sensor performance exist, especially between CO_2 models and also between units of the same model. The most relevant observed drawback is related to the humidity and temperature sensitivity among the majority of CO_2 models. The temperature and humidity sensitivity is a common LCS issue and it was pointed out also in other studies (Castell et al, 2016; Lewis and Edwards, 2016; Arzoumanian et al., 2019; Martin et al, 2017). As example, Lewis and Edwards (2016) mentioned that LCS sensors' readings are subject to interference from prevailing meteorological conditions. However it was found that temperature and humidity correction models can improve the data quality (Arzoumanian et al, 2019; Eugster and Kling, 2012; Martin et al, 2017). Another option to avoid the temperature and humidity interference could be to set up technical arrangements, such as sensor thermal insulation or air desiccation systems. However these technical improvements increase the overall cost and the ease to deploy and use which are the major advantages of LCS sensors.

Despite the highlighted limitations and the need to check the data quality, the lower cost and high portability of these sensors could be an opportunity to overcome the main drawback related to soil chambers, of capturing the spatial heterogeneity of CO_2 fluxes, or to replicate heavier, more expensive eddy covariance sensing systems to measure the storage flux.

Low-cost sensing technology is evolving quickly. The availability of low-cost sensors with better performances will be key for researchers to continue testing the new technologies. Structurate information regarding the sensor performance over different ranges of environmental conditions could lead to better defining the limits of application of these sensors and to develop protocols to monitor the data quality.

In order to validate the laboratory results, and provide further information on the outdoor performance, the sensors have been tested in the field, as described in the following Chapters.

3 Low-cost system approach to measure CO_2 storage fluxes

3.1 Introduction

Net ecosystem exchange (NEE) is a measure of the net carbon exchange of CO_2 between a given ecosystem and the atmosphere, resulting from a balance between the CO_2 taken up via the photosynthesis process and that emitted during respiratory processes of the different ecosystem's components (soil, roots, leaves, branches, fauna) (Baldocchi, 2003; Chapin et al., 2006). By convention, emissions (from ecosystem to atmosphere) are indicated as positive fluxes, and uptake (from atmosphere to ecosystem) are considered negative, so if the NEE is negative the ecosystem under study is a sink of CO_2 and, vice versa, it is a source when NEE is positive (Chapin et al., 2006). It follows that NEE is a primary estimate of ecosystem carbon sink or source strength (Kramer et al., 2002).

One of the common methods used to measure the NEE is the eddy covariance (EC) technique. EC ascertains the CO_2 NEE across the interface between the atmosphere and a plant canopy by measuring the covariance between fluctuations in vertical wind velocity, measured by using a sonic anemometer, and CO_2 mixing ratio, measured using a dedicated gas analyzer (GA) over the control volume representative of the ecosystem (Baldocchi, 2003). NEE related to the scalar of interest (s) is given by (Aubinet et al, 2012; Foken et al, 2006; Rebmann et al, 2018):

$$NEE = \frac{1}{V_m}\overline{w'\chi'_s} + \int_0^z \frac{1}{V_m}\frac{\delta\overline{\chi_s}(z)}{\delta t}\,dz + \int_0^z \frac{1}{V_m}\overline{w}(z)\frac{\delta\overline{\chi_s}(z)}{\delta z}dz + \int_0^z \frac{1}{V_m}\left(\overline{u}(z)\frac{\delta\overline{\chi_s}(z)}{\delta x} + \overline{v}(z)\frac{\delta\overline{\chi_s}(z)}{\delta y}\right)dz \tag{3.1}$$

Where V_m is the molar volume of dry air ($m^3\ mol^{-1}$), t the time (s), u,v and w represent the wind velocity components in the horizontal (x,y) and vertical (z) directions and χ_s is the scalar concentration (expressed as mixing ratio, mol mol^{-1}).

The first term of the Equation (3.1) is the turbulent flux (Fc), the second term is the storage of the scalar of interest (S) in the control volume, the third and fourth term are the vertical and horizontal advection.

This method is based on the assumption of ideal conditions, such as strong turbulent mixing, horizontal homogeneity of surface (topography, surface roughness, canopy density, etc), and a flat terrain with an extended upwind distance, (Aubinet et al., 2012; Baldocchi, 2003).
The vertical and horizontal advection are currently neglected, especially due to technical problems related to the direct measurement (Aubinet and Feigenwinter, 2010), while the storage is often estimated, thus the Eq (3.1) can be simplified as:

$$NEE = Fc + S \qquad (3.2)$$

Under stable atmospheric conditions, when thermal stratification is strong and turbulence is low, typical at night, the non-turbulent fluxes become comparable or dominant with respect to Fc (Nicolini et al, 2018; Montagnani et al, 2018). To reach the best estimation of NEE it is crucial to measure S as accurately as possible, (Nicolini et al., 2018).
The EC system uses a single point of measurement, placed over the canopy, to measure Fc while S is measured using vertical concentration profile (Aubinet et al, 2012; Rebmann et al, 2018; Chapin et al, 2006).
To assess the S vertical profile, two approaches are mostly used: the single point (SP) and the multiple points (MP) approach. The SP approach makes use of the CO_2 dry molar fraction measured by the EC gas analyser, and then it assumes that the CO_2 profile is linear from the measurement point to the ground (Aubinet et la, 2012; Rebmann et al, 2018; Nicolini et al, 2018). For that reason, the SP is used not only in case of short canopies, where S fluxes are expected to be less relevant, but it can be found in other systems too when the budget availability is low (Aubinet et la, 2012; Papale et al, 2006). The MP approach instead consists of one or more CO_2 sensors installed in a vertical line, (Nicolini and Papale, 2017; Montagnani et al, 2018) used to calculate directly the vertical CO_2 profile (see Equation 1.5, Chapter 1). The MP approach is the more accurate (Nicolini et al, 2018), but its complexity and the number of sensors required sum up to an expensive setup, increasing with the height of the canopy (Al-Saidi et al, 2009). In addition to the gas analyzer, whose number depends on the configuration chosen (see section 3.2.1), some hardware installations are also needed to support the sensors, and a system of valves, tubes and pumps is often in place to switch the measurement from one level to the next one (depending on configuration and sensors type). In both the approaches, the measurement point(s) are paired with temperature (AT) and relative humidity (RH) sensors (e.g. thermo-hygrometers) used to collect auxiliary data. The number (n) of sampling points in the vertical profile depends on the EC measurement height, defined by (Nicolini and Papale, 2017):

$$n = \lfloor (h^a) \rfloor \qquad (3.3)$$

where h is the EC measurement height (m), $\lfloor \; \rfloor$ represents the rounding to the next integer and a is a default value equal to ⅔.

In the MP approach it is also possible to spread the sensor in the vertical plane, especially at the lower levels, to include the effect of spatial (horizontal) variability. This however requires an even higher number of sensors deployed, and a further increase in the costs. As example, for an EC measurement height of 35 m, 10 vertical sampling points are required and, concerning the horizontal sampling strategy, a minimum of 4 sampling points should be installed on a plane across the lowest level on the ground, and 2 at the second level, located around the tower, in a radius of minimum 5 meters, (Nicolini and Papale, 2017).

As the number of measurement levels in a profile increases, along both vertical and horizontal directions, the standard errors of S estimate decrease, (Nicolini et al., 2018; Yang et al, 1999). As a consequence, SP configuration not only sacrifices information on spatial variability but also leads to less accurate S measurements. The underestimation of NEE can be huge, by up to the same error magnitude as the night-time NEE (Gu et al., 2012; B. Yang et al., 2007).

In addition to the above, the CO_2 horizontal variability can be large under specific meteorological conditions even in homogeneous forests (Montagnani et al., 2018), especially at night, during calm wind and stable atmosphere, when the storage is mainly represented by a portion of the respiratory CO_2 from soil and plants trapped in the lowest profiles levels (Yang et al., 2007). Under these conditions even the additional horizontal sampling points located a few meters around the tower, could not be enough to properly represent the whole reference control volume. To better represent the CO_2 horizontal spatial variability some researchers suggest to use a ramified design of the lowest profile levels, or a 3D array of instruments (Van Gorsel et al, 2007; Marcolla et al, 2014). The ramified design proposed by Marcolla et al (2014) was made up by a single GA, 3 suction lines located at different heights and configured for 16 sampling points. This methods,despite improving the representativeness of the spatial variability, has showed to have some issues as eventually leakages (e.g. at the level of the manifold, connectors, etc) and some uncertainty due mainly to the discrete temporal sampling as a consequence of the impossibility to have synchronous observations from several sampling points with a single GA (Marcolla et al, 2014). The 3D array, on the other hand, requires a large number of instruments to deploy in fields (Gorsel, Leuning, Cleugh, Keith, & Suni, 2007). These approaches could be cost demanding, not so practical or easy to manage.

As an alternative to such complex and cost-demanding solutions, new low-cost tools and technologies to measure CO_2 concentrations, AT and RH available in the market could be considered to increase the number of sensors used and then the horizontal representativeness. Also, by using low cost sensors, the number of devices in the vertical line could be increased, for a better characterization of the concentration and temperature profile, and/or the number of profiles itself. Having a MP low-cost and easy to deploy equipment to measure the S fluxes could be an opportunity to improve the S measurements. These types of sensors, obviously, do not reach the high accuracy and precision as the traditional GA and thermo-hygrometers, but are up to 100 times less expensive, low powered and easy to deploy and the number increase of direct CO_2 measurements could compensate for the lower accuracy. In addition, they are shown to be good enough for some environmental applications, (Bastviken et al, 2015; Harmon et al., 2015; Martin et al., 2017).
This study presents a new multisampling system prototype (PT) to measure S, using small and easy to mènage low-cost sensors, substantially reducing costs for instruments and setup with respect to the systems currently used. Two experiments were carried out. The aim of the first experiment was comparing S measured by PT against a most accurate MP system and a SP system. The second experiment had the aim to evaluate if this new low-cost system was able to catch the S horizontal spatial variability. Using the prototype, a ramified design was built up mimicking the one suggested by Marcolla et al. (2014), made up of three horizontal transects, about 40 m long and 1.5 m high. S was measured along the horizontal transects and along the MP vertical profile lower levels and the two dataset compared.

3.2 Materials and methods

3.2.1 Low-cost system

Three different MP sampling configurations are currently used in ICOS to assess the S profile: the ‘separate sampling’ configuration, which provides for a dedicated GA at each sampling level, the ‘sequential scheme’ configuration, which is made up by a single GA used to sequentially sample all the levels, and the ‘simultaneous’ configuration, where a single GA is used for the whole sampling levels, (Nicolini and Papale, 2017). PT was developed following the ‘separate sampling’ scheme, which is the only configuration that has the advantage to sample all the profile levels continuously.

PT scheme was designed to replace the GA, AT and RH sensors at each level with a set of corresponding low-cost sensors.

According to the laboratory test results (see Chapter 2), CO_2 low-cost and low-power non dispersive infrared (NDIR) Engine K33-LP T/RH (K33) (0-5000 ppmv, 1/30 Hz) from SenseAir® (www.senseair.com), and the low-cost thermo-hygrometer Sensirion SHT11, (0-50°C/0-100% RH) which has the advantage to be equipped on board on the K33, have been chosen to develop the prototype. Since the K33 has a frequency of measurement equal to 1/30 Hz, a second CO_2 NDIR sensor from the same manufacturer, based on the same circuiting and sensing technology as K33, but with a higher measurement frequency, the Engine K30 FR (K30) (0-5000 ppmv, 1Hz) was added to made up the prototype. Sensors specifications are described in Table 3.1.

One K30 and one K33 have been positioned inside a sealed box (15x12x6 cm) equipped with a little fan to allow surrounding air to circulate inside the box, Figure 3.1. The choice of a fan rather than a sampling tube system with an external pump simplified the experimental design and avoided additional costs.

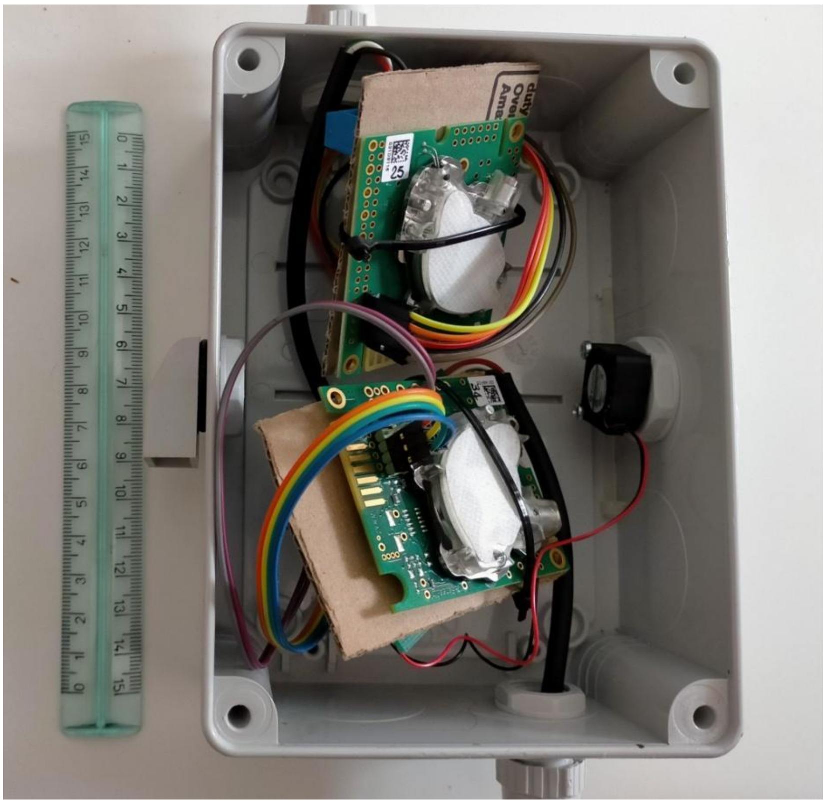

Figure 3.1. Prototype components of each box/measurement point: one NDIR CO2 Engine K33-LP T/RH (0-5000 ppmv, 1/30 Hz), one NDIR CO2 Engine K30 FR (0-5000 ppmv, 1Hz) from Senseair (www.senseair.com) and a little fan to allow air recirculation.

Boxes were connected to each other with a single cable that provided power (12 VDC) and data communication. A Raspberry Pi3B+ (Raspberry Pi Foundation, www.raspberrypi.org), a small (85x56mm^2) single-board computer, was programmed to read and collect data from all sensors and, using an Ethernet connection, sending the data directly to a server every 5 minutes.

The definitive prototype consisted in a multisampling low-cost system made up of two 'chains' of 7 and 6 boxes, respectively. Each chain was connected with its own microcontroller synchronized with each other using the Ethernet connection. The advantage of this configuration was that the sensors were easily replaceable in the event of a malfunction and that additional measuring points (boxes) could easily be added in the chain. This system produced continuous measurements from each sampling point with a frequency of 7s. To avoid any drift, sensors have been programmed to perform an automatic daily calibration at 400 ppm around the daytime when the greatest mixing in the atmosphere was expected. The assumption was that, at that time, the gas concentration along the vertical profile was equal to the mean atmospheric concentration, about 400 ppm.

Sensor model	Operating principle	Range of measurement	Power supply (V)	Resolution @full scale	Accuracy	Frequency of measurement (Hz)	Operating Range	Dimensions (mm - LxWx H)
SenseAir K30	NDIR	0-5000 (ppm)	4.5-14	/	±30 ppm ± 3% readings	1	0 to +50°C 0-95% RH	51 x 57 x 14
SenseAir K33	NDIR	0-5000 (ppm)	5-12	5 ppm	±30 ppm ± 3% readings	1/30	0 to +50°C 0-95% RH	51 x 57 x 12.5
Sensirion SHT11	CMOS/capacitive	0 to 50°C 0-100% RH	2.4 -5.5	0.01 °C 0.05 %RH	±0.4 °C ±3 %RH	1/30	-40 to 125 °C 0-100% RH	7.47 x 4.93 x 2.6

Table 3.1. Catalog specifications of low-cost sensors used to set up the prototype

3.2.2 Field measurements

Field measurements were carried out at the SMEAR II station, located in Hyytiälä, Southern Finland (latitude 61.84741 °N, longitude 24.29477 °E, 181 m asl), during June 2019. The terrain around the station is representative of the boreal coniferous forest, dominated by Scots pine (*Pinus sylvestris* L.) and Norway spruce (*Picea abies* (L.) H. Karst). It is homogenous for about 200 m in all directions, extending to the north for about 1.2 km. The terrain is subject to modest height variation, the annual mean temperature is 3.5° C and precipitation is 711 mm. The SMEAR II station includes a 72-meter high mast, used for collecting meteorological variables, gas concentrations and EC measurements, equipped with a SP and MP measurement system, part of the ICOS network.

SP is running at 27 m, using a LI-COR LI-7200RS gas analyzer (LI-COR, www.licor.com) to measure the eddy and the storage fluxes. Fluxes are calculated over a block averaging period of 30 minutes. MP uses the 'sequential sampling' configuration with a single gas analyser (Picarro, CRDS G1301). The storage profile has 13 sampling points over 9 levels. Each level is equipped with an air temperature/humidity sensor (Rotronic MP102H, www.rotronic.com). Air inlets, from level 1 to 7, are placed along the tower at 27, 21.6, 16.8, 12.5, 8.8, 5.8, 3.3 m from the ground, respectively. The 8th and 9th levels (1.5 and 0.5 m from the ground) have 2 and 4 measurement points, respectively, and are located within a 9 m radius of the mast. Total sampling points are 13. The whole profile cycle of MP measurements completes in 300 s, and GA measurement lasts about 33 s from each level. AT and RH measurements are collected every 30 minutes.

Figure 3.2. **Left panel:** Aerial image of the SMEAR II Forestry station and eddy covariance tower location (red square). **Right panel:** a perspective from the tower base.

3.2.3 Experimental Setup

The first experiment aimed at evaluating PT performances to estimate S against MP and SP approaches. In order to compare the data with MP, each PT box/sampling point was placed near each MP air inlet. One chain of boxes was positioned near the inlets along the tower (levels 1-7), the other one near the inlets above the ground (levels 8th and 9th), for a total of 13 measurement points: one for levels 1-7, two for level 8 and four for level 9, Figure 3.3. The tower was provided with both an Ethernet and a power connection to which microcontrollers were connected. Storage flux measurements lasted one week.

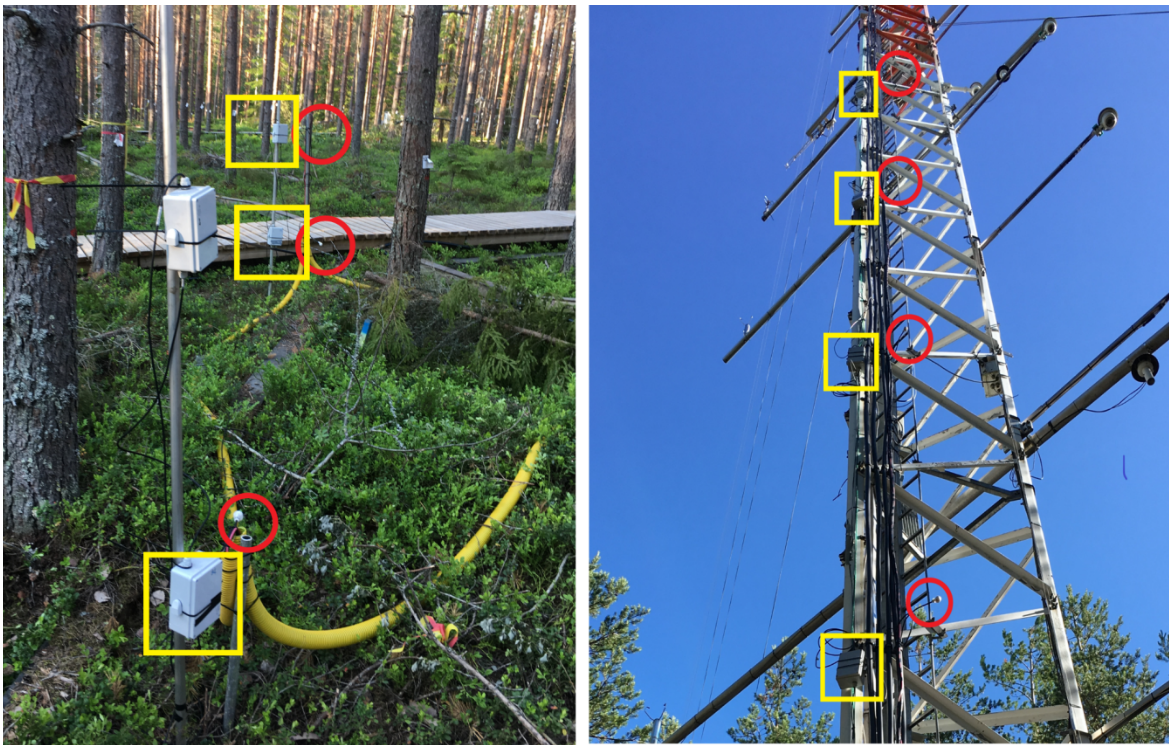

Figure 3.3. Prototype field set-up for storage measurement. The panel on the left shows the system set-up on the lowest profile levels, the panel on the right the system set-up along the EC tower. Red circles indicate the MP inlets and yellow squares the PT measurement points.

The aim of the second experiment was to evaluate if PT could be a useful system to catch the S horizontal spatial variability. Using a ramified design, similar to the one proposed by Marcolla et al (2014), an horizontal branching of the profile levels 8th and 9th was assembled and designed to have 6 sampling points, equipped with two measurement points located at 0.5 and 1.5 m from the ground, to coincide with the 8th and 9th level height of MP profile (Figure 3.4). Only one chain of sensors was used, adding the needed boxes to reach the needed sampling points. Using this set up, it was possible to have continuous measurements of CO_2, AT and RH from each measurement point with a frequency of 7 s. Before proceeding with the measurement along the transects, all the measurement points were left about 12 hours near the MP profile level 8th and 9th inlets (configuration T0). Subsequently, the horizontal branch, or transect, starting from the EC tower and about 40 m long, was directed along three different directions, 150 (T1 configuration), 240 (T2 configuration) and 300 (T3 configuration) °N, clockwise, at different times. The experiment lasted twelve days. The first four days the measurements were carried out along T1. The first sampling point was located 6.30 m from the tower, the distances between the others were 8.00, 6.80, 7.20, 7.80, 5.70 m, for a total length equal to 41.80 m from the tower. The following three days the measurements were carried out along T2. The first sampling point was located 5.90 m from the tower, the distances between the others were 7.10, 5.10, 6.60, 7.70, 6.50 m, for a length equal to 38.90 m from the tower. The last five days the measurements were carried out along T3. The first sampling point was located 7 m from the tower, the distances between the others were 6.10, 5.90, 8.00, 6.40, 5.90 m, for a length equal to 39.30 m from the tower.

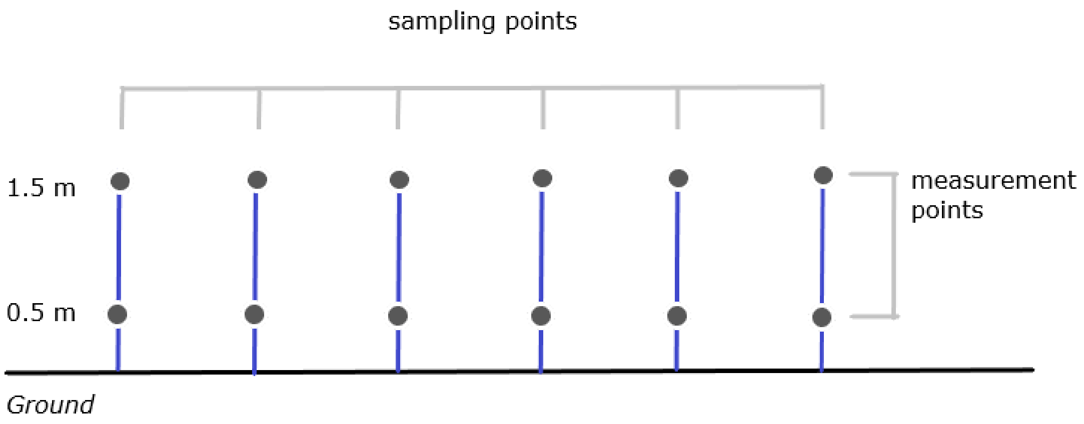

Figure 3.4. Schematic representation of each transect set-up. Each transect was equipped with six sampling points, each provided with two measurement points. Values on the left side indicate the measurement points distance from the ground which coincide with 8th and 9th levels height of MP profile.

3.2.4 Storage fluxes calculation

CO_2, AT and RH readings from PT were cleaned from anomalous data, discarding values out from the expected ranges equal to 350-600 ppm (see Chapter 1), 0-40 °C and 0-100% RH, and averaged over 30 seconds.

AT and RH dataset was used to convert the CO_2 concentrations from molar fraction to mixing ratio (see Chapter 1, section 1.1.1).

Half-hourly storage fluxes are estimated as the difference between instantaneous profiles of CO_2, at the beginning and end of the averaging period, divided by the averaging period, (Finnigan, 2006):

$$S = \overline{\rho_d}(z) \sum_{i=1}^{i=n} \frac{\Delta \bar{c}(z_i)}{\Delta t} \Delta z_i \qquad (3.4)$$

where n is the total number of profile levels, ρ_d is air molar density, Δc is the CO_2 dry molar fraction difference at height z_i over the time period Δt, Δz_i is the vertical extent of the corresponding i-th air layer.

Concerning the first experiment, storage fluxes from MP and PT, (hereinafter referred to as S_{MP} and S_{PT}) were computed using a half hourly averaging period (Δt) equal to 1800 s and vertical profiles with nine levels of measurements (n=9).

Half-hourly storage fluxes from SP (hereinafter referred to as S_{SP}) were assessed using the EddyPro® software (LI-COR,Inc., Lincoln, Nebraska, USA).

Concerning the second experiment, storage fluxes from transects and from MP profile 8th and 9th levels (n=2) were computed using half hourly (Δt = 1800 s) vertical profiles

To avoid concentration profiles were biased away from its mean over the control volume, (e.g by a single gust), in both the experiments, half hourly instantaneous profiles were replaced by averaged profiles over a time interval equal to 300 s and centered on the beginning and the end of the averaging period, (Finnigan, 2006).

3.2.5 Data analysis

3.2.5.1 First experiment: PT performance in storage estimation

To evaluate PT performances to measure the storage in comparison with MP the following statistical analysis were applied.

Ordinary least square regression was used to assess the correlation between storage fluxes. Results are presented with regression and correlation coefficients. The Bland&Altman plot (Bland & Altman, 1999) was used to quantify the effective agreement between methods of measurements. Difference between observations from two methods was plotted against the mean of the two. A systematic error (bias) was evaluated using a confidence interval estimated using the standard error of the difference mean between the paired measurements from the two methods. There will be a bias when the value zero will not lay within the interval. The range of agreement between the two methods, i.e. the confidence interval within which 95% of the differences between one method and the other are included, was estimated by the mean difference ±1.96 standard deviation of the difference, (Bland & Altman, 1999).

Since storage fluxes are expected to be not negligible during low turbulence, to investigate further systems performance, the datasets were analyzed also distinguishing between periods of low and high turbulence. The u* threshold criterion (u^{*crit}) was used at this scope, estimated to be equal to 0.33 m/s for the Hyytiälä site, to identify high ($u^* > u^{*crit}$) from low ($u^* <= u^{*crit}$) turbulence periods (see Chapter 1, section 1.1.1).

The above mentioned analysis was applied on the whole half-hourly storage flux datasets (S_{MP}, S_{PT}) and on the filtered records by $u^* > u^{*crit}$ (i.e. dataset records during high turbulence) and $u^* <= u^{*crit}$ (i.e. dataset records during low turbulence)

Both ordinary least square regression and Bland&Altman plot were performed on SP storage measurements against MP, on the whole half-hourly storage flux datasets (S_{MP}, S_{SP}) and on the filtered records by $u^* > u^{*crit}$ and $u^* <= u^{*crit}$. Results were used to contrast PT performance against SP performance.

After the performance analysis, the S_{PT} and S_{SP} uncertainty, with respect to S_{MP}, was assessed using the mean absolute error (MAE). To evaluate the errors under different conditions (daytime and nighttime) and levels of turbulences, the daytime and nighttime observations were binned by u* values, and the MAE over each bin was computed, using the following equation:

$$MAE = \frac{\sum_{1}^{N}|x_t - y_t|}{N} \quad (3.5)$$

where x_t and y_t are respectively, the reference (S_{MP}) and the estimated half hourly storage fluxes values (S_{PT} and S_{SP}) at time t.

To investigate how errors of low cost sensors impact the storage flux estimation, an error propagation analysis was performed. The absolute errors, between the concentrations measured by PT sensors and the concentrations measured by the MP system, at each storage profile level, were combined in *quadrature,* and propagated over all the computations used to calculate the final storage flux from PT.

3.2.5.2 Second experiment: storage spatial variability

To evaluate if PT could be a useful instrument to quantify the storage horizontal spatial variation, the following analysis were performed on the configuration (T0) and on each transect (T1,T2,T3). First of all, T0 configuration was used as a 'control' configuration, to check if storage fluxes from T0 were compliant with MP storage fluxes computed using the lowest profile levels (8th and 9th) (see section 3.2.4). Deviations between T0 sampling points and MP were analyzed and the mean storage flux along T0 was compared against the storage fluxes from MP using a linear regression. It

should be noted that, in the deviation analysis, values falling within the range of uncertainty calculated with the previous MAE analysis were discarded to have a more conservative approach.
The same deviation analysis applied on T0 was performed on T1, T2 and T3. Subsequently the mean storage flux along T1, T2 and T3 was compared against the storage fluxes from MP profile 8^{th} and 9^{th} levels. To investigate further systems performance, datasets were analyzed also distinguishing between periods of low and high turbulence. The u^{*crit} was used to identify high ($u^* > u^{*crit}$) from low ($u^* <= u^{*crit}$) turbulence periods (see Chapter 1). In order to exclude transition periods from low to high turbulence, during which storage "flush" may occur (Yang et al, 1999), not only half hours characterised by u^* values $> u^{*cri}$ were selected to identify windy events, but those when the previous half hour had $u^* <= u^{*cri}$ were excluded. Results are presented with scatter plots and correlation coefficients. Scatter plots illustrate the data distribution and the correlation coefficient (r) is used as estimator for the correlation between the two measurement system. A lack of correlation could be considered due to the spatial variability captured along the transects by the system of measurement.

3.3 Analysis Results

3.3.1 First experiment. PT performance in storage estimation

Regression results between S_{PT} and S_{MP} are presented graphically in Figure 3.5 (top row). Regression performed on the whole dataset (Figure 3.5, top row A1), on the dataset filtered by $u^* <= u^{*crit}$ (Figure 3.5, top row A2) and on the dataset filtered by $u^* > u^{*crit}$ (Figure 3.5, top row A3), showed respectively the following results: slope values were equal to 0.89, 0.93 and 0.82; intercept values to -0.02, 0.02 and -0.03 μmol $m^{-2}s^{-1}$; correlation coefficients to 0.85, 0.87, 0.81.
Regression results between S_{SP} and S_{MP} are presented graphically in Figure 3.5 (bottom row). Regression performed on the whole dataset (Figure 3.5, bottom row B1), on the dataset filtered by $u^* <= u^{*crit}$ (Figure 3.5, bottom row B2) and on the dataset filtered by $u^* > u^{*crit}$ (Figure 3.5, bottom row B3), showed respectively the following results: slope values were equal to 0.58, 0.37 and 0.93; intercept values to 0, 0.07 and 0.01 μmol $m^{-2}s^{-1}$; correlation coefficients to 0.77, 0.62, 0.96.
Results are collected in Table 3.2

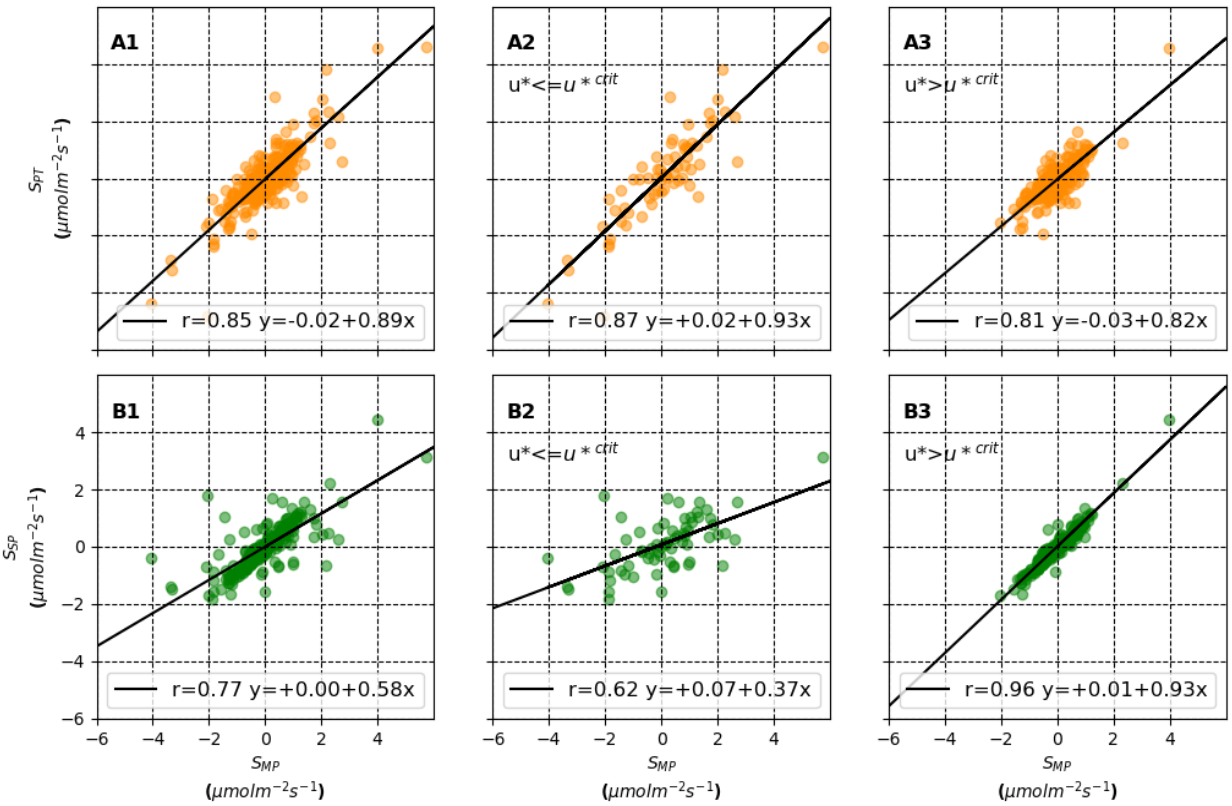

Figure 3.5 OLS regression analysis. Top row: scatter plots, fit lines (black) and regression equation between S_{PT} (y-axis) and S_{MP} (x-axis) for the dataset not filtered (A1), filtered by $u^{*}<=u^{*crit}$, (A2) and filtered by $u^{*}>u^{*crit}$ (A3). **Bottom row:** scatter plots, fit lines (black) and regression equation between S_{SP} (y-axis) and S_{MP} (x-axis) for the dataset not filtered (B1), filtered by $u^{*}<=u^{*crit}$, (B2) and filtered by $u^{*}>u^{*crit}$ (B3). The dotted red lines represent the 1:1 relation.

	S_{PT}			S_{SP}		
Dataset filter criterion	r	slope	intercept	r	slope	intercept
			$\mu mol\ m^{-2}s^{-1}$			$\mu mol\ m^{-2}s^{-1}$
none	0.85	0.89	-0.02	0.77	0.58	0.00
$u^{*}<= u^{*crit}$	0.87	0.93	0.02	0.62	0.37	0.07
$u^{*}<= u^{*crit}$	0.81	0.82	-0.03	0.96	0.93	0.01

Table 3.2 Regression analysis results between S_{PT} and S_{SP} against S_{MP}, for the storage flux dataset not filtered, filtered by $u^{*}<=u^{*crit}$, and filtered by $u^{*}>u^{*crit}$. The table indicates the correlation coefficient (r), the slope and the intercept values.

Analysis of the residuals was performed on regression results between S_{SP} against S_{MP} on the dataset not filtered (Figure 3.6, A1), filtered by $u^{*}<=u^{*crit}$ (Figure 3.6, A2) and on the dataset filtered by $u^{*}>u^{*crit}$ (Figure 3.6, A3). Histogram of residuals and the probability density function (PDF) showed that the distribution of errors was normally distributed.

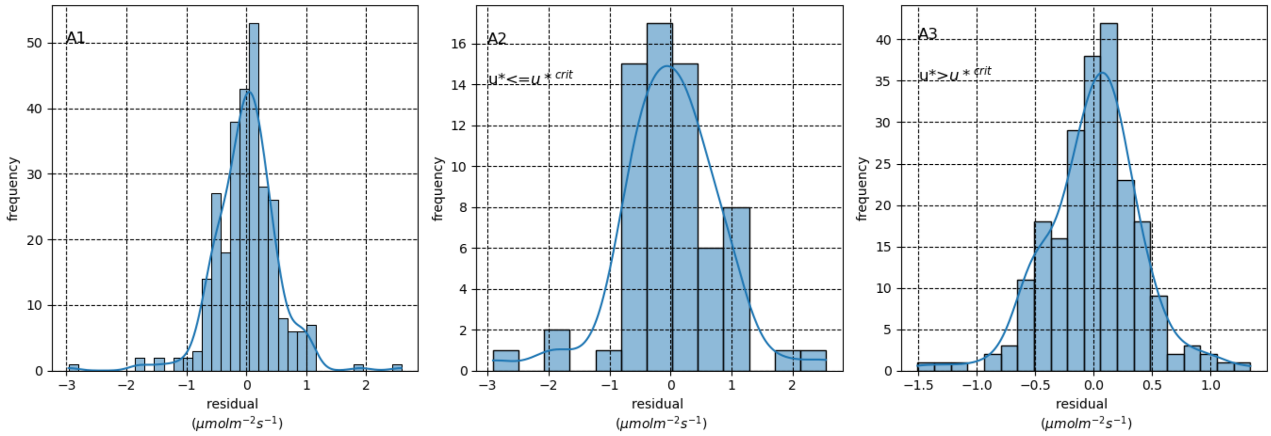

Figure 3.6 Residual histogram and PDF function. Residual histogram and PDF function (blu line), for the dataset not filtered (A1), filtered by $u^{*}<=u^{*crit}$, (A2) and filtered by $u^{*}>u^{*crit}$ (A3).

The Bland&Altman plots (Figure 3.7) were used to quantify the effective agreement between the two methods of measurement and represent the difference between half hourly storage fluxes measured by the two methods (y axis) plotted against the mean of the two (x axis). The confidence interval for the mean of differences gives indications of a systematic error (bias) while the confidence interval for the mean difference ±1.96 standard deviation (SD) of the difference, indicates the range of agreement between the two methods.

Bland&Altman plots between S_{PT} and S_{MP} are presented in Figure 3.7, top row. The range of agreement was equal to $-1.04<CI<1.07$ μmol $m^{-2}s^{-1}$ on the whole dataset (Figure 3.7, A1), to $-1.61<CI<1.59$ μmol $m^{-2}s^{-1}$ on the dataset filtered by $u^{*}<=u^{*crit}$ (Figure 3.7, A2) and to $-0.79<CI<0.84$ μmol $m^{-2}s^{-1}$ on the dataset filtered by $u^{*}>u^{*crit}$ (Figure 3.7, A3).

Bland Altman plots between S_{SP} and S_{MP} are presented in Figure 3.7, bottom row. The range of agreement was equal to $-1.20<CI<1.21$ μmol $m^{-2}s^{-1}$ on the whole dataset (Figure 3.7, B1), to $-2.42<CI<2.40$ μmol $m^{-2}s^{-1}$ on the dataset filtered by $u^{*}<=u^{*crit}$ (Figure 3.7, B2) and to $-0.38<CI<0.36$ μmol $m^{-2}s^{-1}$ on the dataset filtered by $u^{*}>u^{*crit}$ (Figure 3.7, B3), Confidence intervals for the mean of differences crossed the zero line in all the plots, so none of the methods analyzed showed a systematic bias.

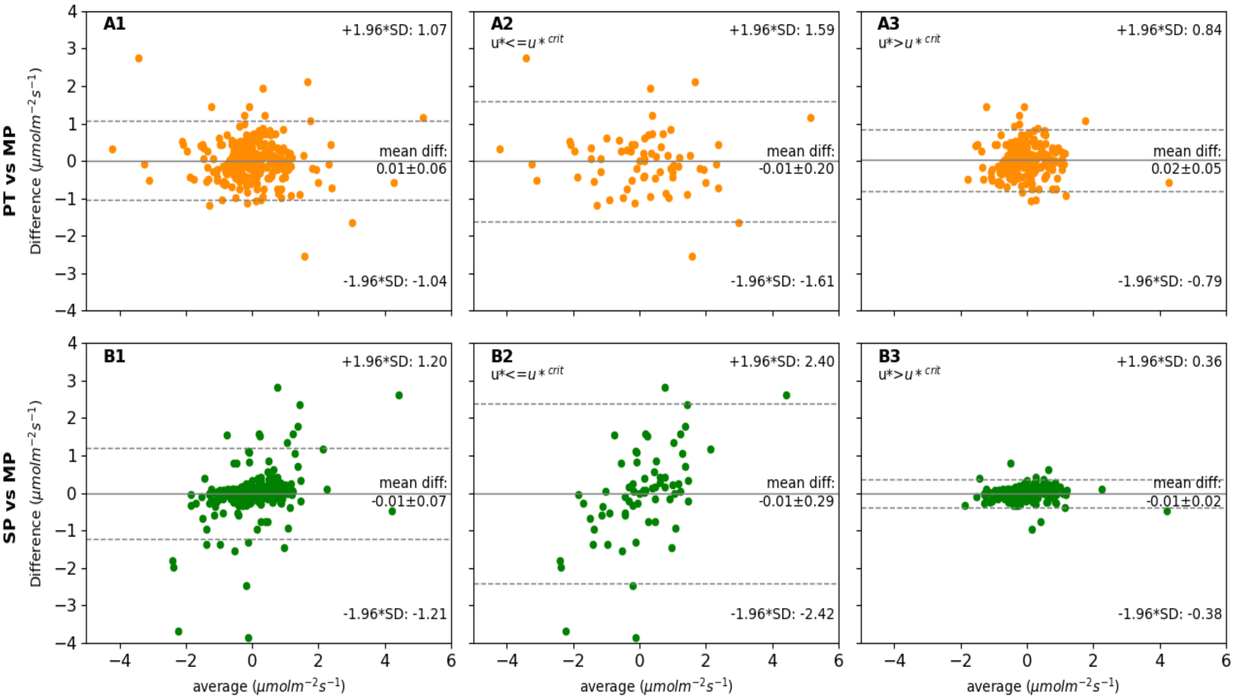

Fig 3.7 Bland Altman analysis. Top row: Bland&Altman plot between S_{PT} and S_{MP} for the dataset not filtered (A1), filtered by u*<=u*^{crit}, (A2) and filtered by u*>u*^{crit} (A3). **Bottom row:** Bland&Altman plot between S_{SP} and S_{MP} for the dataset not filtered (B1), filtered by u*<=u*^{crit}, (B2) and filtered by u*>u*^{crit} (B3). The dotted grey lines represent the limits of agreements alongside their values. Grey lines represent the mean for the differences, alongside with its value and confidence interval.

S_{PT} and S_{SP} uncertainty respect to S_{MP} is graphically shown in Figure 3.8 and presented as the mean absolute error within u* bins and evaluated for daytime and night-time observations. The black dotted line represents the mean storage flux measured by MP, related to the u* bins. Bin range was chosen to have the same number of observations inside each bin. During daytime (fig 3.8 left panel) the mean storage flux measured by MP was equal to 0.42 ±0.11 μmol m^{-2}s^{-1} and S_{PT} MAE spanned from 0.30 to 0.52 μmol m^{-2}s^{-1}, for a mean error equal to ±0.37 μmol m^{-2}s^{-1}, while S_{SP} MAE from 0.07 to 0.26 μmol m^{-2}s^{-1}, for a mean error equal to ±0.13 μmol m^{-2}s^{-1}. During night-time (fig 3.8 right panel) S_{PT} MAE spanned from 0.21 to 0.85 μmol m^{-2}s^{-1}, for a mean error equal to ±0.39 μmol m^{-2}s^{-1}, while S_{SP} MAE spanned from 0.10 to 1.46 μmol m^{-2}s^{-1}, for a mean error equal to ±0.42 μmol m^{-2}s^{-1}. Taking into account only the night-time low turbulence periods (u*<0.33 m/s), the S_{PT} mean error was equal to ±0.63 μmol m^{-2}s^{-1}, while the S_{SP} mean error to ±1.01 μmol m^{-2}s^{-1}. It should be noted that during night-time low turbulence periods the storage measured by MP was up to 3 times higher on average with respect to the daytime high and low turbulence period.

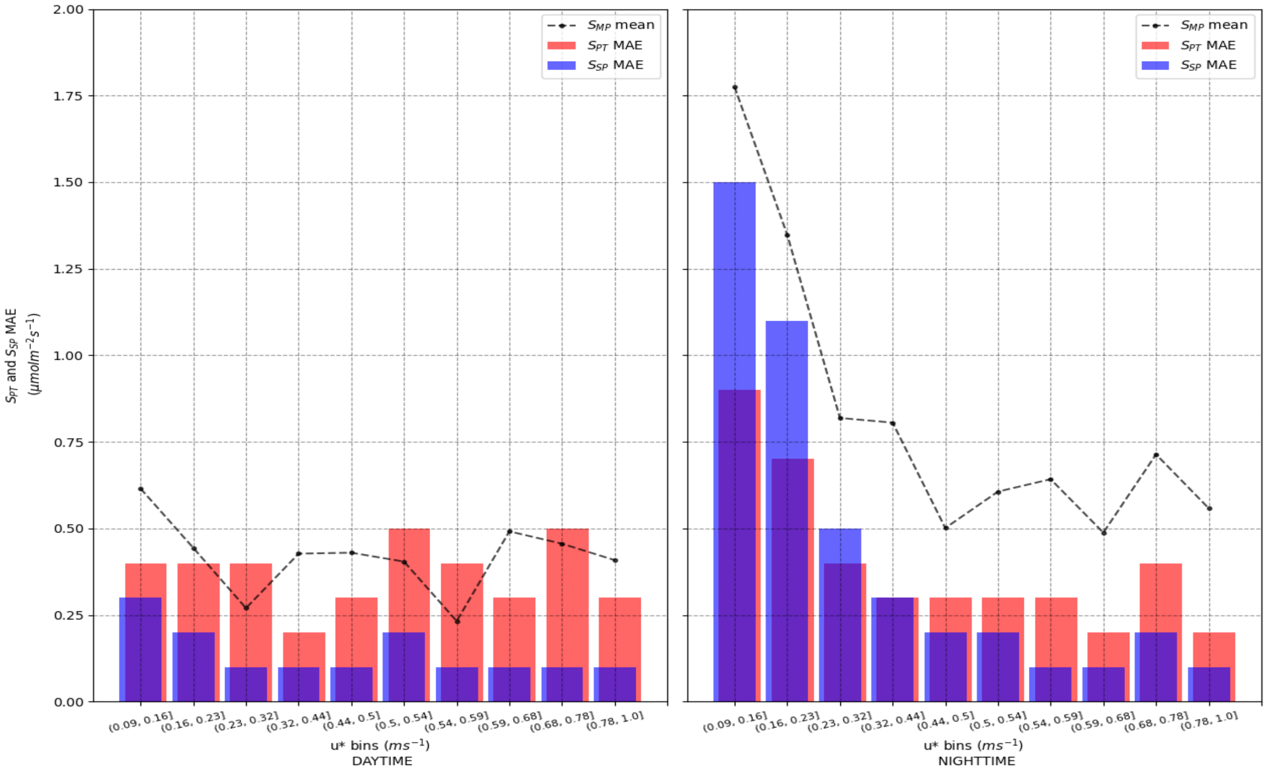

Figure 3.8. S_{PT} (red bars) and S_{SP} (blue bars) mean absolute error respect u* bins and evaluated for daytime (left panel) and night-time (right panel) observations. The black dotted line represent the S_{MP} mean flux respect the u* bins.

The error propagation analysis performed on each PT storage profile level led to the following results. The S_{PT} mean error related to the S_{MP} storage flux was equal to ±0.42 μmol $m^{-2}s^{-1}$, according to the MAE ranges assessed in the previous analysis. The percentage contribution of each PT profile level error on the S_{PT} mean error is shown in Table 3.3. Results suggest that the lower levels contributed in a minor way to the mean error, and data showed an increasing trend starting from the lowest level (9) to the highest (1). The trend is more evident in Figure 3.9, which represents the boxplots of percentage error that contribute to the mean error referred to each PT level.

S_{PT} Error (%)	PT Profile levels								
	1	2	3	4	5	6	7	8	9
mean	0.92	1.54	1.21	1.09	0.95	0.74	0.62	0.33	0.09
std	0.39	0.81	0.75	0.63	0.54	0.45	0.47	0.17	0.05

Table 3.3 S_{PT} error propagation analysis results. Results are presented as the percentage of error from each single profile level that contributes to S_{PT} mean error.

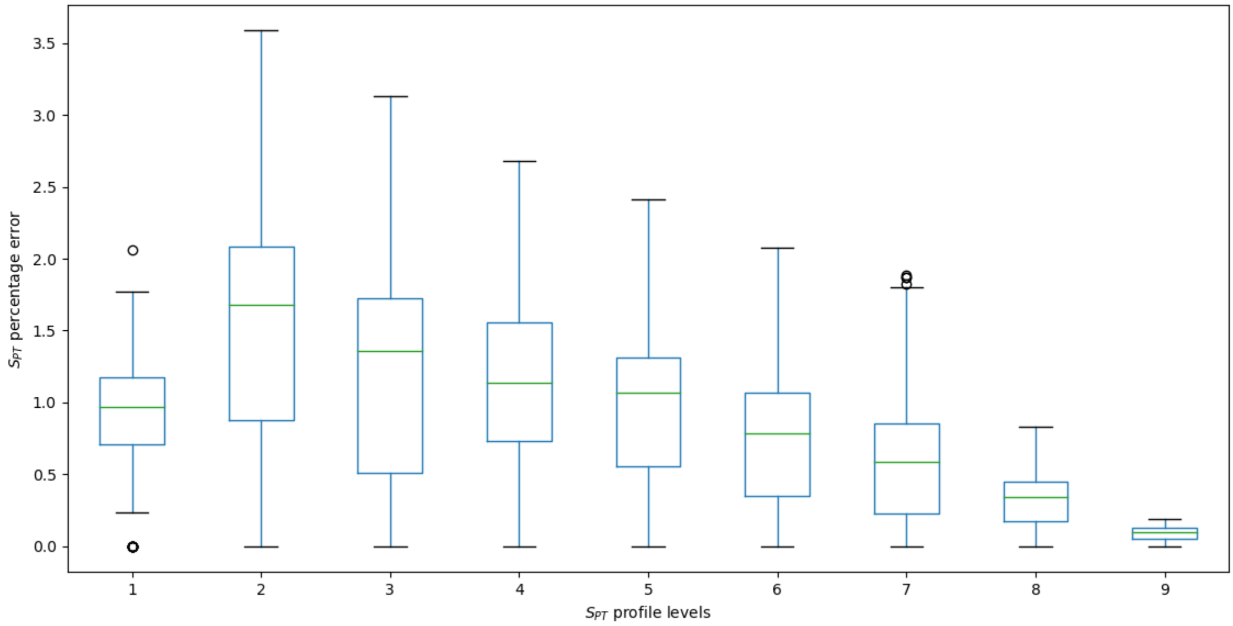

Figure 3.9 Comparison of S_{PT} error from each storage profile level. Boxplots indicate the range of percentage error from each single profile level that contributes to S_{PT} mean error. The green line indicates the median, the box the interquartile range and the blue lines extending above and below the box show the extent of the rest of the sample. Dots represent the outliers.

3.3.2 Second experiment. Storage spatial variability

In order to assess if the low cost system was able to catch the storage spatial variability, 4 configurations (T0, T1, T2, T3) were set up using the PT low-cost system. The T0 configuration was used as a 'control' configuration. Each PT sampling point was placed for 12 hours near the MP profile 8th and 9th level inlets. Half hourly storage fluxes were computed over each T0 sampling point and over MP profile 8th and 9th levels ($S_{MP(8\text{-}9)}$). Deviations between these fluxes were analyzed. None of the T0 sampling points showed a significant deviation from MP (results not shown). Fluxes from each PT measurement point were averaged and the mean flux (S_{T0mean}) was compared with $S_{MP(8\text{-}9)}$. The correlation coefficient r, resulting from the regression analysis between S_{T0mean} and $S_{MP(8\text{-}9)}$ was equal to 0.95, with slope equal to 0.94, Figure 3.10. These results showed a high correlation between the two measurement systems, and fluxes measured by T0 were considered compliant with MP.

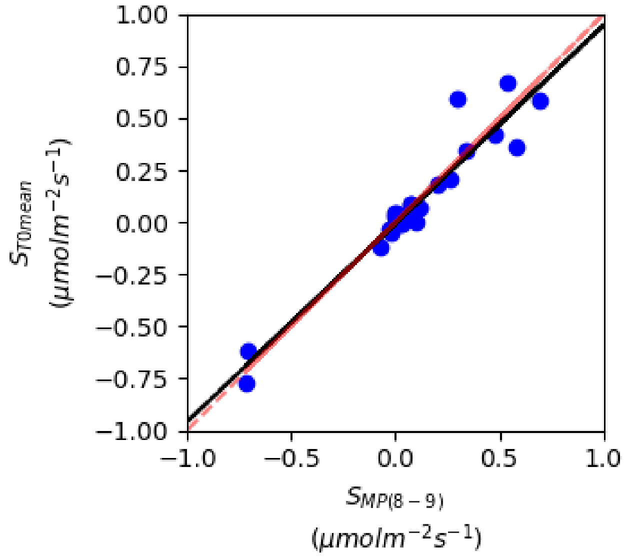

Figure 3.10. Scatter plot between the half-hourly mean storage fluxes from T0 configuration (S_{T0mean}) against the storage flux from MP (level 8 and 9), ($S_{MP(8\text{-}9)}$), with fit line (black) and the 1:1 relation line (red)

T1, T2 and T3 configuration, i.e. three horizontal branching of the MP profile levels 8th and 9th, about 40 m long, were directed along three different directions starting from the MP location. Each transect was designed to have six sampling points, (see section 3.2.3 and Figure 3.4). Half hourly storage fluxes were computed over each sampling point. These fluxes were compared with half-hourly storage fluxes from MP profile 8th and 9th levels ($S_{MP(8\text{-}9)}$). T1, T2 and T3 deviations from MP, are presented in Figure 3.11. In order to have a more conservative approach, deviation values lower than the night-time MAE computed in the uncertainty analysis (section 3.3.1, Figure 3.8), equal to ±0.63 µmol m^{-2}s^{-}1, were discarded. Deviations, observed especially during night-time, ranged between -2.00 and 1.19, -1.49 and 1.03, -1.32 and 1.79 µmol m^{-2} s^{-1}, for T1, T2 and T3, respectively.

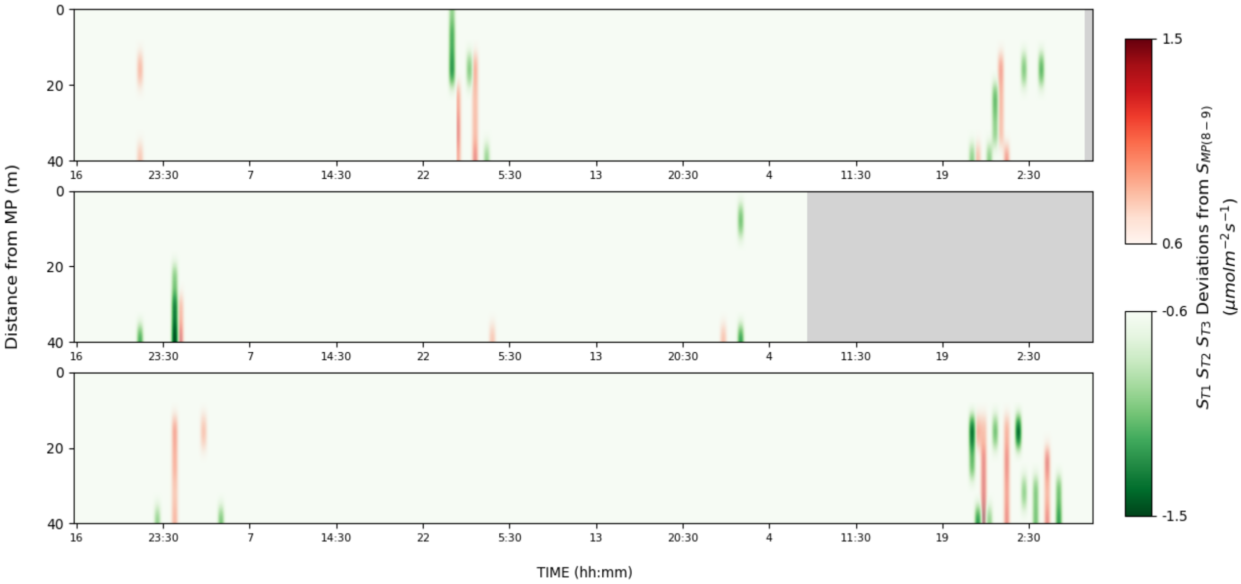

Figure 3.11. Time series of deviations between half-hourly storage flux from MP profile 8th and 9th levels and half-hourly storage flux from each transect sampling point, (T1: top panel, T2: central panel, T3: bottom panel). The y axis represents the distance between each sampling point along the transects and the MP system, located on the EC tower.

Secondly, fluxes from sampling points were averaged to obtain the mean flux along each transect, (S_{T1mean} - S_{T2mean} - S_{T3mean}). Mean fluxes were compared with $S_{MP(8-9)}$.$S_{T1\ mean}$, $S_{T2\ mean}$ and S_{T3mean} were compared against the $S_{MP(8-9)}$ distinguishing between periods of low turbulence ($u^*<=u^{*crit}$) and well mixed periods, i.e. half hours characterised by u* values > u^{*crit} were selected but those when the previous half hour had $u^*<=u^{*cri}$ were discarded (see section 3.2.5.2). Scatter plots are presented in Figure 3.12.

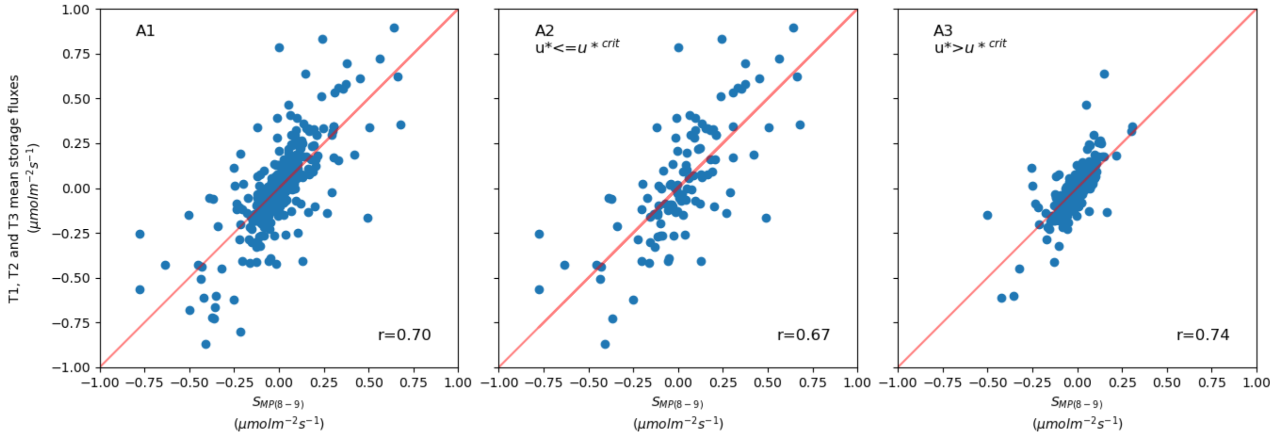

Figure 3.12 A1: Scatter plots between the mean storage flux along all the transect ($S_{T1\ mean}$, $S_{T2\ mean}$ and S_{T3mean}) against the storage flux from MP profile 8th and 9th levels, ($S_{MP(8-9)}$), with the 1:1 relation line (red). **A2:** Scatter plots between the mean storage flux along all the transect ($S_{T1\ mean}$, $S_{T2\ mean}$ and S_{T3mean}) against the storage flux from MP profile 8th and 9th levels, ($S_{MP(8-9)}$) during low turbulence periods ($u^*<=u^{*crit}$), with the 1:1 relation line (red). **A3:** Scatter plots between the mean storage flux along all the transect ($S_{T1\ mean}$, $S_{T2\ mean}$ and S_{T3mean}) against the storage flux from MP profile 8th and 9th levels, ($S_{MP(8-9)}$) during well mixed conditions (see section 3.2.5.2), with the 1:1 relation line (red).

Scatter plots highlight that the correlation between the transect datasets and MP is equal to 0.70,(Figure 3.12, A1). During well mixed periods, (Figure 3.12, A3), the correlation coefficient increased up to 0.74, and decreased during low turbulence periods (Figure 3.12, A2), upl to 0.64. Results suggest that the lack of correlation between the transect datasets and MP is mainly due to the storage fluxes that occurred during low turbulence (low u* values).

3.4 Discussion

In this paper a new low-cost approach was introduced to measure S fluxes and improve their spatial representativeness. A multisampling system (PT) was developed and equipped with CO_2, T and RH low-cost sensors for continuous data measurement. Field tests were carried out at the SMEAR II station, (Hyytiälä, Southern Finland).

The first experiment had the final aim to evaluate the PT performance against a most accurate MP system and against the SP system, both using high precision gas analyzers. Technically speaking, the use of PT led to several benefits: the system was easy to deploy, minimizing the impact on the environments monitored. A simple infrastructure is necessary for its deployment in view of its small size and weight. The system design allowed us to consider each PT measurement point as an individual unit, easy to replace in case of sensor malfunctioning. In addition, the whole system needed a low power supply to work (12V). The continuous measurements were logged to a server, using an Ethernet connection, and remotely monitored.

PT performance analysis compared to the standard system, i.e. the multipoint approach (MP), highlighted that the low cost approach can't reach the accuracy of a MP system. Half-hourly storage fluxes were underestimated by 11%, with an uncertainty range between -1.04 and 1.07 $\mu mol\ m^{-2}s^{-1}$, (Figure 3.5, A1 – Figure 3.7, A1). However, the most significant observation emerges in comparing PT against SP performance. From the data analysis, the SP underestimation of storage fluxes with respect to MP was equal to 42%, and the uncertainty range between -1.21 and 1.20 $\mu mol\ m^{-2}s^{-1}$, (Figure 3.5, B1 – Figure 3.7, B1). SP underestimation was 4 times greater than the PT underestimation, with an uncertainty greater about 10%. These results are due mainly to PT and SP performance in fluxes estimations during low turbulence, shown by the regression analysis (Figure 3.5, A2 – Figure 3.5, B2). The underestimation shown by SP was equal to 63% with an uncertainty range between -2.42 and 2.40 $\mu mol\ m^{-2}\ s^{-}1$. On the other hand, the underestimation shown by PT was equal to 7% with an uncertainty range between -1.61 and 1.59 $\mu mol\ m^{-2}s^{-1}$. Taken together these results suggest that with respect to measuring S by SP, using PT during low turbulence, involved a reduction in the uncertainty of about ± 0.8 $\mu mol\ m^{-2}s^{-1}$.

Anyway it should be noted that during high turbulence, PT showed a decreasing performance. The underestimation showed by PT was equal to 18% and the uncertainty range between -0.79 and 0.84 $\mu mol\ m^{-2}s^{-1}$, while the underestimation showed by SP was equal to 7% and the uncertainty range between -0.38 and 0.36 $\mu mol\ m^{-2}s^{-1}$, (Figure 3.5- A2/B2, Figure 3.7 A2/B2). These results were expected and due mainly to two aspects. Firstly, during high turbulence the storage flux is expected low, and the air mixing leads to a linear profile, i.e. the gas concentration is similar over all the profile measurement levels. Under these conditions, the SP approach, using a high precision gas analyzer, is more representative of the linear profile from the measurement point to the ground. Secondly, the mean standard deviation of half hourly concentration difference, used to assess storage fluxes during high turbulence, was equal to ±1.50 ppm. The low-cost CO_2 sensors, with resolution, equal to 5 ppm, and accuracy, equal to ±30 ppm ±3% of readings (Table 3.1), were not able to catch these variations.

The error propagation analysis pointed out this aspect. The error contribution of each single level (i.e. sensor) to the PT storage flux mean error with respect to MP could be related to the half hourly concentration difference magnitude, lower in the higher levels and higher in the lower profile levels, Figure 3.13. Comparing the error propagation results from each level (Figure 3.9) with the magnitude of the half hourly concentration measured by the MP system (Figure 3.13), it's possible to speculate that the two quantities were inversely proportional.

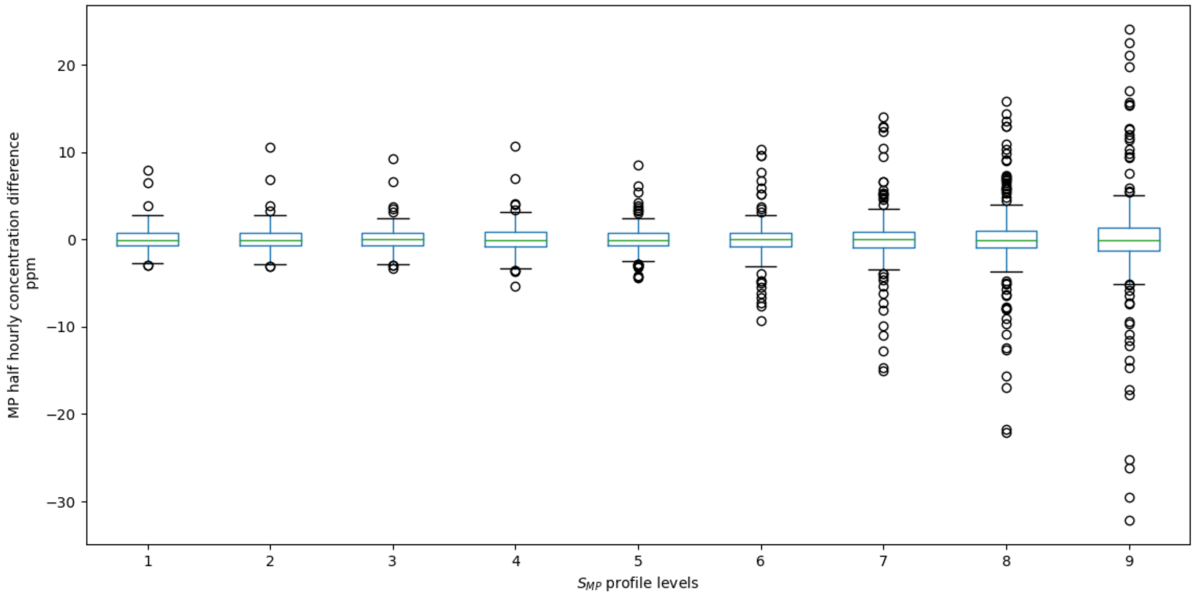

Figure 3.13 MP half hourly concentration difference from each storage profile level. The green line indicates the median, the box the interquartile range and the blue lines extending above and below the box show the extent of the rest of the sample. Dots represent the outliers.

It follows that PT uncertainty was mainly related to the magnitude of concentrations measured by the system and consequently to the storage fluxes magnitude: during high turbulence, the error in storage estimation was up to the same magnitude of the storage flux measured by MP (Figure 3.8, left side). During nocturnal low turbulence, when the storage flux increased over ±0.80 µmol $m^{-2}s^{-1}$, the PT error in storage estimation, decreased up to 50% of the magnitude of the storage flux measured by MP, lower with respect to the SP approach (Figure 3.8, right side).

It is possible to speculate that this promising low cost system could be a suitable tool especially in ecosystems with tall canopies where the storage flux is expected to be high, such as, but not limited to, tropical forest (-12 to 7 µmol $m^{-2}s^{-1}$) or Mediterranean forests (±3 µmol $m^{-2}s^{-1}$) (Montagnani et al, 2018). In order to overcome the uncertainty shown during low turbulence in measuring the lower storage fluxes, PT could be used in conjunction with the SP approach. As a consequence, increasing

the number of sampling points along the vertical profile could lead to a more accurate storage estimation with respect to using the only SP approach.
The second experiment had the aim to evaluate if this new measurement system was able to capture the S horizontal spatial representativeness. A 'control' configuration (T0) was set up before realizing three horizontal branchings, (T1, T2 and T3 configurations), of the MP profile levels 8^{th} and 9^{th}. Set up of the low-cost system led to the same technical benefits of the first experiment.
The 'control' configuration, compared with MP, showed a good correlation between the two measurement systems in storage estimations, (Figure 3.10). On the other hand, analysis results on T1, T2 and T3 configurations revealed that, especially during night-time, the low-cost system measured a storage difference along the transects with respect to the 8 and 9 levels of MP profile (Figure 3.11). In addition, the comparison between the mean storage fluxes measured along the transects and along the (8^{th} and 9^{th}) levels of MP profile, highlighted that, with respect to the 'control configuration' the correlation between the two measurement systems decreased from 0.95 to 0.70 (Figure 3.12-A1). The major lack of correlation occurred especially during low turbulence periods (Figure 3.12-A2). The difference from the MP standard system could be related to horizontal non-homogeneity of the subcanopy space. If the supposition is correct, the PT system set-up could be a useful tool to catch the horizontal storage spatial variability. On the other hand, it should be noted that measurements along the transects were not carried out alongside a reference system, and it's impossible to exclude *'a priori'* that difference could be related to a PT system measurement error.

3.5 Conclusions

In this study the performance of a low-cost approach based on small, low-cost sensors, to measure storage fluxes and its potential to catch the storage spatial variability have been evaluated. The system has proven to have advantages such as limitations. Experiment results suggest that the low cost system can't reach the accuracy of MP, or the accuracy of SP during high turbulence to estimate the storage fluxes. However the low-cost system has proven to be an efficient tool during low turbulence, leading to more accurate storage estimates with respect to the SP approach. It could be used in conjunction with the SP approach to increase the storage estimations, allowing the spread of sampling points along the vertical profile or inside the ecosystem. It could be suitable to set up a sensor network, e.g. multiple profiles, to account for the storage spatial variability, especially in ecosystems characterized by heterogeneous surfaces, different local emissions or canopy closure, where the spatial variability is expected to be high, e.g. tropical forests. These ecosystems play a key role in the carbon cycle, and there is a need for structured data on gas exchange over these areas. However the majority of the area covered by tropical forest belongs to developing countries which cannot invest in costly sensing systems such as EC equipment. The lower cost, the lower power consumption and the high portability of these sensors could be an opportunity to replicate heavier, more expensive sensing systems to measure the storage fluxes. Currently, to our knowledge, this is the first study on low-cost sensors used for storage flux measurements, so it's impossible to compare results with other researchers. However many studies on low-cost sensor networks to monitor the air quality are available (Castell et al, 2016; Lewis and Edwards, 2016; Arzoumanian et al., 2019; Martin et al, 2017). These works highlight the need to account for LCS temperature and relative humidity sensitivity and to check for the data quality. Structurate information regarding the low-cost sensor performance to measure storage fluxes over different ranges of environmental conditions can be useful to compare the results, validate the robustness of data quality and better define the range of application. For example, in this study the low-cost system was tested for one month, and future works could evaluate the sensor performance over longer periods, of the order of six months to a few years, or apply temperature and humidity correction models to sensor readings, or procedure of sensor cross-comparison or cross-correction during different meteorological conditions (i.e. high wind conditions), with the aim of improving the accuracy of measurements. In addition, in order to compare and validate the experimental results concerning the horizontal storage variability, future field tests could be performed with the set-up suggested in this study, alongside with a reference instrumentation.

In addition, low-cost sensors are currently available on the market not only for CO_2 concentration measurements, but also for other greenhouse gases. The growth of new technologies and improvement in sensor performance could also open supplementary paths toward the applications of these tools to estimate other GHGs, such as CH_4 and N_2O, that require a more expensive and higher precision sensing system than CO_2 measurements, due to their characteristic pattern of emission.

4 Potentiality of Low-cost approach for measuring CO_2 soil fluxes

4.1. Introduction

Automated and manually closed chambers are the most common approach for CO_2 soil fluxes measurements (Livingston & Hutchinson 1995; Rochette and Hutchinson, 2005; Butterbach-Bahl et al., 2016). The first is made up of a chamber connected to a gas analyzer which cyclically measures the gas concentrations in the chamber headspace (Rochette & Hutchinson, 2005; Butterbach-Bahl et al., 2016). The latter consist in a closed chamber placed in the field and gas samples are collected manually during an enclosure period, and subsequently analyzed by gas chromatography (Rochette and Hutchinson, 2005). The rate of CO_2 change over time, inside the chamber, is used to calculate the flux, (Davidson et al., 2002), using the following general equation (Rochette and Hutchinson, 2005):

$$Fc = \partial C/\partial t \left(\frac{V}{A} \right)/Mv \qquad (4.1)$$

where, $\partial C/\partial t$ is the CO_2 rate of accumulation (μmol mol^{-1} s^{-1}), V/A the chamber volume/area ratio and Mv the molar volume of air at chamber air temperature and pressure (m^{3}mol^{-1}).

To obtain reliable estimations of fluxes and to account the soil respiration spatial variability, many researchers recommend to use short-term deployments with several samplings during each deployment (e.g., sampling every fifth minute for 30 min) and to perform repeated deployments integrated over time and space, (Rochette & Hutchinson, 2005). Therefore, measurements accounting for spatial variability tend to be laborious if relying on manual sampling or costly in terms of equipment if automated chamber systems are used. At the same time, chamber measurements are often the only option because the requirements (in terms of topography, homogeneity etc.) are minimal.

Currently low-cost sensors (LCS) are available to measure CO_2 concentrations. These types of sensors, obviously, do not reach the high accuracy and precision as the traditional gas analyzer, but are several-times less expensive, low powered and easy to deploy. In addition, low-cost sensors are shown to be good enough for some environmental applications, (Harmon et al., 2015; Martin et al., 2017). Having a low-cost and easy to deploy equipment to measure the soil fluxes could be an opportunity to improve spatial accuracy of measurements.

A portable prototype to measure CO_2 concentration was developed using low-cost sensors, and it has been only tested in one single application to explore sensor potential use for soil flux measurements.

4.2 Prototype and test

A CO_2 NDIR model was used to set up the prototype.The IRC-A1 (0-5000 ppm, 1Hz, www.alphasense.com) from Alphasense®, was selected according to the laboratory test results described in Chapter 2. This model, indeed, showed the best performance in measuring the CO_2 increasing concentrations, (see Chapter 2, section 2.3.2). In addition, this sensor is equipped with a transmitter board, provided with a MINI USB socket that allows data communication using a simple USB cable. Sensors specifications are described in Table 4.1.

A Raspberry Pi3B+ (Raspberry Pi Foundation, www.raspberrypi.org), a small (85x56mm^2) single-board computer, was programmed to read data from the sensors to and log the measures on an SD memory card. Sensors and microcontroller were powered using a 12V battery.

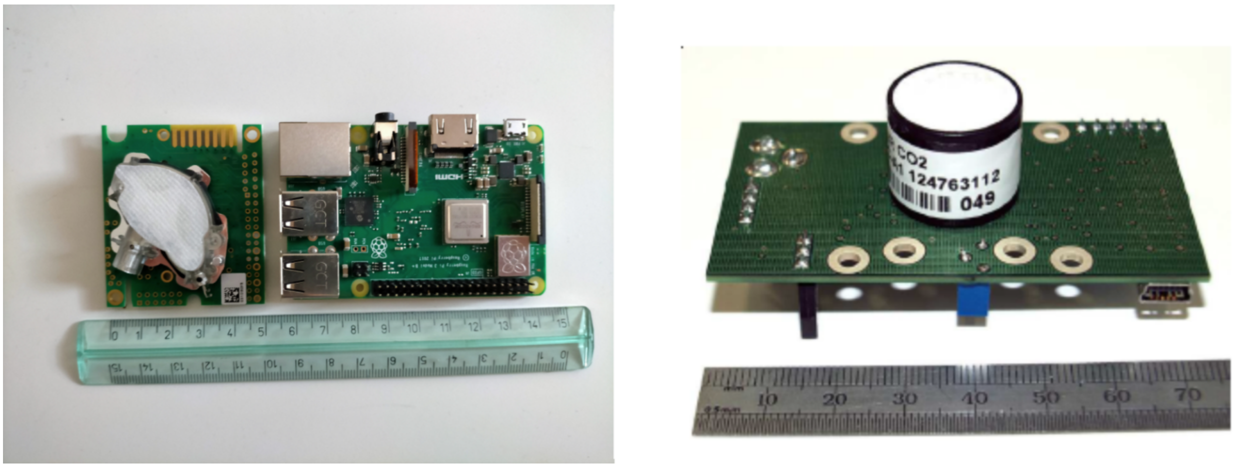

Figure 4.1 Left panel: NDIR CO_2 sensor Engine K30 FR by SenseAir (0-5000 ppm, 1Hz, www.senseair.com) and the microcontroller Raspberry Pi3B+ (Raspberry Pi Foundation, www.raspberrypi.org). **Right panel:** NDIR CO_2 sensor IRC-A1 with transmitter board by Alphasense (0-5000 ppm, 1Hz, www.alphasense.com)

Sensor dimensions allowed the use of the sensors directly inside the chamber headspace. However in this study it was not possible to place the sensors inside the chamber headspace, so two units from each model were sealed in a box, (20x12x7 cm) equipped with an air inlet and outlet. Box dimensions were suitable to accommodate inside only the sensors. In order to power both sensors and microcontroller and carry out field measurements, CO_2 sensors with their dedicated box, battery and microcontroller were positioned inside a second larger box (40x30x15 com), to make the whole system easily transportable. For the field test, a metal closed chamber (7.5 L volume, 30 cm diameter) was connected to a high precision CO_2 gas analyzer (DX4015 FTIR, Gasmet, www.gasmet.com), the benchmark. The flux measurements from soil were based on monitoring the concentration of CO_2 over time inside the chamber, taking simultaneous measurements from the sensors and the reference. The test set up was the following: the chamber was connected to the reference gas analyzer with an inlet air tube. The outlet tube from the gas analyzer was connected to the air inlet on the sensor box, and the sensor air outlet back to the chamber. The air was forced to pass through the gas analyzer first, then through the sensor box using the internal pump inside the Gasmet. The field work consisted of starting the units, deploying chambers, manual flushing of the chamber headspace at the desired time intervals and restarting measurements.

CO_2 concentrations inside the chamber headspace were collected over time at 5 min intervals throughout measurement periods of about two hours, for a total of 15 trials.

CO_2 concentrations from the sensors were compared with the Gasmet gas analyzer. An ordinary least squares regression between each sensor and the reference was performed over all the 15 trials. Results showed a clear lack of correlation between the sensors and reference measurements, with mean values of r^2 and slope equal to 0.18±0.24 and 0.21±1.55, respectively, and data was discarded.

A second sensor, the CO_2 Engine K30 FR by SenseAir (0-5000 ppm, 1Hz, www.senseair.com) was selected because of the good performance obtained during the field test described in Chapter 3. Sensors specifications are described in Table 4.1.

Manufacturer	Alphasense www.alphasense.com	SenseAir www.senseair.com
Model	IRC-A1 with transmitter board	CO_2 Engine K30 FR
Range of measurement (ppm)	0-5000	0-5000
Power supply (V)	10-30	5-12
Average current consumption (mA)	20	< 1.5
Peak current consumption (mA)	100	<600

Resolution (ppm)		15	n.a.
Accuracy (ppm)		±50	±30 ± 3% readings
Frequency of measurement (Hz)		1	1
Operating range	**T (°C)**	-30 to +50	0 to +50
	RH (% RH)	0-95 non condensing	0-95 non condensing
Dimensions (mm -LxWxH)		72 x39x16.5	51x57x12.5

Table 4.1. Catalog specifications of NDIR CO_2 models chosen for the tests

The sensors were replaced and a further cycle of measurements was carried out. CO_2 concentrations inside the chamber headspace were collected over time at 5 min intervals throughout measurement periods of about two hours, for a total of 12 trials.

K30 sensors led to reliable measurements and the dataset was used in the following analysis to assess the correlation between the sensors and the reference readings.

CO_2 concentrations from the sensors were compared with the Gasmet gas analyzer. An ordinary least squares regression between each sensor ($K30_1$ and $K30_2$) and the reference (Gasmet) was performed over all the 12 trials. Results are presented graphically in Figure 4.2 ($K30_1$) and Figure 4.3 ($K30_2$) while values are summarized and collected in Table 4.2.

CO_2 concentrations measured by K30 sensors showed a good correlation if compared to the reference data: slope ranges were equal to 1.04 ±0.08 and 1.04 ±0.07, correlation coefficient ranges to 0.98±0.03 and 1.00±0.00 for $K30_1$ and $K30_2$, respectively. Intercept range, equal to -77.06 ±88.80 and -88.15±82.28 ppm for $K30_1$ and $K30_2$, respectively, showed that both sensors had an offset with respect to the reference readings.

	$K30_1$			$K30_2$		
	r^2	**slope**	**intercept (ppm)**	**r^2**	**slope**	**intercept (ppm)**
mean	0.98	1.04	-77.06	1.00	1.04	-88.15
std	0.03	0.08	88.80	0.00	0.07	82.28
min	0.89	0.90	-210.68	0.98	0.93	-232.32
25%	0.99	1.01	-129.24	0.99	1.01	-131.87
50%	0.99	1.05	-85.58	1.00	1.06	-93.98
75%	1.00	1.07	-23.86	1.00	1.06	-34.05
max	1.00	1.15	71.14	1.00	1.14	39.48

Table 4.2 Descriptive statistics of result distributions for the regression analysis between $K30_1$ and $K30_2$ against the reference instruments, over the 12 trials. The table indicates the mean, the standard deviation (std), the minimum and maximum value (min, max) and the percentiles (25%, 50%, 75%).

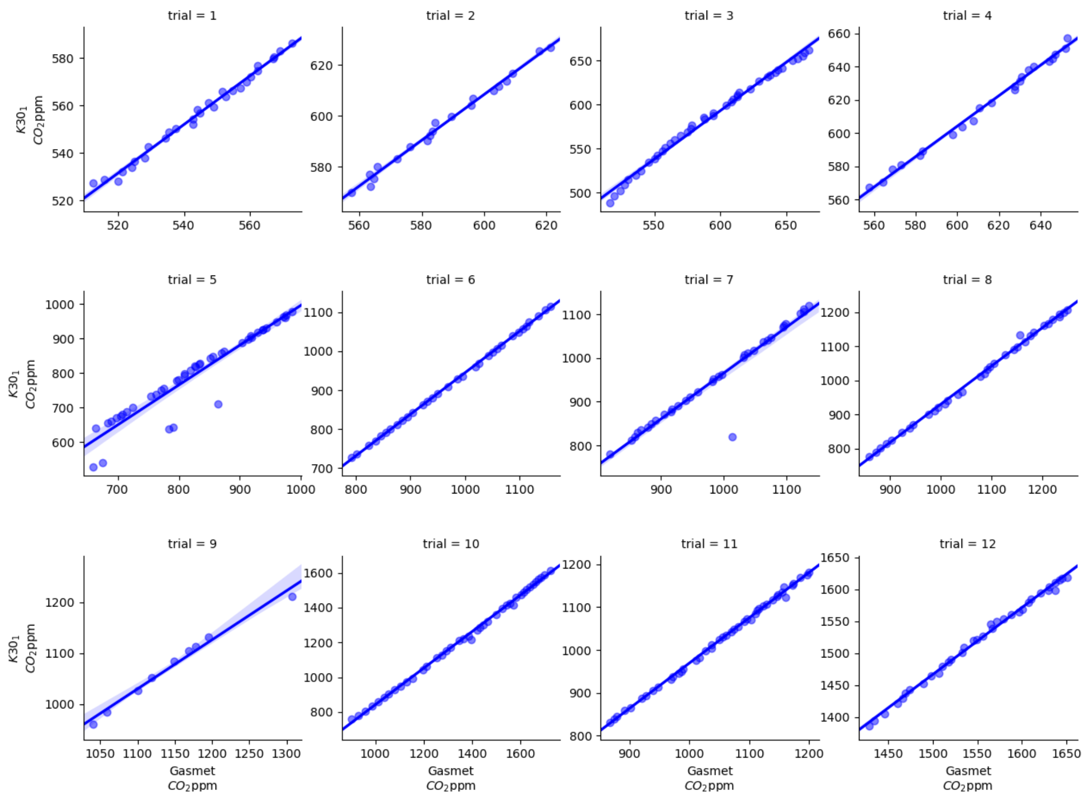

Figure 4.2. Regression analysis. Each plot represents the CO_2 concentrations measured during one trial by the K30 sensor unit n.1 (y axis, $K30_1$) against the Gasmet gas analyzer (x axis), with the fit line (blu line).

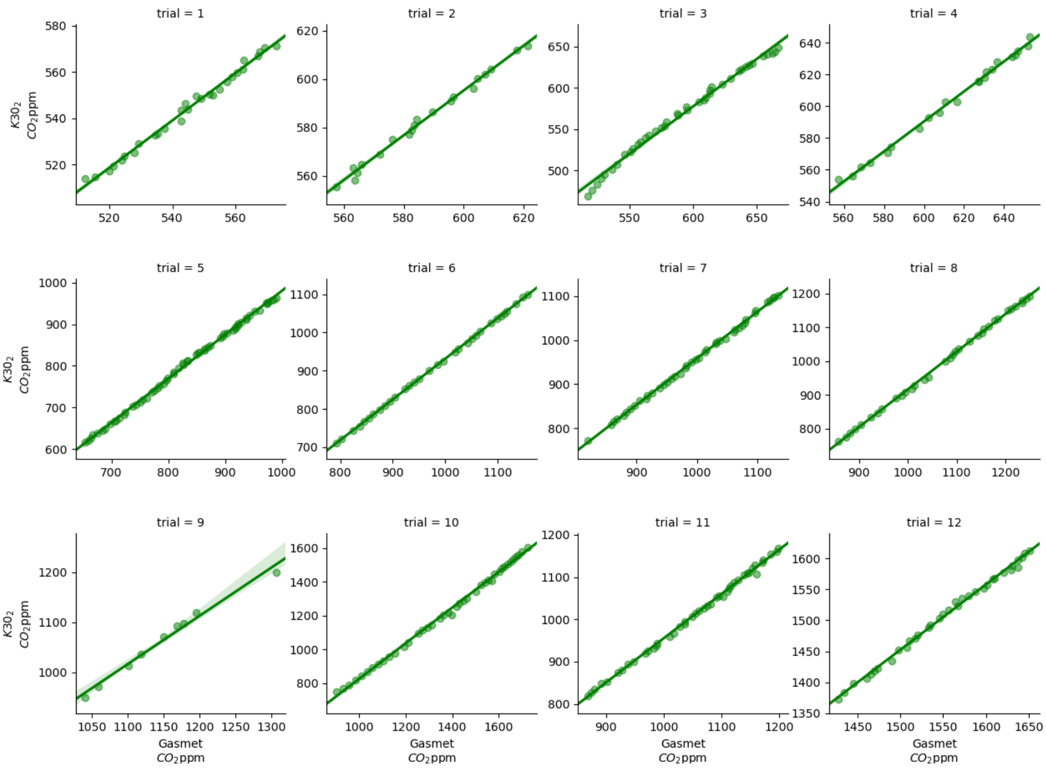

Figure 4.3. Regression analysis. Each plot represents the CO_2 concentrations measured during one trial by the K30 sensor unit n.2 (y axis, $K30_2$) against the Gasmet gas analyzer (x axis), with the fit line (green line)

CO_2 rates of accumulation, $\partial C/\partial t$(see Equation 4.1), i.e. the slope of the gas change in the chamber headspace during the deployment time, were calculated from the linear portion of the observed time series. The CO_2 rate of accumulation inside the chamber, measured by the sensors, was compared against the CO_2 rate of accumulation measured by the reference system, Figure 4.4 and Figure 4.5.

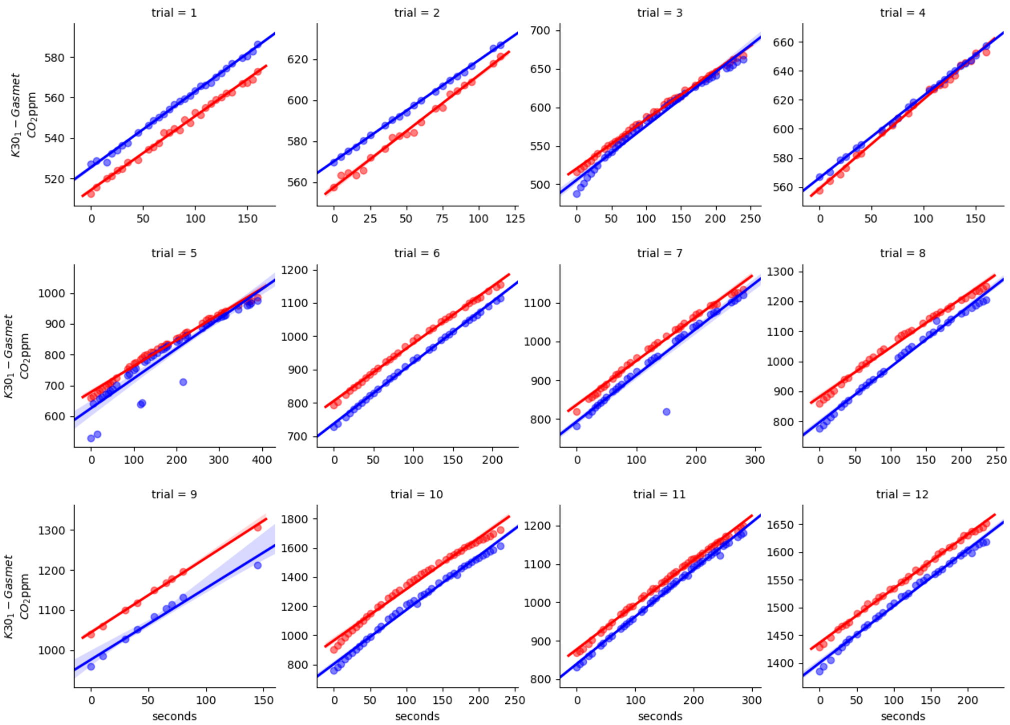

Figure 4.4. Comparison of CO_2 rate of accumulation inside the chamber measured with Gasmet gas analyzer (red dot) and the unit n.1 of the K30 (blue dot) over 12 trials. Each scatter plot represents the concentration measured by the sensor and by the gas analyzer against the chamber closure time, with the fit line.

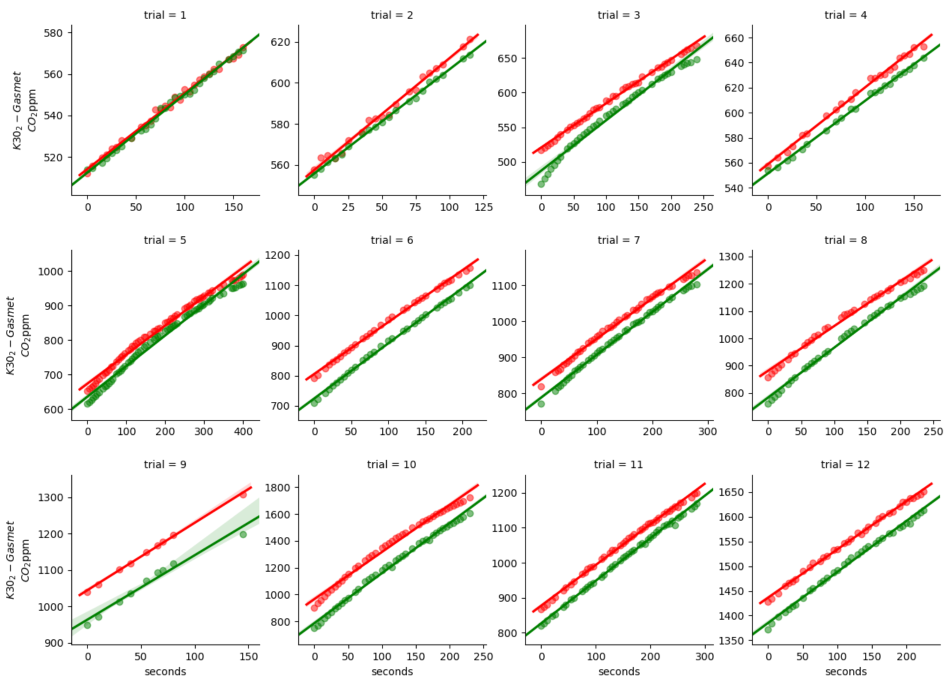

Figure 4.5. Comparison of CO_2 rate of accumulation inside the chamber measured with Gasmet gas analyzer (red dots) and the unit n.2 of the K30 sensors (green dots) over 12 trials. Each scatter plot represents the concentration measured by the sensor and by the gas analyzer against the chamber closure time, with the fit line.

The rate of accumulation measured by the two low cost sensors, over the 12 trials, was comparable with the rate of accumulation measured by the Gasmet, as shown in Figure 4.6, with a mean error equal to 0.05 ± 0.08 µmol mol^{-1} s^{-1}.

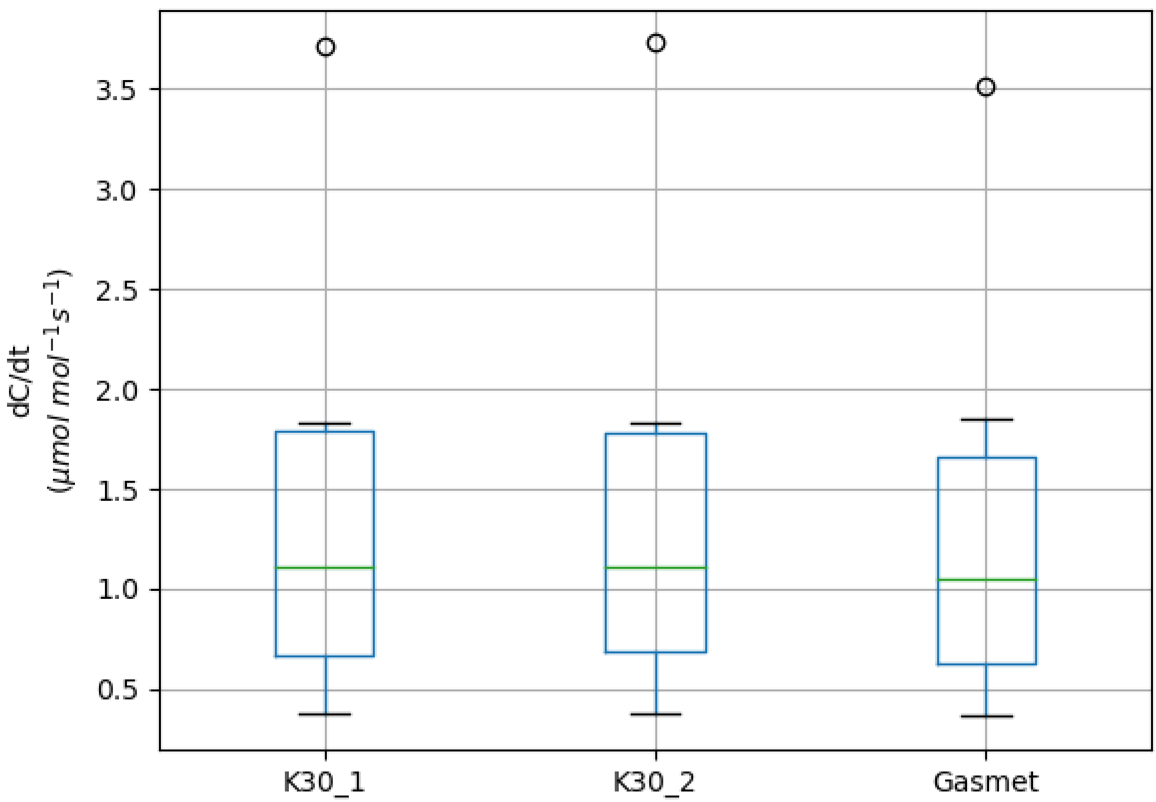

Figure 4.6. Comparison of CO_2 rate of accumulation inside the chamber measured by the two K30 sensors (K30_1 and K30_2) and the Gasmet gas analyzer (Gasmet). Boxplots indicate the range of rate of accumulation values. The green line indicates the median, the box the interquartile range and the blue lines extending above and below the box show the extent of the rest of the sample. Dots represent the outliers.

4.3 Conclusions

The measurements described in this Chapter are a simple test of low-cost sensors suitability for soil fluxes estimation. The test procedure, indeed, didn't follow the common recommendations regarding soil chambers (e.g., having pre-installed frames) and sensors were tested in one single application, but had the final aim to show if CO_2 low-cost sensors were suitable for soil measurements. A portable prototype to measure CO_2 concentration was realized using two models of NDIR CO2 low-cost sensors, a microcontroller to read and collect data and a 12 V battery. The prototype was tested in the field, alongside a reference system, in a single application with 12 trials. The use of LSC showed advantages such as limitations. Technically speaking, LCS led to several benefits: the system was easy to deploy, easy to carry and mènage respect to the heavier, more expensive sensing systems to measure the soil fluxes. In addition, the system needed a low power supply to work (12V). The major drawback was encountered in the fact that one of the two models (NDIR CO_2 IRC-A1 with transmitter board, by Alphasense) used in the first field led to an unreliable dataset. One the other hand, the second model (NDIR CO_2 Engine K30 FR, by Senseair) led to reliable measurements that were used to analyze the sensor performance. Plots and regression analysis results between reference and sensors showed clearly that K30 sensor measurements were well correlated with the reference, anyway the intercept values showed that both sensors had an offset respect to the reference instrument (Figure 4.3, Figure 4.4 and Table 4.2). However, analysis on the rate of accumulation measured from the sensors and the reference system, over the 12 trials, showed comparable values and a mean error respect to the reference equal to 0.05 ± 0.08 µmol mol^{-1} s^{-1}. These results suggest that the major limitation of these sensors, the low accuracy respect to traditional high precision gas analyzers, pointed out by the intercept values in the regression analysis (Table 4.2), i.e. the offset, can be overcome in soil chamber application. Soil flux measurements, indeed, are based on relative CO_2 changes (the rate of accumulation), which are not sensitive to exact absolute values. The test results show that these sensors could have a great potential for this type of measurement. As an example, sensors could be placed inside the chamber headspace, allowing chambers to be individual units that can be distributed over the surface more widely than a system where the chambers are connected to the external analyzer. This potential setup is important, indeed, for capturing the soil flux spatial variability, extending the sampling site from the limited area around the gas analyzer. In addition, AT and RH low-cost sensors could easily be added to the system to monitor the chamber conditions during the deployment period.

Trends in the development and deployment of low-cost approaches to measure gas fluxes in conjunction with chamber methods are increasing (Bastviken et al, 2015; Harmon et al., 2015). Bastiviken et al (2015) developed a low cost system to measure CO_2 fluxes in terrestrial and aquatic environments using mini loggers, with promising results. However the effect of temperature and relative humidity variation on sensor reading are unavoidable, especially if used inside a closed chamber and should be further investigated. Information regarding this aspect could be useful to assess a protocol for the use of low-cost systems for chamber measurements and to reach a higher data quality. In addition supplementary studies on low-cost platforms could be useful to share information on equipment and software design, facilitating the adoption of these new technologies.

5 General conclusions

The structure of this thesis, composed of autonomous chapters, allowed the discussion of each topic at the end of each session. In this chapter there will be reported the overall conclusions on the work.

Quantifying CO_2 emissions and uptakes is crucial to assess global policy to reduce climate warming. Well-constrained CO_2 fluxes estimations are critical for the global carbon balance, and there is a need to improve the availability of data-base on direct CO_2 measurements. However the main measurement methods, flux-chambers and eddy covariance techniques, have the major drawback related to the high cost of instruments used that reduce the spatial resolution of measurements. The aim of this PhD research was to develop low-cost approaches for measuring CO_2 concentration, and auxiliary data, such as air temperature and relative humidity, and to explore the possibility to use these systems in support/conjunction with flux chambers and eddy covariance techniques for storage flux measurements. A set of CO_2, temperature and relative humidity low-cost sensors were tested in the laboratory and the test results used to explore their potential use with the considered applications. Laboratory test results suggested that three out of four tested CO_2 models could be used for daily measurement with soil chambers, and one out of four CO_2 models could be suitable for long-term measurement with soil-chamber methods to account for the soil flux spatial variability and with eddy covariance techniques for storage estimations. Concerning the low-cost thermo-hygrometer models two out of four models could be suitable for the long-term deployment needed for storage measurement. Laboratory tests pointed out that the most relevant drawback is related to the CO_2 models sensitivity to humidity and temperature.

According to the test results, sensors were selected and two low-cost prototypes to measure CO_2 soil and storage fluxes were set up. The first prototype, a multisampling low-cost system for storage fluxes measurements, was tested in the field and its performance compared with the standard system, (a multipoint measurement system), and the most used approach, (a single point system) to estimate the storage fluxes. In addition, its potential to catch the storage horizontal spatial variability has been evaluated.

The low-cost system to measure storage fluxes obviously didn't reach the accuracy of the standard system, however the most significant observation emerges in comparing the low cost prototype performances with the most used approach. Storage fluxes were underestimated by the prototype and the single point with a magnitude equal to 11% and 42% respectively. These results are due mainly to system performances in fluxes estimations during low turbulence periods: the prototype underestimated the storage flux by 7%, the single point by 63%. On the other hand, the prototype performances decreased during high turbulence periods; its underestimation increased up to 18% while the single point approach underestimation decreased to 7%.

Considering that the storage flux is expected to be not negligible during low turbulence periods and should be measured as accurately as possible, the prototype could be a low-cost and labour-efficient system to spread measurements of the storage fluxes and if used in conjunction with the single point approach, could lead to a more accurate measure of the storage term. In addition, the second field experiment carried out with the prototype has shown that it could be an efficient tool to catch the storage spatial representativeness.

The second prototype, a low-cost approach for CO_2 soil flux measurements, was set up and tested in the field, with the final aim to explore the potential use of LCS with soil-flux chamber measurements.

The low-cost system to measure soil fluxes was equipped with two LCS sensor models and tested in one single application. One of the two chosen model sensors wasn't able to lead to reliable data, while the second model showed promising results. The rate of accumulation measured by the sensors was compliant to the reference instrumentation with a mean error equal to 0.05 ± 0.08 μmol mol-1 s-1 suggesting that these sensors could be a suitable tool for chamber measurements.

However, LCS technology and its use for ecological science applications is rather new and there is a need for supplementary studies on low-cost platforms over a wider range of environmental conditions to share information on equipment, software used and uncertainty in measurements. Trends in the development and deployment of low-cost approaches are increasing and the quick evolving of technology, to enhance sensor performance, could open supplementary paths toward the application of LCS in the context of greenhouse gas measurements.

The greater advantage in using LCS is represented by the possibility to replicate the heavier, more expensive sensing system used to measure the GHGs. Research on GHG emissions requires, indeed, high-quality, long-term and vast spatial scale measurements, collected using advanced and high-precision sensing systems (López-Ballesteros et al., 2018). Due to these requirements, many developing countries cannot conduct the necessary research (López-Ballesteros et al, 2018; Kim et al., 2016) and the critical lack of data leads to a not accurate estimation of GHG sources or emission, failing to establish proper mitigation strategies (Kim et al, 2021). Despite the needed attention to the data quality, the integration of low-cost approaches to monitoring networks could fill the gap between the costly research instrumentation and the enhancing of spatial and temporal measurement resolution and an opportunity for enhancing GHGs estimations.

References

Al-Saidi, A., Fukuzawa, Y., Furukawa, N., Ueno, M., Baba, S., & Kawamitsu, Y. (2009). A System for the Measurement of Vertical Gradients of CO2, H2O and Air Temperature within and above the Canopy of Plant. *Plant Production Science*, *12*(2), 139–149. https://doi.org/10.1626/pps.12.139

Anderson, D.E., Verma, S.B., Rosenberg, N.J., (1984). Eddy correlation measurements of CO2: latent heat and sensible heat fluxes over a crop surface. Agric For Meteorol 29:263–272

Arzoumanian, E., Vogel, F. R., Bastos, A., Gaynullin, B., Laurent, O., Ramonet, M., & Ciais, P. (2019). Characterization of a commercial lower-cost medium-precision non-dispersive infrared sensor for atmospheric CO2 monitoring in urban areas. *Atmospheric Measurement Techniques*, *12*(5), 2665–2677. https://doi.org/10.5194/amt-12-2665-2019

Aubinet M., Grelle A., Ibrom A., Rannik Ü., Moncrieff J., Foken T., et al., 2000. Estimates of the annual net carbon and water exchange of forests: the EUROFLUX methodology. Adv. Ecol. Res., 30. doi:10.1016/ s0065-2504(08)60018-5.

Aubinet, M., Berbigier, P., Bernhofer, C., Cescatti, A., Feigenwinter, C., Granier, A., … Sedlak, P. (2005). Comparing CO2 storage and advection conditions at night at different carboeuroflux sites. *Boundary-Layer Meteorology*, *116*(1), 63–94.

https://doi.org/10.1007/s10546-004-7091-8

Aubinet M, Feigenwinter C. (2010) Direct CO2 advection measurements and the night flux problem. Agric For Meteorol 150:651–654. doi:10.1016/j.agrformet.2010.03.007

Aubinet, M., Vesala, T., & Papale, D. (2012). *Eddy Covariance A Practical Guide to measurement and data Analysis*. Springer. https://doi.org/10.1007/978-94-007-2351-1

Baldocchi D., Falge E., Gu L.H., Olson R., Hollinger D., Running S., et al., 2001. FLUXNET: A new tool to study the temporal and spatial variability of ecosystem-scale carbon dioxide, water vapor, and energy flux densities. Bull. Am. Meteorol. Soc., 82: 2415-2434

Baldocchi, D. D. (2003). Assessing the eddy covariance technique for evaluating carbon dioxide exchange rates of ecosystems: past, present and future. *Global Change Biology*, *9*(4), 479–492. https://doi.org/10.1046/j.1365-2486.2003.00629.x

Bastviken, D., Sundgren, I., Natchimuthu, S., Reyier, H., & Gålfalk, M. (2015). Technical Note: Cost-efficient approaches to measure carbon dioxide (CO2) fluxes and concentrations in terrestrial and aquatic environments using mini loggers. *Biogeosciences*, *12*(12), 3849–3859. https://doi.org/10.5194/bg-12-3849-2015

Bland, J. M., & Altman, D. G. (1999). Measuring agreement in method comparison studies. *Statistical Methods in Medical Research*, *8*(2), 135–160. https://doi.org/10.1191/096228099673819272

Bryan, K., Komro, F.G. , Manabe, S. and Spelman, M.J. (1982). Transient Climate Response to Increasing Atmospheric Carbon Dioxide. *Science*, *215*, 56–58. https://doi.org/10.5840/enviroethics19835132

Butterbach-Bahl, K., Sander, O., Pelster, D., Díaz-Pinés, E., Butterbach-Bahl, K., Sander, B. O., & Pelster, D. (2016). Quantifying Greenhouse Gas Emissions from Managed and Natural Soils. https://doi.org/10.1007/978-3-319-29794-1_4

Cahoon, C., & Baker, R. J. (2008). Low-Voltage CMOS Temperature Sensor Design Using Schottky Diode-Based References. *IEEE Workshop on Microelectronics and Electron Devices*, 2008, pp. 16-19. https://doi.org/10.1109/WMED.2008.4510657.

Castell, N., Dauge, F. R., Schneider, P., Vogt, M., Lerner, U., Fishbain, B., … Bartonova, A. (2016). Can commercial low-cost sensor platforms contribute to air quality monitoring and exposure estimates? https://doi.org/10.1016/j.envint.2016.12.007

Chapin, F. S., Woodwell, G. M., Randerson, J. T., Rastetter, E. B., Lovett, G. M., Baldocchi, D. D., … Schulze, E. D. (2006). Reconciling carbon-cycle concepts, terminology, and methods. *Ecosystems*, *9*(7), 1041–1050. https://doi.org/10.1007/s10021-005-0105-7

Davidson, E. A., Savage, K., Verchot, L. V., & Navarro, R. (2002). Minimizing artifacts and biases in chamber-based measurements of soil respiration. *Agricultural and Forest*

Meteorology, *113*, 21–37.

Denman, K.L., G. Brasseur, A. Chidthaisong, R. Ciais, P.M. Cox, R.E. Dickinson, D. Hauglustaine, C. Heinze, E. Holland, D. Jacob, U. Lohmann, S. Ramachandran, P.L. da Silva Dias, S.C. Wofsy, and X. Zhang. (2007). Couplings between changes in the climate system and biogeochemistry. p. 499–587. In S. Solomon et al (ed.) Climate change 2007: Th e physical science basis. Contribution of Working Group I to the Fourth Assessment Report of the Intergovernmental Panel on Climate Change. Cambridge Univ. Press, New York, NY

Dinh, T.-V., Son, Y.-S., & Kim, J.-C. (2016). A review on non-dispersive infrared gas sensors: Improvement of sensor detection limit and interference correction, Sensors and Actuators B: Chemical, Volume 231, 2016, Pages 529-538, ISSN 0925-4005, https://doi.org/10.1016/j.snb.2016.03.040.

Falge, E., Baldocchi, D., Olson, R., Anthoni, P., Aubinet, M., Bern- hofer, C., Burba, G., Ceulemans, R., Clement, R., Dolman, H., Granier, A., Gross, P., Grunwald, T., Hollinger, D., Jensen, N. O., Katul, G., Keronen, P., Kowalski, A., Lai, C. T., Law, B. E., Meyers, T., Moncrieff, H., Moors, E., Munger, J. W., Pilegaard, K., Rannik, U., Rebmann, C., Suyker, A., Tenhunen, J., Tu, K., Verma, S., Vesala, T., Wilson, K., and Wofsy, S.(2001). Gap filling strategies for defensible annual sums of net ecosystem ex- change, Agr. Forest Meteorol., 107, 43–69, 2001

Farahani, H., Wagiran, R., & Hamidon, M. N. (2014). Humidity sensors principle, mechanism, and fabrication technologies: A comprehensive review. Sensors (Switzerland) (Vol. 14). https://doi.org/10.3390/s140507881

Finnigan, J. (2006). The storage term in eddy flux calculations. *Agricultural and Forest Meteorology*, *136*(3–4), 108–113. https://doi.org/10.1016/j.agrformet.2004.12.010

Finnigan J.J., Clement R., Malhi Y., Leuning R., and Cleugh H.A., 2003. A re-evaluation of long-term flux measurement techniques – Part I: Averaging and coordinate rotation. Bound. Lay. Met., 107: 1-48.

Foken, T., Wimmer, F., Mauder, M., Thomas, C., & Liebethal, C. (2006). Some aspects of the energy balance closure problem. *Atmos. Chem. Phys. Atmospheric Chemistry and Physics*, *6*, 4395–4402.

Foken, T. (2008), The energy balance closure problem: An overview, Ecol. Appl., 18, 1351–1367, https://doi.org/10.1890/06-0922.1

Foken T., Aubinet M., and Leuning R., 2012. The eddy covariance method. In: Eddy Covariance: A Practical Guide to Measurement and Data Analysis (Eds M. Aubinet, T. Vesala and D. Papale). Springer, Dordrecht

Fowler, D., Pilegaard, K., Sutton, M. A., Ambus, P., Raivonen, M., Duyzer, J., … Erisman, J. W. (2009). Atmospheric composition change: Ecosystems-Atmosphere interactions. *Atmospheric Environment*. https://doi.org/10.1016/j.atmosenv.2009.07.068

Franz D., et al., 2018. Towards long-term standardised carbon and greenhouse gas observations for monitoring Europe´s terrestrial ecosystems. Int. Agrophys., 32, 439-455.

Gorsel, E. Van, Leuning, R., Cleugh, H. A., Keith, H., & Suni, T. (2007). Nocturnal carbon efflux: reconciliation of eddy covariance and chamber measurements using an alternative to the u * -threshold filtering technique . *Tellus B*, *59*(3). https://doi.org/10.3402/tellusb.v59i3.17001

Goulden, M. L., Munger, J., Fan, S., Daube, B. C., & Wofsy, S. C. (1996). Measurements of carbon sequestration by long-term eddy covariance: methods and a critical evaluation of accuracy. *Global Change Biology*, *2*, 169–182.

Greenspan, L. (1977). Humidity Fixed Points of Binary Saturated Aqueous Solutions. *JOURNAL OF RESEARCH of the National Bureau of Standards -A. Phys Ics and Chemistry*, *81*(1). Retrieved from https://nvlpubs.nist.gov/nistpubs/jres/81A/jresv81An1p89_A1b.pdf

Gu, L., Falge, E., Boden, T., Baldocchi, D.D., Black, T.A., Saleska, S.R., Suni, T., Vesala, T., Wofsy, S., Xu, L., 2005. Objective threshold determination for nighttime eddy flux filtering. Agric. For. Meteorol. 128, 179–197.

Gu, L., Massman, W. J., Leuning, R., Pallardy, S. G., Meyers, T., Hanson, P. J., … Yang, B.

(2012). The fundamental equation of eddy covariance and its application in flux measurements. *Agricultural and Forest Meteorology*, *152*(1), 135–148. https://doi.org/10.1016/j.agrformet.2011.09.014

Guidolotti G, De Dato G, Liberati D, De Angelis P (2017). Canopy Chamber: a useful tool to monitor the CO_2 exchange dynamics of shrubland. iForest 10: 597-604. doi:10.3832/ifor2209-010

Harmon, T. C., Dierick, D., Trahan, N., Allen, M. F., Rundel, P. W., Oberbauer, S. F., … Zelikova, T. J. (2015). Low-cost soil CO2 efflux and point concentration sensing systems for terrestrial ecology applications. *Methods in Ecology and Evolution*, *6*(11), 1358–1362. https://doi.org/10.1111/2041-210X.12426

Hensen, A., Skiba, U. and Famulari, D. (2013) 'Low cost and state of the art methods to measure nitrous oxide emissions', *Environmental Research Letters*, 8(2), p. 025022. doi: 10.1088/1748-9326/8/2/025022

Holland, E.A., Robertson, G.P., Greenberg, J., Groffman, P., Boon, R. and Gosz J. (1999). Soil CO_2, N_2O and CH_4 exchange. In Robertson G.P., Bledsoe C.S., Coleman D.C., Sollins P. (eds), Standard soil methods for long term ecological research, Oxford University Press, New York, pp 185-201

Houghton, J. (1997).Global warming: The complete briefing. Cambridge, UK, Cambridge UniversityPress.

ICOS Handbook (2019). Publisher: ICOS ERIC. Editor: Syed Ashraful Alam, Janne-Markus Rintala, Katri Ahlgren, Eija Juurola ISBN: 978-952-94-1950-0

IPCC (2001). Climate Change 2001: The Scientific Basis. Contribution of Working Group I to the Third Assessment Report of the Intergovernmental Panel on Climate Change. Houghton, J.T., et al. (eds.). Cambridge University Press, Cambridge, United Kingdom and New York, NY, USA, 881 pp.

IPCC (2015). Climate Change 2014: Synthesis report. Contribution of Working Groups I, II and III to the Fifth Assessment Report of the Intergovernmental Panel on Climate

Change. IPCC, Geneva, Switzerland. https://doi.org/10.1016/S0022-0248(00)00575-3

Jiao, W., Hagler, G., Williams, R., Sharpe, R., Brown, R., Garver, D., … Buckley, K. (2016). Community Air Sensor Network (CAIRSENSE) project: Evaluation of low-cost sensor performance in a suburban environment in the southeastern United States. *Atmospheric Measurement Techniques*, *9*(11), 5281–5292. https://doi.org/10.5194/amt-9-5281-2016

Karl, T.R., Trenberth, K.E. Modern global climate change. Science 2003, 302, 1719–1723

Kim, D.-G., Thomas, A., Pelster, D., Rosenstock, T. S., and Sanz-Cobena, A.: Greenhouse gas emissions from natural ecosystems and agricultural lands in sub-Saharan Agrica: synthesis of available data and suggestions for further research, Biogeosci., 13, 4789-4809, 2016

Kim, D.-G., Bond-Lamberty, B., Ryu, Y., Seo, B., and Papale, D.: Reviews and syntheses: Enhancing research and monitoring of land-to-atmosphere greenhouse gases exchange in developing countries, Biogeosciences Discuss. [preprint],

https://doi.org/10.5194/bg-2021-85, in review, 2021.

Kramer, K., Leinonen, I., Bartelink, H. H., Berbigier, P., Borghetti, M., Bernhofer, C., … Vesala, T. (2002). Evaluation of six process-based forest growth models using eddy-covariance measurements of CO2 and H2O fluxes at six forest sites in Europe. *Global Change Biology*, *8*(3), 213–230. https://doi.org/10.1046/j.1365-2486.2002.00471.x

Lavigne, M. B., Foster, R. J., Goodine, G., (2004). Seasonal and annual changes in soil respiration in relation to soil temperature, water potential and trenching, Tree Physiology, Volume 24, Issue 4, April 2004, Pages 415–424, https://doi.org/10.1093/treephys/24.4.415

Lee, X., Massman, W., and Law, B. (2004). Handbook of Micrometeorology: A Guide for Surface Flux Measurement and Analysis, Kluwer Academic Publishers, Dordrecht, the Netherlands, 2004.

Lewis, A. C., Lee, J. D., Edwards, P. M., Shaw, M. D., Evans, M. J., Moller, S. J., Smith, K.

R., Buckley, J.W., Ellis, M., Gillot, S. R., & Whited, A. (2016). Evaluating the performance of low cost chemical sensors for air pollution research. Faraday Discussions, 189, 85–103.

Livingston G, Hutchinson G (1995). Enclosure- based measurement of trace gas-exchange: applications and sources of error. In: "Biogenic Trace Gases: Measuring Emissions from Soil and Water" (Matson PA, Harris RC eds). Black- well Scientific Publication, London, UK, pp. 14- 51. [online] URL: http://books.google.com/book s?id=WDjpgK7IQAgC

López-Ballesteros, A., Beck, J., Bombelli, A., Grieco, E., Lorencová, E. K., Merbold, L., Brümmer, C., Hugo, W., Scholes, R., Vačkář, D., Vermeulen, A., Acosta, M., Butterbach-Bahl, K., Helmschrot, J., Kim, D.-G., Jones, M., Jorch, V., Pavelka, M., Skjelvan, I., and Saunders, M. (2018): Towards a feasible and representative pan-African research infrastructure network for GHG observations, Environ. Res. Lett., 13, 085003

Makinwa K.A.A., (2010). Smart temperature sensors in standard CMOS, Procedia Engineering, Volume 5, Pages 930-939, ISSN 1877-7058, https://doi.org/10.1016/j.proeng.2010.09.262.

Marcolla, B., Cobbe, I., Minerbi, S., Montagnani, L., & Cescatti, A. (2014). Methods and uncertainties in the experimental assessment of horizontal advection. *Agricultural and Forest Meteorology*, *198–199*, 62–71. https://doi.org/10.1016/j.agrformet.2014.08.002

Martin, C. R., Zeng, N., Karion, A., Dickerson, R. R., Ren, X., Turpie, B. N., & Weber, K. J. (2017). Evaluation and environmental correction of ambient CO2 measurements from a low-cost NDIR sensor. *Atmospheric Measurement Techniques*, *10*(7), 2383–2395. https://doi.org/10.5194/amt-10-2383-2017

Matthews, H.D., Weaver, A.J., Meissner, K.J. et al (2004). Natural and anthropogenic climate change: incorporating historical land cover change, vegetation dynamics and the global carbon cycle. *Climate Dynamics* **22,** 461–479. https://doi.org/10.1007/s00382-004-0392-2

Montagnani, L., Grünwald, T., Kowalski, A., Mammarella, I., Merbold, L., Metzger, S., … Siebicke, L. (2018). Estimating the storage term in eddy covariance measurements: The ICOS methodology. *International Agrophysics*, *32*(4), 551–567.

https://doi.org/10.1515/intag-2017-0037.

Montgomery, R. B., 1948. Vertical eddy flux of heat in the atmosphere. J. Meteor., 5, 265–274.

Nicolini, G., & Papale, D. (2017). ICOS Ecosystem Instructions for Storage Fluxes Measurements (CO2, H2O, CH4 and N2O). ICOS Ecosystem Thematic Centre.

Nicolini, G., Aubinet, M., Feigenwinter, C., Heinesch, B., Lindroth, A., Mamadou, O., … Papale, D. (2018). Impact of CO2 storage flux sampling uncertainty on net ecosystem exchange measured by eddy covariance. *Agricultural and Forest Meteorology*, *248*(November), 228–239. https://doi.org/10.1016/j.agrformet.2017.09.025

Oertel, C., Matschullat, J., Zurba, K., Zimmermann, F., & Erasmi, S. (2016). Greenhouse gas emissions from soils - A review. Geochemistry, Volume 76, Issue 3, Pages 327-352, ISSN 0009-2819, https://doi.org/10.1016/j.chemer.2016.04.002.

Ohtaki, E., (1984). Application of an infrared carbon dioxide and humidity instrument to studies of turbulent transport. Bound Layer Meteorol 29:85–107

Papale, D. and Valentini, R.(2003). A new assessment of European forests carbon exchanges by eddy fluxes and artificial neural network spatialization, Global Change Biol., 9, 525–535

Papale, D., Reichstein, M., Aubinet, M., Canfora, E., Bernhofer, C., Kutsch, W., … Yakir, D. (2006). Towards a standardized processing of Net Ecosystem Exchange measured with eddy covariance technique: algorithms and uncertainty estimation. *Biogeosciences*, *3*(4), 571–583. https://doi.org/10.5194/bg-3-571-2006

Parkin, T. and Venterea, R. (2010). Chapter 3. Chamber-based trace gas flux measurements, in: Sampling Protocols, edited by: Follet, R., available at: www.ars.usda.gov/research/GRACEnet (last access: 20 March 2016), 3-1 to 3-39.

Pihlatie, M. K., Christiansen, J. R., Aaltonen, H., Korhonen, J. F. J., Nordbo, A., Rasilo, T., … Pumpanen, J. (2013). Comparison of static chambers to measure CH 4 emissions from soils. *Agricultural and Forest Meteorology*, *171–172*, 124–136.

https://doi.org/10.1016/j.agrformet.2012.11.008

Pinty, B., Ciais, P., Dee, D., Dolman, H., Dowell, M., Engelen, R., … Kentarchos, A. (2019). *An Operational Anthropogenic CO_2 Emissions Monitoring & Verification Support Capacity*. https://doi.org/10.2760/182790

Polidori, A., Papapostolou, V., & Zhang, H. (2016). Laboratory Evaluation of Low-Cost Air Quality Sensors. Retrieved from http://www.aqmd.gov/docs/default-source/aq-spec/protocols/sensors-lab-testing-protocol6087afefc2b66f27bf6fff00004a91a9.pdf?sfvrsn=2

Primicerio, J., Matese, A., Gennaro, S. F. Di, Albanese, L., Guidoni, S., & Gay, P. (2013). Development of an integrated , low-cost and open-source system for precision viticulture : from UAV to WSN. *EFITA-WCCA-CIGR Conference "Sustainable Agriculture through ICT Innovation" Turin, Italy*, (June 2013), 24–27.

Prentice I.C. et al. (2001). The Carbon Cycle and Atmospheric Carbon Dioxide. Climate Change 2001: the Scientific Basis. Contributions of Working Group I to the Third Assessment Report of the Intergovernmental Panel on Climate Change. , ed. by Houghton, J.T., Ding, Y., Griggs, D.J., Noguer, M., van der Linden, P.J., Dai, X., Maskel. Cambridge University Press, Cambridge, UK. https://doi.org/10.1029/eo067i015p00191

Ramaswamy, V., et al. (2000). Radiative forcing of climate change. In: Climate Change 2001: The Scientific Basis. Contribution of Working Group I to the Third Assessment Report of the 83 Intergovernmental Panel on Climate Change [Houghton, J.T., et al. (eds.)]. In *Space Science Reviews* (Vol. 94, pp. 363–373). , Cambridge, United Kingdom and New York, NY, USA, pp. 349–416.: Cambridge University Press. https://doi.org/10.1023/A:1026752230256

Raupach, M. R., Rayner, P. J., Barrett, D. J., Defries, R. S., Heimann, M., Ojima, D. S., … Schmullius, C. C. (2005). Model-data synthesis in terrestrial carbon observation: Methods, data requirements and data uncertainty specifications. *Global Change Biology*, *11*(3), 378–397. https://doi.org/10.1111/j.1365-2486.2005.00917.x

Rebmann, C., Aubinet, M., Schmid, H., Arriga, N., Aurela, M., Burba, G., … Franz, D.

(2018). ICOS eddy covariance flux-station site setup: A review. *International Agrophysics*, *32*(4), 471–494. https://doi.org/10.1515/intag-2017-0044

Reichstein, M., Falge, E., Baldocchi, D., Papale, D., Aubinet, M., Berbigier, P., Bernhofer, C., Buchmann, N., Gilmanov, T., Granier, A., Gr¨unwald, T., Havr´ankov´a, K., Ilvesniemi, H., Janous, D., Knohl, A., Laurila, T., Lohila, A., Loustau, D., Mat- teucci, G., Meyers, T., Miglietta, F., Ourcival, J.-M., Pumpanen, J., Rambal, S., Rotenberg, E., Sanz, M., Tenhunen, J., Seufert, G., Vaccari, F., Vesala, T., Yakir, D., and Valentini, R. (2005). On the separation of net ecosystem exchange into assimilation and ecosystem respiration: review and improved algorithm, Global Change Biol., 11, 1424–1439

Rochette, P., & Hutchinson, G. L. (2005). Measurement of Soil Respiration in situ: Chamber Techniques. *Publications from USDA-ARS / UNL Faculty. Paper 1379*. Retrieved from http://digitalcommons.unl.edu/usdaarsfacpub

Savage, K. E., & Davidson, E. A. (2003). A comparison of manual and automated system for soil CO2 flux measurements: trade-offs between spatial and temporal resolution. *Journal of Experimental Botany*, *54*, 891–899. Retrieved from http://proclima.cetesb.sp.gov.br/wp-content/uploads/sites/28/2014/04/co2flux.pdf

Savage, K., Phillips, R., & Davidson, E. (2014). High temporal frequency measurements of greenhouse gas emissions from soils. *Biogeosciences*, *11*, 2709–2720. https://doi.org/10.5194/bg-11-2709-2014

Shevliakova, E., Stouffer, R. J., Malyshev, S., Krasting, J. P., Hurtt, G. C., & Pacala, S. W. (2013). Historical warming reduced due to enhanced land carbon uptake. Proceedings of the National Academy of Sciences of the United States of America, 110, 16730–16735. https://doi. org/10.1073/pnas.1314047110

Shrestha, S. S. (2009). Performance evaluation of carbon-dioxide sensors used in building HVAC applications, (Graduate Theses and Dissertations, 10507).

Snyder, C. W. (2016). Evolution of global temperature over the past two million years. *Nature* 538, (7624), 226–228. https://doi.org/10.1038/nature19798

Spinelle, L., Aleixandre, M., & Gerboles, M. (2013). *Protocol of evaluation and calibration of* *low-cost gas sensors for the monitoring of air pollution*. Publications Office of the European Union. https://doi.org/10.2788/9916

Stull, R. B., (1988): An introduction to Boundary Layer Meteorology. Kluwer Academic Publishers.

Van Gorsel, E., Delpierre, N., Leuning, R., Black, A., Munger, J.W., Wofsy, S., Aubinet, M., Feigenwinter, C., Beringer, J., Bonal, D., Chen, B., Chen, J., Clement, R., Davis, K.J., Desai, A.R., Dragoni, D., Etzold, S., Grünwald, T., Gu, L., Heinesch, B., Hutyra, L.R., Jans, W.W.P., Kutsch, W., Law, B.E., Leclerc, M.Y., Mammarella, I., Montagnani, L., Noormets, A., Rebmann, C., Wharton, S., 2009. Estimating nocturnal ecosystem respiration from the vertical turbulent flux and change in storage of CO2. Agric. For. Meteorol. 149, 1919–1930. http://dx.doi.org/10.1016/j.agrformet.2009.06.020.

Wallington, T.J., Srinivasan, J., Nielsen O.J. , Highwood, E. J. (2004). Greenhouse gases and global warming. In Environmental and Ecological Chemistry, Ed. Aleksandar Sabljic, in Encyclopedia of Life Support Systems (EOLSS), Developed under the Auspices of the UNESCO. Oxford ,UK

Wang, K-Y, Zheng, X., Pihlatie, M., Vesala, T., Liu, C., Haapanala, S., Mammarella, I., Rannik, Ü., and Liu, H., (2013). Comparison between static chamber and tunable diode laser-based eddy covariance techniques for measuring nitrous oxide fluxes from a cotton field, Agr. Forest Meteorol., 171–172, 9–19

Webb E. K., Pearman G. I., Leuning R., 1980. Correction of flux measurements for density effects due to heat and water vapour transfer. Quart. J. Met. Soc., 106, 85-100. doi: 10.1002/qj.49710644707.

Wohlfahrt, G., Anfang, C., Bahn, M., Haslwanter, A., Newesely, C., Schmitt, M., Drösler, M., Pfadenhauer, J., Cernusca, A. (2005). Quantifying nighttime ecosystem respiration of a meadow using eddy covariance, chambers and modelling, Agricultural and Forest Meteorology, Volume 128, Issues 3–4, 2005, Pages 141-162, ISSN 0168-1923, https://doi.org/10.1016/j.agrformet.2004.11.003.

Yang, P. C., Black, T. A., Neumann, H. H., Novak, M. D., & Blanken, P. D. (1999). Spatial and temporal variability of CO2 concentration and flux in a boreal aspen forest. *Journal of Geophysical Research-Atmospheres*, *104*(D22), 27653–27661. https://doi.org/10.1029/1999jd900295

Yang, B., Hanson, P. J., Riggs, J. S., Pallardy, S. G., Heuer, M., Hosman, K. P., … Gu, L. H. (2007). Biases of CO2 storage in eddy flux measurements in a forest pertinent to vertical configurations of a profile system and CO2 density averaging. *Journal of Geophysical Research Atmospheres*, *112*(20), 1–15. https://doi.org/10.1029/2006JD008243

Yasuda, T., Yonemura, S., & Tani, A. (2012). Comparison of the Characteristics of Small Commercial NDIR CO 2 Sensor Models and Development of a Portable CO 2 Measurement Device. *Sensors*, *12*, 3641–3655. https://doi.org/10.3390/s120303641

Young, D. T., Chapman, L., Muller, C. L. and Cai X.M., (2014) ‘A low-cost wireless temperature sensor: Evaluation for use in environmental monitoring applications’, *Journal of Atmospheric and Oceanic Technology*, 31(4), pp. 938–944. doi: 10.1175/JTECH-D-13-00217.1.

Zha, T. S., Kellomäki, S., Wang, K‐Y. (2003). Seasonal Variation in Respiration of 1‐year‐old Shoots of Scots Pine Exposed to Elevated Carbon Dioxide and Temperature for 4 Years, Annals of Botany, Volume 92, Issue 1, July 2003, Pages 89–96, https://doi.org/10.1093/aob/mcg118